Digital Comprehensive Summaries of Uppsala Dissertations
from the Faculty of Science and Technology 2290

Carbenes: The Gathering

Photophysics of Transition Metal Carbene Complexes

NIDHI KAUL

ACTA UNIVERSITATIS
UPSALIENSIS
2023

ISSN 1651-6214
ISBN 978-91-513-1860-8
urn:nbn:se:uu:diva-508707

UPPSALA
UNIVERSITET

Dissertation presented at Uppsala University to be publicly examined in Pohlemsalen, Ångströmlaboritoriet, Lägerhyddsvägen 1, Uppsala, Monday, 25 September 2023 at 13:15 for the degree of Doctor of Philosophy. The examination will be conducted in English. Faculty examiner: James K. McCusker (Michigan State University).

Abstract

Kaul, N. 2023. Carbenes: The Gathering. Photophysics of Transition Metal Carbene Complexes. *Digital Comprehensive Summaries of Uppsala Dissertations from the Faculty of Science and Technology* 2290. 101 pp. Uppsala: Acta Universitatis Upsaliensis. ISBN 978-91-513-1860-8.

This thesis explores the photophysics of some transition-metal complexes (TMCs) which utilize N-heterocyclic carbenes as ligands. After a historical interlude which traces the development of the broader field of transition metal complexes and their photophysical investigations, there is an overview of theoretical concepts and the spectroscopic methods employed. The focus thereafter is placed on complexes of the type $[ML_2]^{n+}$ (where M=Fe and Mn) which feature the tripodal 'Scorpionate' motif, i.e. L=[phenyl(tris(3-methylimidazol-1-ylidene))borate]$^-$. L, like many carbenes, is an exceptional sigma-donor, and by some metrics is the strongest tripodal donor known. It is therefore able to sufficiently destabilize metal-centred states in conjunction with several 3d metals, allowing for the realization of long-lived charge-transfer states on the nanosecond timescale, in sharp contrast to many complexes based on polypyridyl ligand motifs previously investigated.

$[Fe^{III}L_2]^+$ features a 2 ns doublet ligand-to-metal charge transfer (LMCT) excited state, which is substantially energetic and is shown to be capable of engaging in photoinduced electron transfer reactions with both donors and acceptors. The strong ligand field imposed on the iron centre furthermore makes possible the occurrence of two metal-centred redox events before the ligand oxidation – this translates to the unusual situation of the LMCT excited state of $[Fe^{III}L_2]^+$ being able to oxidize or reduce its own ground state: a phenomenon called photoinduced symmetry-breaking charge separation. The finding is the first documented case with direct evidence for a transition-metal complex, and the only one which proceeds with a substantial driving force generally. $[Mn^{IV}L_2]^{2+}$ features a long-lived LMCT excited state, which is found to be a potent photo-oxidant, capable of oxidizing a range of substrates including solvents such as methanol. Its excited state lifetime of 16 ns also presents a near order of magnitude improvement over the iron counterpart. One possible cause is traced to the spin-forbidden nature of the transition back to the ground state, highlighting the importance of such a design principle for the realization of longer lifetimes, as has been the case previously for excited states based on precious metals. The last half of the thesis features benzothiadiazole-Au-carbene (and phosphine) chromophores that are bright phosphors in room temperature solution – it is found that the carbene is inconsequential to the photophysics in this case, which is instead contingent on the direct linkage of the gold atom to a heteroarene moiety, causing an efficient population of its triplet manifold. Concluding remarks are furnished.

Keywords: photophysics, time-resolved spectroscopy, transition-metal complexes

Nidhi Kaul, Department of Chemistry - Ångström, Physical Chemistry, Box 523, Uppsala University, SE-75120 Uppsala, Sweden.

ISSN 1651-6214
ISBN 978-91-513-1860-8
URN urn:nbn:se:uu:diva-508707 (http://urn.kb.se/resolve?urn=urn:nbn:se:uu:diva-508707)

नासदासीन्नो सदासीत्तदानीं नासीद्रजो नो व्योमा परो यत् |

किमावरीवः कुह कस्य शर्मन्नम्भः किमासीद्गहनं गभीरम् ॥

...

इयं विसृष्टिर्यत आबभूव यदि वा दधे यदि वा न |

यो अस्याध्यक्षः परमे व्योमन्त्सो अङ्ग वेद यदि वा न वेद ॥

— **ऋग्वेद** १०.१२९

List of Papers included

This thesis is based on the following papers, which are referred to in the text by their Roman numerals.

I. **Luminescence and reactivity of a charge-transfer excited iron complex with nanosecond lifetime**
Kasper Skov Kjær†, Nidhi Kaul†, Om Prakash†, Pavel Chábera, Nils W Rosemann, Alireza Honarfar, Olga Gordivska, Lisa A Fredin, Karl-Erik Bergquist, Lennart Häggström, Tore Ericsson, Linnea Lindh, Arkady Yartsev, Stenbjörn Styring, Ping Huang, Jens Uhlig, Jesper Bendix, Daniel Strand, Villy Sundström, Petter Persson, Reiner Lomoth, Kenneth Wärnmark. **2019** Science *363*, 6424, 249–253.
Contribution: Investigation, Methodology, Formal Analysis, Validation, Visualization (lead) for reactivity studies.

II. **The Carbene Cannibal: Photoinduced Symmetry-Breaking Charge Separation in an Fe(III) N-Heterocyclic Carbene**
Nidhi Kaul and Reiner Lomoth. **2021** Journal of the American Chemical Society *143*, 29, 10816–10821.
Contribution: Conceptualization (equal), Investigation, Methodology, Formal Analysis, Validation, Visualization, Writing – original draft (lead), review, editing (equal) for all photophysical studies.

III. **A Mn(IV)-carbene complex with a long-lived charge transfer excited state**
Nidhi Kaul, Juan A. Valdez-Moreira, Jeremy M. Smith, Leif Hammarström. *Submitted.*
Contribution: Conceptualization, Investigation, Methodology, Formal Analysis, Validation, Visualization, Writing – original draft (lead), review, editing (equal) for all photophysical, electrochemical, spectro-electrochemical, and reactivity studies.

IV. Benzothiadiazole-Au(I) complexes as efficient room-temperature phosphors in solution
Mauricio Posada Urrutia,† Nidhi Kaul,† Tobias Kaper, Dustin Hurell, Linus Chiang, Fredric Ingner, Jordann Wells, Andreas Orthaber, Leif Hammarström, Lukasz T. Pilarski, and Christine Dyrager. *In Manuscript.*
Contribution: Conceptualization (supporting), Investigation (equal), Methodology (equal), Formal Analysis, Validation, Visualization, Writing – original draft (lead), review, editing (equal) for all photophysical studies.

Contributions according to CRediT, see: https://credit.niso.org.

†Equal contribution.

Initial reactivity results in Paper I were published in the Masters thesis, entitled, 'Excited State Reactivity of $[\{PhB(MeIm)_3\}_2Fe]^+$'. In the paper, however, reductive quenching data is new, and erroneously determined cage-escape yields were corrected. All quenching rate constants were also revised using time-resolved emission spectroscopy.

Papers not included in this thesis

V. Photophysical Integrity of the Iron(III) Scorpionate Framework in Iron(III)–NHC Complexes with Long-Lived ^{2}LMCT Excited States
Om Prakash†, Linnea Lindh†, Nidhi Kaul†, Nils W. Rosemann, Bolaño Losada, Catherine Johnson, Pavel Chábera, Aleksandra Ilic, Jesper Schwarz, Arvind Kumar Gupta, Jens Uhlig, Tore Ericsson, Lennart Häggström, Ping Huang, Jesper Bendix, Daniel Strand, Arkady Yartsev, Reiner Lomoth, Petter Persson, and Kenneth Wärnmark. **2022** Inorganic Chemistry *61*, 44, 17515–17526.

VI. How Rigidity and Conjugation of Bidentate Ligands Affect the Geometry and Photophysics of Iron *N*-heterocyclic Complexes – A Comparative Study
Om Prakash†, Pavel Chábera†, Nidhi Kaul†, Valtýr F. Hlynsson †, Nils W. Rosemann, Iria Bolano Losada, Yen Tran Hoang Hai, Ping Huang, Jesper Bendix, Tore Ericsson, Lennart Häggström, Arvind Gupta, Daniel Strand, Arkady Yartsev, Reiner Lomoth, Petter Persson, Kenneth Wärnmark. *Submitted.*

VII. ^{3}MLCT excited state dynamics of a Homoleptic Iron(II) Hexa *N*-heterocyclic Carbene Scorpionate Complex
Nidhi Kaul, Mawuli Deegbey, Aleksandra Ilic, Catherine Johnson, Om Prakash, Kenneth Wärnmark, Elena Jakubikova, Reiner Lomoth. *In Manuscript.*

VIII. Realizing Symmetry-Breaking Architectures in Soap Films
Hongwei Song†, Nidhi Kaul†, Agnese Amati, Gabriele Falciani, Luca Bergamasco, Cees J. M. van Rijn, Eliodoro Chiavazzo, Indraneel Sen, Sylvestre Bonnet, Leif Hammarström. *Submitted.*

IX. **Surface plasmon-enhanced photo-driven CO_2 hydrogenation by hydroxy-terminated nickel nitride nanosheets**
Saideep Singh†, Rishi Verma†, Nidhi Kaul†, Jacinto Sa, Ajinkya Punjal, Shriganesh Prabhu, Vivek Polshettiwar. **2023** Nature Communications *14*, 1, Article: 2551 1–18.

†Equal contribution.

Contents

Key Abbreviations and Symbols

bpy	2,2'-bipyridine
FWHM	Full-width-half-maximum
HOMO	highest occupied molecular orbital
ILCT/ICT	inter-ligand charge-transfer
IRF	instrument response function
LMCT	ligand-to-metal charge transfer
LUMO	lowest unoccupied molecular orbital
MC	metal-centred
MLCT	metal-to-ligand charge transfer
MO	molecular orbital
MV^{2+}	1,1′-Dimethyl-4,4′-bipyridinium dication
NHC	N-heterocylic carbene
Q	Quencher
SCE	Saturated Calomel Electrode
SV	Stern-Volmer
TMC	Transition-metal complex
UV	Ultraviolet
Vis	Visible

A	Absorbance
ΔA	Differential absorbance
c	concentration
$E_{0\text{-}0}$	0-0 spectroscopic transition energy
$\Delta\varepsilon$	Differential extinction coefficient
ε	Molar extinction coefficient in M^{-1} cm^{-1}
E	Energy
Δ_o	Ligand-field splitting parameter in an octahedral field
Fc^+/Fc	Ferrocene ferrocenium couple
η_{ce}	Cage escape efficiency
ΔG^o	Standard Gibbs free energy change in a chemical process / reaction
$\hbar$	Reduced Planck's constant: $h/2\pi$
I	Intensity of light
µM	Micromolar (10^{-6})
mM	Millimolar (10^{-3})
M	Molar
K_{sv}	Stern-Volmer constant
k_q	Bimolecular quenching rate constant
k_{bet}	Rate constant of back electron transfer
k_{et}	Rate constant of forward electron transfer
k_{ce}	Rate constant of cage escape
k_d/k_{-d}	Rate constant of diffusion
k_r	Rate constant of radiative decay
k_{nr}	Rate constant of non-radiative decay
κ_{el}	Electronic transmission coefficient
k_{sub}	Rate constant; sub=defined in text
Q / $[Q]$	Quencher / Quencher concentration

q	Coordinate
λ	Reorganization energy
τ	Excited state lifetime in the presence of quencher
τ_o	Excited state lifetime in the absence of quencher

Prologue

It is so difficult to find the beginning. Or better: it is difficult to begin at the beginning. And try not to go further back.

– Ludwig Wittgenstein, *On Certainty*

"What kind of field defines itself as a negation?" a wise man questioned[a] – presumably half in jest – referring to the field of *in*organic chemistry. Inasmuch as G.N. Lewis characterized physical chemistry as 'encompassing all that is interesting', it may be worthwhile to make the broad subject of this condensed treatise – physical inorganic chemistry – somewhat less vacuous and accessible *before* beginning in earnest.

The wise man's seemingly innocent query turns out to be a loaded one as a brief stroll through history would indicate: inorganic chemistry has known many definitions, depending on individual, time-period, and even geographic location. Deriving from ancient Greek *ὄργανον*, the classification of substances as "organic bodies" in the early 1700s by philosophers and chemists hearkened to the Aristotelian thought of living beings as organised bodies, with non-living – *i.e.* everything else – as inorganic, and unorganized, though little was known of their composition in a chemical sense. Berzelius, together with others, using combustion analysis, made substantial contributions to the understanding of the chemical constituents of materials. He also espoused the vital-force theory[b], which conferred on elements in living beings a special function inaccessible via purely inorganic 'non-living' means. This doctrine was dismantled by Wöhler's synthesis of urea from ammonium cyanate, without use of – as understood at the time – organic sources. Kolbe's synthesis of acetic acid from the elements drove further nails into the coffin – and the implication of organic changed from "life-based" to "carbon-based", which is what we typically think of in current parlance.

Accordingly, the negation that is inorganic chemistry proceeded to include

[a] In conversation with Professor Leif Hammarström, April 29 2021.

[b] It is worth noting that Berzelius had re-used the nomenclature and concepts from Bergman and Gren, both of whom had died by that point, and were not cited. Bergman was based in Uppsala; for a recent, thorough account of the origins of organic chemistry, see: C. Wentrup, *Eur. J. Org. Chem.* **2022**, e202101492, and references therein.

everything that is *not* based on carbon – at least *prima facie*. In truth, not only are the roots of modern synthetic organic chemistry markedly 'inorganic' in character, hardly any organic synthesis of appreciable complexity may be achieved without the involvement of a metal, or, more specifically, a transition metal complex. Indeed, as reflected in textbooks and symposia, the present implication of inorganic chemistry (besides metallurgy[c]) is commonly regarded as equivalent to coordination chemistry, which invariably involves a central metal atom bonded to several molecular units called ligands (from Latin *ligare* "to bind"), that are organic or inorganic. Yet, it is the former – organometallic complexes – which are oftentimes far more interesting than the latter. We need only look to Nature to confirm the fact: everything from photosynthesis to respiration relies on the involvement of metals or their complexes. We are carbon-based lifeforms, whose critical functionalities are mostly impossible without first-row transition metals[d].

Suffice to say, the distinction between branches is an artifice more rooted in tradition, perspective, and convenience of study, rather than an honest conceptual one. Alfred Werner had noted already in 1914 in the context of isomerism, '…the distinction between organic and purely inorganic compounds disappears' and that the chemistry of carbon fell in the broader scope and rules of coordination chemistry, rather than the other way round. Decades later, in 1988, Lehn would echo such a sentiment in relation to supramolecular chemistry: '…the chemistry of receptor molecules may be considered a generalized coordination chemistry, not limited to transition metal ions, but extending to all types of receptees: cationic, anionic or neutral species of organic, inorganic or biological nature.' Ultimately, one is forced to acknowledge that the (structural) study of matter reduces itself to the classifications of ordered arrangements and the interactions which hold these arrangements together – the most encompassing definition of coordination chemistry.

Perhaps the most powerful tool at our disposal to gain insight into the aforementioned arrangements – both in space and time – is spectroscopy. Nearly all introductory courses begin with a reflection on the telling origins of the word: Latin *spectron,* "ghost or spirit", and Greek *σκοπειν*, "to see". Unable to be directly seen, the spectres that are molecules unravel themselves in their response to the stimulus of electromagnetic radiation, i.e. light. A measurement of the response to this perturbation furnishes all sorts of information about the physical properties of the molecular world: structures, symmetries, energies of states, dynamics, etc. Many coordination complexes display

[c] More generally, smelting and metallurgy – the cornerstones of the development of human civilization – fall in the ambit of the modern conception of inorganic chemistry as well.
[d] So entwined they are since antiquity that the Sanskrit root word for iron/metal, लोह, was equivalently substituted to mean blood in Vedic texts.

vibrant colours: a direct manifestation of the quantum mechanical principles which govern their electronic arrangement, easily measured even by the primitive detector that is our eye. Absorption of a visible photons by molecules leads to the promotion of their electrons to higher energy levels, resulting in the formation of excited states. Both steady-state and time-resolved spectroscopic methods – the latter typically using pulsed light sources such as lasers – may be used to gain insight into the nature, energetics and dynamics of these electronically excited states. The study of such light-matter interactions and resulting phenomena fall specifically within the realm of molecular photophysics, and forms the core content of the pages that follow. As alluded to before, the subjects are a set of novel organometallic complexes, which happen to exhibit certain photophysical properties hitherto unseen in coordination complexes based on first-row metals – the findings may thus be thought to be of substantial interest from both fundamental and applied perspectives. Although the systems under study are highly specific, the aim is to gain some general insight.

The first chapter serves to set the stage with appropriate historical and contemporary context of the research field, and a more formal motivation (in addition to curiosity)! The second chapter brushes up on old concepts that are readily applied to the study of these new complexes, while the third chapter revisits the well-known spectroscopic and other methods employed. The next few chapters delve into the systems under study, tackling one by one complexes of Fe and Mn, followed by a comparative account of the properties of these complexes in several oxidation states. The seventh chapter sees a segue to organo-Au complexes that function as an important contrasting example. The final chapter summarizes findings, presents a future outlook, and notes challenges. An attempt has been made to make the text self-contained, largely accessible to an individual with an undergraduate training in chemistry or physics, and enjoyable for one who should like to call themselves an expert in molecular photophysics – all the while qualifying for a doctoral degree in Chemical Physics! Time will tell if these lofty ambitions were achieved, but it is important to say that the good things contained herein are undoubtedly a product of the inspiration imparted by my mentors, collaborators, and friends, while the errors and missteps are all my own.

Nidhi Kaul

Uppsala, Sweden
July 2023

1. Introduction

It is not what you look at that matters, but what you see.

– Henry David Thoreau, *Walden*

Essential to the understanding of molecular photophysics are both structure and dynamics. Structure can be considered in a nuclear as well as electronic sense, and at the level of principle the former is a consequence of the latter. The electronic arrangement of a molecule determines how it interacts with light; put conversely, interaction with light – spectroscopy – can furnish structural information about a molecule. The type of information gained depends on the wavelength of light used (i.e. the energy of the incident photons), and what is probed (absorption, diffraction, resonances, etc.). Dynamics comes into play because electromagnetic perturbation necessarily generates a transient metastable state of a molecule, different from its ground state. How this state proceeds to evolve *in time* to return to its original configuration (though this is not always the case) is contingent on the states available in the molecule, and their relative energies. Structure and dynamics are thus intimately tied, and correlated with function. Further, dynamical measurements, particularly in the solution phase (which are the kind this thesis concerns itself with) are carried out on ensembles and not individual molecules: a population-averaged signal is measured. Finally, the evolution of populations is frequently also tied to the solvation environment. These considerations in coordination complexes can sometimes be particularly nuanced: a clarity of their structure was not developed until the second quarter of the 20th century, and dynamical investigations followed only thereafter.

Indeed, coordination chemistry speaks of a coloured past – both literally and figuratively. This has been documented in painstaking detail by George Kauffman[1,2], and also others[3,4]. A compressed rendition follows, unavoidably coloured by the author's biases which determine what is told and what is left out – the reader is encouraged to explore the aforementioned references for a more complete picture.

1.1 Metal Complexes

Alizarin is perhaps one of the oldest dyes, its usage well-known to Indians and Egyptians as far back as 1500 BC. The principle component, orange 1,2–dihydroxyanthraquinone, was extracted from the roots of the Madder plant, *Rubia tinctorum* and in conjunction with a metal salt could give rise to shades of red, pink, and brown (Figure 1.11) – the resulting colour a consequence of chelation (Latin *chela*, "crab's claw") with the metals Al, Sn and Fe, respectively. Even at the time, the importance of the constituents was known, although the specific way they interacted or were arranged was not.

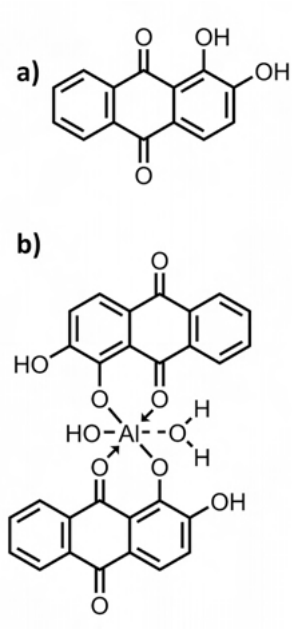

Figure 1.11. a) Protonated form of 1,2–dihydroxyanthraquinone, i.e. Alizarin. b) Alizarin coordinated to Al, resulting in a crimson-coloured complex.

This continued to be the case well into the 18th century: coordination complexes were discovered sporadically, typically on accident (and many likely went unreported despite being used). On the higher energy end of the spectrum, the accidental discovery of Prussian Blue by German manufacturer Diesbach in 1704 is notable, especially since it presents one of the first examples of a coordination complex possessing transition-metal–carbon bonds[5], even if the fact was delineated over two centuries later. We skip another century – and some intermediary findings – to mention the work of Gmelin[6], to whom the discovery of several double salts such as ferricyanides and cobalticyanides is credited[7]. It was only in 1856 that the first extensive, systematic study of coordination compounds appeared, however: a series of Co(III)-ammine cations (*e.g.* $[Co^{III}(NH_3)_6]X_3$, $[Co^{III}(NH_3)_5Cl]X_2$ etc. – here modern nomenclature is used for clarity) was characterized in detail by Gibbs and Genth[8] – and several of them would assume centre stage in the founding of modern coordination theory. Indeed, during the latter half of the 19th century, understanding the structure of such – at the time referred to as – 'molecular compounds' was a substantial challenge and a central question in the theory of chemical bonding. In fact, the lack of clarity on how such entities were held together is exactly what earned them the moniker, 'complex'.

Swiss chemist Alfred Werner was a 26 year-old unsalaried docent when he found an answer to this problem. It came to him in a dream at 2 AM, and he

woke up and wrote without pause until evening the next day, resulting in his seminal publication in 1893[9]. Therein, he proposed without any experimental proof of his own, the concepts of primary and secondary valence, and the octahedral arrangement of the primary coordination sphere of the central metal atom. This was considered as one unit, whose net charge was neutralized by the (ionizable) secondary valence. He also criticized the 'choo-choo train' chain theory of Scandinavian pair Blomstrand–Jørgensen[e], well accepted at the time, which successfully explained the behaviour of cobalt-ammines based on structures as shown to the left of Figure 1.12.

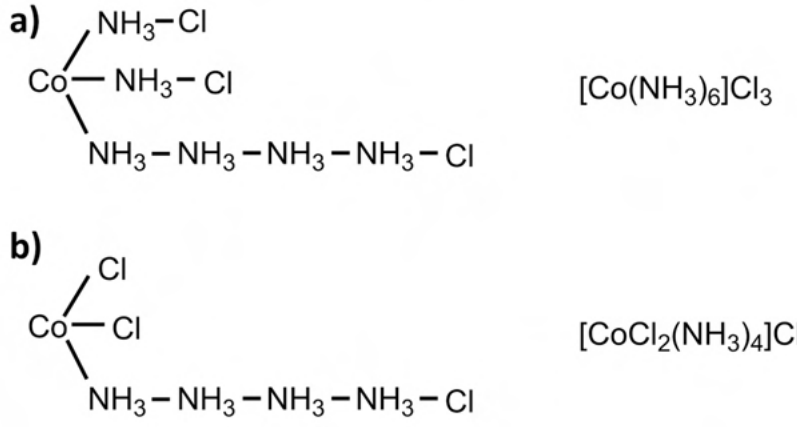

Figure 1.12. Structures of Cobalt-ammines as proposed by Blomstrand–Jørgensen and Werner, left and right, respectively. a: Cobalt hexaammine, and b: Cobalt tetraammine.

To modern eyes, the Blomstrand–Jørgensen structures appear immediately unphysical, not the least due to the pentavalent nitrogen. However, put in the perspective of those times, they were reasonable: the chemistry of carbon compounds was far more extensively studied, and a nitrogen with valence five arranging itself in chains – in analogy to tetravalent carbon – was not regarded as unusual. The theory was simple: groups directly bound, i.e. 'nearer' to the metal were difficult to release, while those further away could be easily ionized. As is evident from Figure 1.12, the structures from both theories predicted the same number of ions (and free chlorides) for both Cobalt hexa- and tetraammines, easily verified by conductivity measurements and precipitation with silver salts. They were thus equally likely, and Werner's ideas were more radical.

[e] Christian Wilhelm Blomstrand (1826 – 1897) was a Professor at Lund University, and initially proposed the theory; Sophus Mads Jørgensen (1837 – 1914), Professor at University of Copenhagen, was eleven years his junior, and his good friend. He was the one to meticulously apply the theory to a large number of complexes and became its primary proponent – as well as Werner's principal adversary.

The battle began to swing in Werner's favour with triammines, where the two theories predicted different number of ions, as seen in Figure 1.13. In 1893–1894, together with former student Miolati, Werner could confirm by a series of conductance measurements on ammines (including nitro-complexes) that they were in accord with his theory for all considered complexes, and that the solution had a conductivity close to zero for the triammine in particular. Sympathizers should like to declare at this point Werner's theory had triumphed, but this was far from the case.

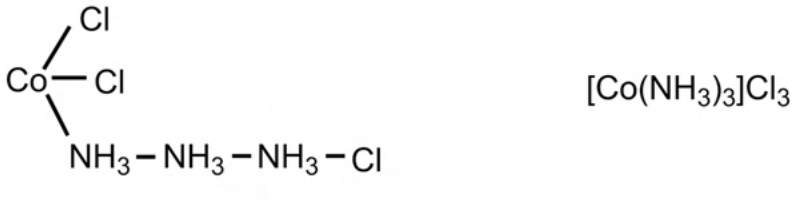

Figure 1.13. Structures of Cobalt-triammines as proposed by Blomstrand–Jørgensen and Werner, left and right, respectively. The former should result in two ions, while the latter in none.

A coordination of six around the metal does not imply an octahedral arrangement *apriori*, and three other possibilities exist: trigonal prismatic, hexagonal pyramidal, and hexagonal planar (the third one could well be considered a special case of the second). In order to decisively established the octahedron, Werner needed to rely on the technique of 'isomer counting' – the different arrangement would give rise to different numbers of optical isomers, i.e. bend polarized light differently[f]. Challenges were met in the form of unstable isomers which could not be isolated (Werner was thus criticized for postulating structures which did not exist). At the same time, if another arrangement (say trigonal prismatic) predicted an extra isomer which could not be isolated, its existence was not precluded.

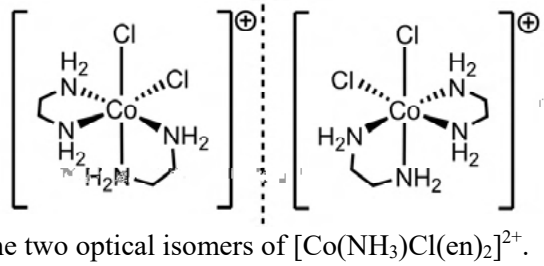

Figure 1.14. The two optical isomers of $[Co(NH_3)Cl(en)_2]^{2+}$.

[f] Isomer counting as a technique was known since the 1870s to van't Hoff and Le Bel – the history of optical activity, starting from the late 17th century discovery of polarized light by Huygens is a very interesting one, but beyond the scope of this text.

It therefore took nearly two decades for Werner to find decisive proof, which came in the form of the successful preparation and optical resolution of cis-amminechlorobis(ethylenediamine)Co(III) salts (see Figure 1.14) in 1911, with the help of his American PhD student Victor L. King. Two years later, Werner became the first inorganic chemist to win the Nobel Prize. Interestingly, a few skeptics still remained, who believed that the chirality was due to the organic ligand (although ethylene diamine by itself was shown to be optically inactive). The last of Werner's critics were silenced by the optical resolution of the entirely 'inorganic' tris[tetraammine-μ-dihydroxocobalt(III)]Cobalt(III)bromide in 1914 – a compound, poetically enough, first prepared by Jørgensen. A new era had finally dawned, and coordination chemistry flourished.

Much of the interest in coordination complexes in the late 19th and early 20th century had to do with their use as dyes, redox indicators, and importantly, as sensitive colorimeters, clearly seen in the survey published by Morgan and Burstall in 1936[10]. Colorimetry, of course, was made possible by the synthesis of novel organic ligands – chelates – that could bind to biologically relevant metals of interest such as Fe and produce an intense colour, serving as both qualitative and quantitative probe for the analysis of samples. Fritz Blau must be mentioned, the first to report the synthesis of 2,2'–bipyridine (bpy) in 1888[11,12]. Already then, he had noted an intense red colour upon addition of $FeSO_4$, but went into no further details. A year later he confirmed the finding[13], but it was only a decade hence, in 1898, that he formally reported the characteristics of $[Fe(bpy)_3]^{2+}$, describing its structure in accord with Werner's formulation[14]. This was confirmed by Werner himself[15] in 1912, by resolution of its isomers (this was somewhat non-trivial as the system racemized easily).

It is useful at this stage to take a macro-view of the extant scientific climate at the time (to the late 1930s), which is impossible to document in detail, owing to both the rapidity and variety of findings. Two years after Werner's demise, in 1921, Wyckoff and Posnjak using X-ray diffraction published the crystal structure of $[PtCl_6](NH_4)_2$ and found a perfect octahedron[16]. In 1922, Dickinson[17] could likewise confirm Werner's prediction of the planar structure for Pt(II). In hindsight, one can wonder how much easier the acceptance of theory would have been, were the method readily available!

Contemporary developments at the time also included a more complete theoretical understanding of chemical bonding thanks to Pauling, Lewis, Mulliken, Hund, Condon, Slater, among others. The foundations of quantum mechanics were laid in tandem, where the observation of distinct atomic spectral lines forced a reconsideration of classical views of continuous energies. Electronic structure, and its consequences, became tractable. Some relevant details of these matters are reviewed in Chapter 2.

1.2 Photophysics of Transition-Metal Complexes

Advances outlined in the previous section meant that the time was ripe for a shift to queries of a more fundamental photophysical character: the first electronic absorption spectrum of $[Fe(bpy)_3]^{2+}$ was reported by Yamasaki in 1937[18]. While in the decades to follow $[Ru(bpy)_3]^{2+}$ would play a pivotal role in the development of the photophysics and photochemistry of coordination compounds, its synthesis was reported by Burstall only in 1936[19], and its absorption spectrum was not published until 1954[20]. The authors note in the very first sentence, "*The accumulation of considerable information on the Fe(II) complexes with 2,2'-bipyridine made the investigation of the corresponding ruthenium system seem desirable, especially in view of the similarity of the coordination chemistry of the two metals.*"

One can speculate why – rightfully christened by Wenger[21] – the fruit-fly of photophysics trailed behind, and the reason could have been as simple as the biological irrelevance of Ruthenium, coupled with its scarcity. The sophistication of the instrumentation available was of course a general limitation. In this regard, the advent of pulsed light sources – particularly the laser in 1960 – can be considered a milestone, without which the detailed study of excited state dynamics, and consequently an understanding of their reactivity, would not be possible. We return to this matter shortly. Meanwhile, it would be remiss to not mention that the very first laser was based on the crystal Ruby, which is nothing but Cr^{3+} ions doped in Al_2O_3.

Returning to the matter of electronic structure, transition-metal complexes (TMCs) are colourful, i.e. they absorb visible light (more broadly, they absorb from the UV to the near infrared, ca. 200 to 1100 nm). Visible photons pack around 170 to 300 kJ/mol of energy, and their absorption by a complex leads to a rearrangement in its electronic structure, and it is said to be in an (electronically) excited state. It is these *electronic transitions* which dominate the absorption spectra of TMCs. $[Fe(bpy)_3]^{2+}$ and $[Ru(bpy)_3]^{2+}$, for instance, are the colour of red wine and whiskey, respectively, when dissolved in a solvent such as water or acetonitrile. This translates to absorption maxima of ca. 520 nm and 450 nm in the visible: absorption spectra are a quantitative measure of what we see (or don't) with our eyes. A unique feature of TMCs is the variety of electronic states, and consequently, transitions available[g], oftentimes due to the presence of partially filled orbitals on the metal or empty orbitals on the ligand. As an example, the transition responsible for the colour of $[Ru(bpy)_3]^{2+}$ or $[Fe(bpy)_3]^{2+}$ is entirely different than the one which

[g] See 2.1 for details; for the purpose of this discussion, however, it is sufficient to think of the complex's orbitals as comprised of those based on the metal, and those on the ligand

underlies the emission of the Ruby laser mentioned previously. The former is a so-called (metal-to-ligand) charge-transfer (MLCT) transition, characterized by the movement of an electron from a primarily metal-based to ligand-based orbital; the latter on the other hand is a ligand-field transition: the electron moves from one metal-based orbital to another (see Figure 3.11 for a representative illustration). The transitions which characterize their emissions (if any), likewise involve different electronic states.

This complexity of electronic structure meant that coordination complexes were once again at the forefront of the application and refinement of electronic theory[22,23]: the molecular orbital approach was first applied to TMCs in 1952; correlation diagrams which tracked the energies of various electronic states were published by Tanabe and Sugano in 1954[24,25], and remain an invaluable tool in the analysis of spectra even today. Needless to say, the rich landscape of electronic states presents a myriad of possibilities from both a perspective of fundamental understanding and practical use.

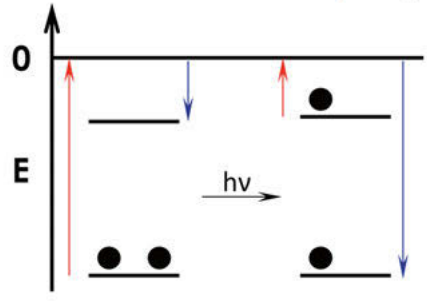

Figure 1.21. A molecular orbital picture of why the excited state is a better oxidant and reductant. Ground state on the left, excited state on the right. The red arrows indicate ionization potential, while the dark blue arrows indicate electron affinity. '0' indicates continuum, or the electron in vacuum.

Given the altered electronic structure, the excited state can be regarded as a distinct species – it is more energetic, and is a more potent oxidant and reductant, which can be simply visualized in Figure 1.21. Excited states are transient species, and several pathways may allow them to shed their excess energy in order to return to the ground state. The principle two are radiative (emission of a photon) and non-radiative decay. The latter is vibrational in character, and is called intersystem crossing when accompanied by a change in spin, otherwise called internal conversion. The importance of knowing the timescales of occurrence of these processes is made evident by once again considering the cases of congeners $[Fe(bpy)_3]^{2+}$ and $[Ru(bpy)_3]^{2+}$.

The luminescence spectrum of $[Ru(bpy)_3]^{2+}$ was reported in 1959 by Brandt[26], and the corresponding spectrum for the iron analogue does not exist. This is not due to a lack of measurement – the complex does not emit. Furthermore,

$[Ru(bpy)_3]^{2+}$ finds extensive use as a photosensitizer, the first quenching experiments demonstrating its photochemical activity having been conducted by Balzani and co-workers, as well as Meyer and co-workers in 1974[27,28]. Such is not true for the iron counterpart. The two are isoelectronic (d^6 configuration) and superficially isostructural[29] (bite angles and M–N bond lengths are not drastically different, although the bond lengths for $[Fe(bpy)_3]^{2+}$ are around 5% shorter: 78.8±0.5° / 2.064 Å for Ru, and 81.8±0.6° / 1.961 Å for Fe), so the observed difference cannot be explained by these metrics alone. On the other hand, the difference is immediately unravelled upon a consideration of the state energetics and dynamics, which are summarized in Figure 1.22 (this picture was built on, cumulatively, several decades of steady-state and time-resolved spectroscopic measurements26,[31–39], some of them conducted – and still debated – as late as 2014-15[40,41], and work still continues[42,43]).

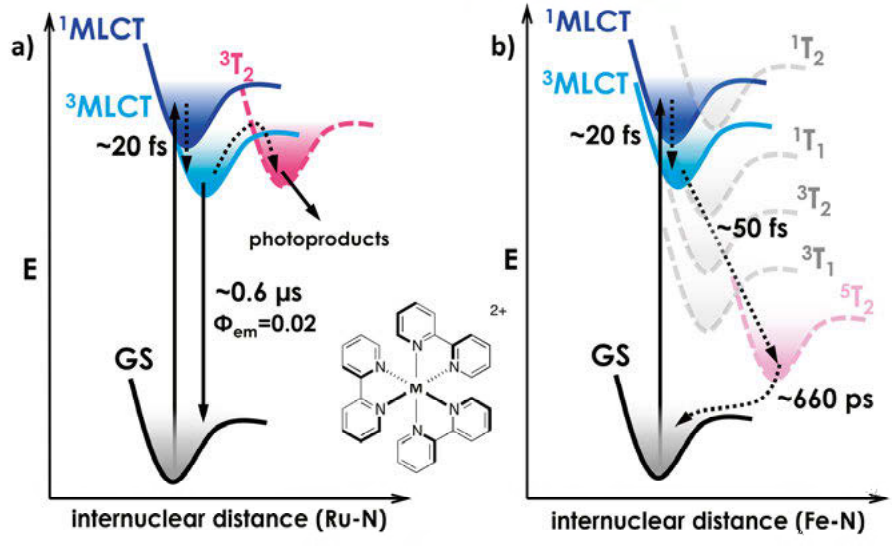

Figure 1.22. State energetics for the isoelectronic, and geometrically isostructural oligopyridyl complexes, **a:** $[Ru(bpy)_3]^{2+}$ and **b:** $[Fe(bpy)_3]^{2+}$, where bpy = 2,2'–bipyridine. Note that the exact cascade in **b** is disputed; here the picture suggested from ref 26 is drawn.

Excitation into the MLCT bands of both complexes results in the population of the ^{1}MLCT state, which then undergoes rapid intersystem crossing on the timescale of 20–40 fs to the ^{3}MLCT state. In $[Ru(bpy)_3]^{2+}$, the ^{3}MLCT is the lowest lying excited state – the thermalized state delocalized over the three bpy ligands[44] – which is luminescent and proceeds to decay with a lifetime of ca. 0.6 µs in room temperature solution. Although some 0.5 eV is lost during the intersystem crossing process, the ^{3}MLCT is still rather energetic (2.1 eV), and has a long enough lifetime to allow for bimolecular reactivity in the solution phase. By contrast, in $[Fe(bpy)_3]^{2+}$, the lowest lying state is the metal-centred quintet state, $^5T_2$, which is populated from the ^{3}MLCT on a sub-

picosecond timescale. This state deactivates with a lifetime of around 660 picoseconds – even if one may consider this just enough for reactivity using rather high quencher concentrations, the fact remains that it is too low in energy (0.6 to 0.8 eV) for most photochemical applications, although some recent reports exist[45,46]. Thus, as expected from the identical electronic configurations, the available electronic states in both systems are the same, but their energetic ordering is very different. The concepts illustrated here are applicable for polypyridyl complexes of the first-row generally, compared to their heavier counterparts from the second and third rows, thus precluding their use as photosensitizers or light harvesters of any merit. Recent developments, however, have begun to see this paradigm slowly shift[47–50].

At this stage, it is right to ask ourselves *why* – despite being nearly isostructural in the ground state and possessing the same ligand set – are the metal-centred state energies so different in $[Fe(bpy)_3]^{2+}$? The answer lies, coarsely put, in the proximity of the 3d orbitals to the metal[51] – the ligands must approach far closer to achieve a good orbital overlap, but this is not possible due to electronic repulsion. They are thus pre-disposed to experiencing a smaller ligand-field compared to 4d and 5d metals, and low-lying metal-centred states result. Armed with all this information, we are in a position to approach the central premise of this thesis.

1.21 Objectives and Motivation

A natural question emerges from the discussion above: is it possible to achieve the energetic paradigm of a 4d or 5d metal with a 3d one? Put differently, can we generate long-lived, energetic charge-transfer states with first-row transition metal complexes? Can the proverbial torch exchange hands once again from Ru to Fe? Clearly, the metals themselves cannot be changed, so the effort must be directed towards a different design of the ligand framework, if such an outcome is to be achieved. This thesis explores one such strategy, which utilizes N-heterocyclic carbene ligands in a unique tripodal – *scorpionate* – motif in conjunction with 3d metals Mn, Fe, and Co. The general structure of the complex can be seen in Figure 1.23. Throughout the text, we will refer to it as $[M^xL_2]^{n+}$ (where M=Mn, Fe, or Co, x is the oxidation state of the metal, and L=[phenyl(tris(3-methylimidazol-1-ylidene))borate]$^-$. Sometimes, we will also use the shorthand M-carbene or M-NHC, where M is the metal, but only when it precludes any confusion.

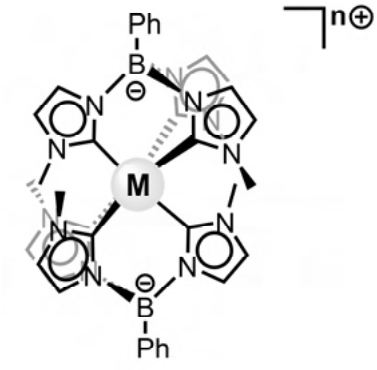

Figure 1.23. General structure of the complex(es) investigated in this thesis (apart from Chapter 7), $[M^xL_2]^{n+}$. M=metal, x=oxidation state of the metal, and n=charge of the complex. L=[phenyl(tris(3-methylimidazol-1-ylidene))borate]$^-$, which is the tridentate Scorpionate ligand.

Should the answer to the aforementioned questions be a positive one – and we mildly spoil the reader by saying yes – then several corollaries emerge: what are the energetics and dynamics of these excited states? What is their reactivity? How is the structural and dynamic paradigm in these complexes similar or different from the ones already studied?

Finally, the motivation for answering such questions can be twofold. To begin with, there is the matter of fundamental photophysical insight: not only was a mechanistic understanding of the underlying photophysics of transition-metal complexes useful to explain their behaviour, it altered the dogma established from organic photophysics regarding the timescales of processes. For a large suite of organic chromophores, vibrational relaxation always occurs first, followed by internal conversion, and finally intersystem crossing. This is hardly the case for metal polypyridyls, however, where any generality seems a luxury[52]. Thus, as always, with this new class of complexes comes the possibility of unforeseen photophysics. The second motivation can admit of a social context[h]: several first-row metals are orders of magnitude more abundant than rare metals such as Ru and Ir, and can also be relatively non-toxic. The realization of first-row based excited states with similar or better properties, enabling them, for e.g., to harvest sunlight, can thus be thought to contribute towards a more sustainable future.

[h] whether one considers it philosophically tenable is another matter entirely.

2. Fundamentals of Molecular Photophysics

The universe is an enormous direct product of representations of symmetry groups.

– Steven Weinberg

We refresh here some key theoretical concepts that are used in the chapters that follow. Nothing new is presented, per se, and the treatment is essential and far from exhaustive. It takes inspiration from well-known texts on quantum mechanics[53,54], physical inorganic chemistry[55,56] and molecular photophysics[57] – the reader is directed there for any missed details or clarifications.

2.1 The Theoretical Minimum

The electronic structure of matter cannot be explained by classical theories of physics. One must instead use quantum theory, the core axiom of which is Schrödinger's equation (here it is written in one dimension, but can be generalized to three):

$$-\frac{\hbar}{i}\frac{\partial \boldsymbol{\Psi}(x,t)}{\partial t} = -\frac{\hbar^2}{2m}\frac{\partial^2 \boldsymbol{\Psi}(x,t)}{\partial x^2} + V\boldsymbol{\Psi}(x,t) \tag{2.1}$$

$\hbar$ is the reduced Planck's constant, m is the mass of the particle, and V is the potential energy function (that does not depend on time). $\boldsymbol{\Psi}$ is the particle's *wavefunction* – which in principle contains all information about the particle – and what we try to solve for. Visual inspection suggests we may look for solutions of the form $\boldsymbol{\Psi}(x,t) = f(t)\psi(x)$. If we take this expression and differentiate with respect to time and twice with respect to position, we get:

$$\frac{\partial \boldsymbol{\Psi}(x,t)}{\partial t} = \frac{df(t)}{dt}\psi(x) \; and \; \frac{\partial^2 \boldsymbol{\Psi}(x,t)}{\partial x^2} = \frac{d^2\psi(x)}{dx^2}f(t)$$

Substituting these equations into 2.1 yields:

$$-\frac{\hbar}{i}\frac{1}{f(t)}\frac{df(t)}{dt} = -\frac{\hbar^2}{2m}\frac{1}{\psi(x)}\frac{d^2\psi(x)}{dx^2} + V(x) \tag{2.2}$$

We can observe that the left-hand side of 2.2 is exclusively a function of t, while the right-hand side is a function x: we can therefore set both sides equal to an arbitrary constant, 'E', and solve. The solution of the left-hand side gives us the time-dependence of the wavefunction:

$$-\frac{\hbar}{i}\frac{1}{f(t)}\frac{df(t)}{dt} = E;\ f(t) = Ae^{-iEt/\hbar} \tag{2.3}$$

The right-hand side gives us the *time-independent* Schrödinger's equation:

$$\left[-\frac{\hbar^2}{2m}\frac{d^2}{dx^2} + V(x)\right]\psi(x) = E\psi(x) \tag{2.4}$$

In principle, multiplying $\psi(x)$ with 2.3 can give us a general solution which maps the evolution of the wavefunction in space and time. The correspondence of the term in brackets with the classical Hamiltonian, $\frac{{p_x}^2}{2m} + V(x)$, is immediately evident. 2.4 is therefore often written as:

$$\widehat{\boldsymbol{H}}\psi = E\psi \tag{2.5}$$

where $\widehat{\boldsymbol{H}}$ is the Hamiltonian. The correspondence between physical quantities in classical mechanics and operators in quantum mechanics is general, and *every physical observable has a corresponding operator*. In order to obtain $\psi(x)$ from 2.4, we need $V(x)$ and this is determined by the problem of interest. Unfortunately, 2.4 is only exactly analytically solvable for very few systems (types of $V(x)$). *Fortunately*, these simple potentials (such as $V(x) = 0$ for a free particle, or a Hooke's law style potential, $V(x) = {}^1\!/_2\, kx^2$ for the harmonic oscillator, etc.) are sufficient to model a lot of physically interesting problems.

One such solvable problem is that of the one-electron atom, where $V(x)$ takes the form of the spherically symmetric Coulomb potential, $-\left({}^{Z|e|^2}\!/_x\right)$. Z is atomic number, e is the electronic charge and x is the distance from the nucleus. The solution wavefunction gives rise to the three quantum numbers n, l, and m. It is a product function consisting of a radial part which determines the distance of the electron from the nucleus and an angular part (spherical harmonics) which decides how it is positioned with respect to the nucleus. The latter is what gives the 'shapes' of atomic orbitals. It was not mentioned thus far, but the actual probability of finding a particle (or in this case, the electron) will be given not by the wavefunction itself. Rather it is determined by its product with its complex conjugate, i.e. $|\psi(x)|^2$, termed the probability density. This is plotted for the 3d orbitals in Figure 2.11.

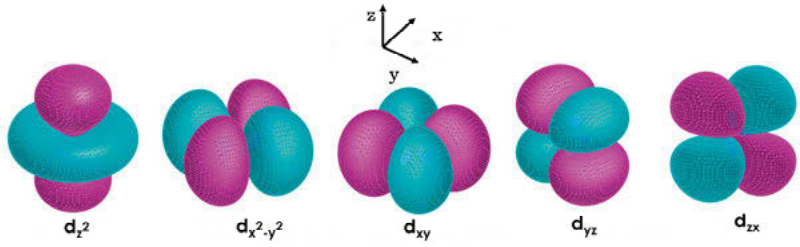

Figure 2.11. Shapes of the 3d orbitals as obtained by plotting the probability density obtained for the solutions of the Schrödinger equation for hydrogenic atoms.

Our approximation of the shape also holds up reasonably well in a multielectron system (surprisingly enough!). So what is the fate of the 3d-orbitals in a typical octahedral[i] transition metal complex? Crystal-field theory (CFT) offers a first explanation from a purely electrostatic point of view. If the ligands are thought of as negative point charges surrounding the central metal atom, we can see that the d_{z^2} and $d_{x^2-y^2}$ orbitals which point along the axis will experience greater repulsion. Accordingly, under the influence of the ligand's field orbital degeneracy will be lifted as illustrated in Figure 2.12. Δ_o is the crystal-field splitting parameter for the octahedral case; d_{z^2} and $d_{x^2-y^2}$ are *destabilized* by $\frac{2}{5}\Delta_o$ and d_{xy}, d_{yz}, d_{xz} are *stabilized* by $\frac{3}{5}\Delta_o$.

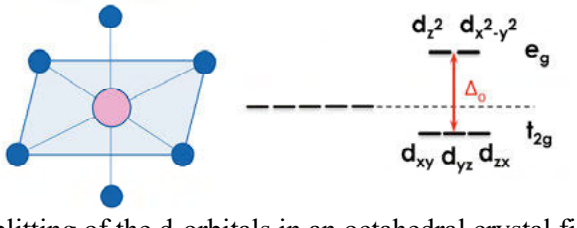

Figure 2.12. Splitting of the d-orbitals in an octahedral crystal field.

Ligands may be classified as 'strong' or 'weak' field depending on the magnitude of Δ_o, with those generating a larger splitting labeled as strong-field. After the third electron is added, there is a choice to pair-up or to fill an empty orbital which is at higher energy (but is favorable from the point of view of Hund's rule of maximum multiplicity). What happens is determined by Δ_o: if it is larger than the energetic cost of pairing up electrons (pairing energy), then the fourth electron would rather pair-up. If it is smaller, then the electron will go to a higher energy d-orbital. Accordingly, strong-field ligands with large values of Δ_o favour low-spin complexes, while weak-field ligands result in high-spin complexes. A concept called 'spectro-electrochemical series' exists,

[i] there are of course other geometries of complexes, but we restrict ourselves to the octahedral / pseudo-octahedral case here

where the ligands are arranged according to their field-strength, and a partial one is shown below:

$I^- < Br^- < SCN^-$ (S–bonded) $< Cl^- < NO_3^- < F^- < OH^- < C_2O_4^{2-} < H_2O < NCS^-$ (N–bonded) < py (pyridine) < NH_3 < en (ethylenediamine) < bpy (2,2'-bipyridine) < phen (1,10-phenanthroline) < PPh_3 (Triphenylphosphine) < CN^-

The series embeds the weakness of CFT: neutral ligands such as bpy and phen generate a stronger field as opposed to the doubly-charged oxalate. A purely ionic description of bonding in TMCs is therefore inadequate, and we must consider covalency. Before we introduce a more refined theory, we take a small detour. The alert reader may have noticed that the d_z^2 and $d_{x^2-y^2}$ orbitals in Figure 2.12 carry a label called 'e_g' beside them. Likewise, d_{xy}, d_{yz}, and d_{xz} are denoted as 't_{2g}'. These are symmetry symbols which belong to group theory. In a simple way, group theory may be understood as a formal system of classifying objects according to their symmetry operations. The latter include transformations such as reflection in a plane[j], rotating about an axis, doing nothing (it's math, you see, so the 'identity' operation i.e. multiplying by '1' which changes nothing must always appear to ensure completeness…), etc.

Some core ideas are understood even without the use of formalism: for instance, we can see that rotating the axis 90° (a 'C_4' operation) can transform the d_{xy}, d_{yz} and d_{xz} orbitals into one another: they are *triply degenerate*. Hence the symbol 't'. Note that lower case will be used for orbitals, while upper case for states (t_{2g} or T_{2g}). Likewise, the e_g set is doubly degenerate (though this is not as simple to visualize – but we can at least see that changing the axis labels can 'mix' the two orbitals). A character table of a given 'point group' tells us how an orbital with a given symmetry symbol transforms under different symmetry operations. For instance, the character table for the octahedral point group collects *all* its symmetry operations, and the aforementioned symmetry symbols are found there.

For our purposes, without getting into details, the important point from the context of molecular orbital (MO) theory is that only ligand and metal orbitals with the *same symmetry properties* may interact to generate molecular orbitals. This gives rise to MO diagrams, which are illustrated in Figure 2.13 for an octahedral complex. In the MO perspective, one can rationalize larger field splittings for ligands such as bpy, for instance, by noting that ligand π orbitals (depending on their energy) can interact with the metal t_{2g} orbitals and stabilize them. Similarly, ligand σ orbitals influence the field-splitting by changing the energy of the e_g* orbitals.

[j] Note the corresponding symmetry *elements* which are mirror planes, axes of rotation etc.

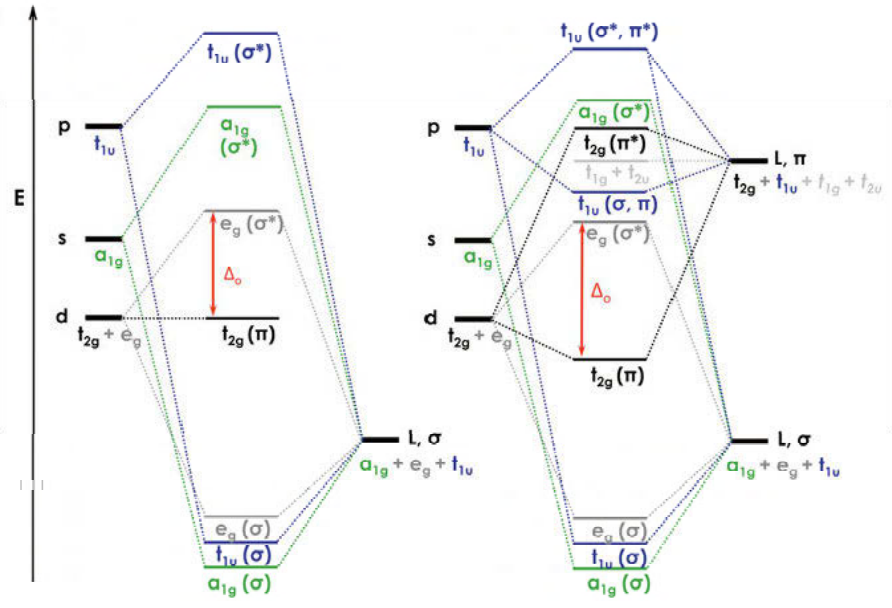

Figure 2.13. Molecular orbital diagrams for an octahedral complex. *Left:* For ligands which do not possess π orbitals or do not have substantial π interactions. *Right:* Showing both ligand σ and π interactions.

We can draw a generic and simplified MO diagram in order to illustrate the many transitions we mentioned in the introductory chapter. These include metal-to-ligand charge transfer (MLCT), ligand-to-metal charge transfer (LMCT), ligand-centred (LC), and metal-centred (MC) transitions.

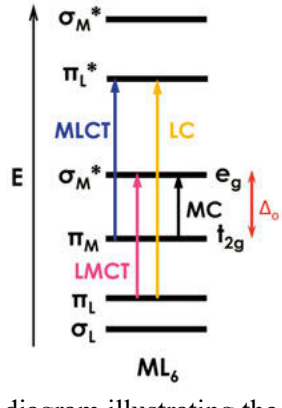

Figure 2.14. Generic MO diagram illustrating the several types of transitions possible in an octahedral complex. See text for details. Figure concept from ref 56.

We bring this section to a close by mentioning one more handy tool: the Tanabe-Sugano (TS) diagram. These diagrams can be made for different d-

electron configurations, and track the energies of the different electronic states available as a function of Δ_o. One for a d^3 electron configuration is illustrated in Figure 2.15. The abscissa is the ground term, which is arbitrarily set to zero energy; B is a Racah parameter (there are also Racah parameters A and C, but they are typically less important) which accounts for electron repulsion. An important point to bear in mind is that a lot of TS diagrams will be plotted with some arbitrary C/B value (the one shown has a C/B = 4.5), while in reality B will be different for every complex, so the relative energies will be different as well. Nevertheless, a generic TS diagram is still an excellent qualitative guide. In a crystal-field approach, B can be taken as the free-ion value obtained from atomic spectral data. However, it has been found that metal complexes will typically have a smaller B value than that of the free-ion (usually obtained as a fit parameter). We once again see the consequence of covalency: the electrons are in fact delocalized over the ligands, and the effective charge on the metal is also reduced, resulting in a lowered B value than from a purely ionic perspective.

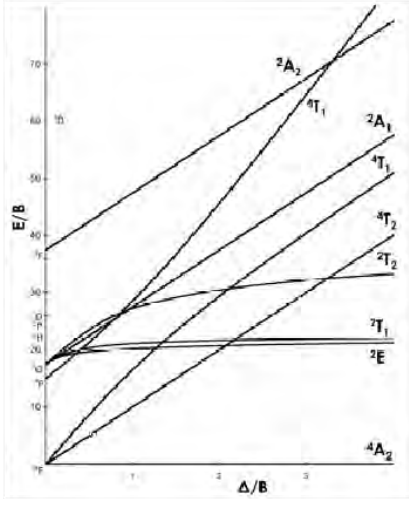

Figure 2.15. Tanabe-Sugano diagram for a d^3 electron configuration. See text for details.

A few more caveats are good to note[58]: TS diagrams do not feature charge-transfer states, and the excited state energies are determined at the ground state geometry (but excited states will typically feature some distortion). If the complex is not perfectly octahedral, then degeneracy will be further lifted, resulting in more terms.

2.2 Transitions

The electronic transitions between different molecular orbitals that we have illustrated towards the end of the previous section (Figure 2.14) are a consequence of the radiation field coupling two quantum states. In fact, the most general descriptor (at least for weakly coupled systems) of the transition

probability between two quantum states is the 'golden rule', obtained using Schrödinger's equation and time-dependent perturbation theory:

$$P_{i\to f} = \frac{2\pi}{\hbar}|\boldsymbol{V}|^2\rho(E_f) \tag{2.6}$$

P is the transition probability per unit time between initial state, *i*, and final state, *f*, and $\boldsymbol{V}$ is the coupling between the two states (note this is not to be confused with the potential energy function we have discussed in section 2.1). $\rho(E_f)$ is the density of states at the energy of the final state, E_f. $\boldsymbol{V}$ takes the form of the transition matrix element:

$$V \equiv \langle f|\mathbf{H}'|i\rangle \tag{2.7}$$

Which is shorthand for $\int \Psi_f{}^*\mathbf{H}'\Psi_i d\tau$ and $\mathbf{H}'$ is the interaction Hamiltonian. When we consider radiative transitions, 2.6 is modified slightly in that a photon is exchanged with the radiation field – absorption (supplied from the field) and stimulated emission (taken up by the field)[k]. The density of states is rather the mode density of electromagnetic waves in space; but the essential point is that of the transition rate depending on the *square of the matrix element*. $\mathbf{H}'$ takes the form of the dipole moment operator, $\boldsymbol{\mu} = e.\boldsymbol{r}$ and the matrix element is $\langle\Psi_f|\boldsymbol{\mu}|\Psi_i\rangle$, also called the transition moment. The latter must be totally symmetric in order to be non-zero, and results in *selection rules* for transitions, such as those between d-orbitals in an octahedral complex being formally forbidden by symmetry[l]. We may apply the Born-Oppenheimer approximation, which allows for a separation of the wavefunction into nuclear (φ) and electronic (ψ) parts:

$$\langle\psi_f|\langle\varphi_f|\boldsymbol{\mu}|\varphi_i\rangle|\psi_i\rangle \tag{2.8}$$

And the more restrictive Condon approximation, that considers the dipole operator acts only on the electronic part, which allows us to write:

$$\langle\psi_f|\boldsymbol{\mu}|\psi_i\rangle\langle\varphi_f|\varphi_i\rangle \tag{2.9}$$

[k] spontaneous emission is a bit trickier in that vacuum fluctuations of the field constitute the perturbation; but we stick with a handwavy approach in the interest of brevity

[l] octahedral complexes have something called a 'centre of inversion': if you translate each point through the centre the same distance on the other side, you obtain the same shape. the d-orbitals are 'gerade' i.e. symmetric with respect to the inversion centre, hence the 'g' subscript in the symmetry label. g x g = g and the dipole operator has u (ungerade, antisymmetric) symmetry, giving an anti-symmetric product in the integral: g x g x u = u, making it zero. So *why* do we see these transitions at all? Because the rules are meant to be broken, of course. Vibrations of appropriate symmetry can mix a forbidden state with an allowed one, resulting in some intensity stealing – formally this is a breakdown of the Born-Oppenheimer approximation.

$\langle \varphi_f | \varphi_i \rangle^2$ are the Franck-Condon factors, and hence the principle essentially states that the most probable transitions occur between states which maximize the vibrational overlap. The situation is illustrated in Figure 2.21. The vibrational wavefunctions may be obtained by solving the time-independent Schrödinger equation for potential function of a mass tied to the end of a spring, as mentioned previously. Note that a closer approximation of a real system is a Morse potential, and the density of states will get much larger at the higher energy levels.

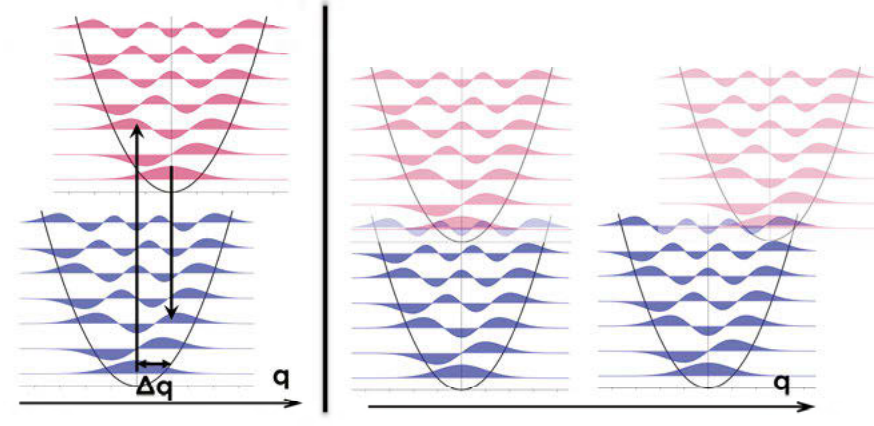

Figure 2.21. Potential energy surfaces with possible transitions; blue is the ground state, red is the excited state. *Left:* Vertical transitions corresponding to absorption and emission (solid arrows), showing how transitions which maximize vibrational wavefunction overlap are favored, in accord with the Condon approximation. Δq is the displacement of the excited state minimum with respect to the ground state. *Right:* Non-radiative transitions (not illustrated by arrows but should occur horizontally) between differently distorted excited states and the ground state.

Finally, we can make a further approximation where we separate the electronic part into a one-electron wavefunction (orbital, θ) and a spin part (S), to obtain:

$$\langle \theta_f | \boldsymbol{\mu} | \theta_i \rangle \langle S_f | S_i \rangle \langle \varphi_f | \varphi_i \rangle \tag{2.10}$$

We can therefore view the transition probability in terms of the squares of these three matrix elements: the electronic transition moment, contingent on orbital overlap and symmetry, the spin integral which accounts for change in spin between the states (if any), and the vibrational overlap, i.e. the Franck-Condon factors just described. By portioning the electronic part, we see that transitions which will involve a spin-change are formally forbidden. On the other hand, much like for symmetry-forbidden transitions, in this case, spin-orbit coupling (particularly for metals which are heavy) can make these

transitions allowed. It is convenient, perhaps, to look at the situation in kinetic terms as the final observed rate constant being a function of these three 'retardation' factors:

$$k_{obs} = k_0 \times f_e f_s f_v \tag{2.11}$$

where k_{obs} is the observed rate constant, and k_0 is the hypothetical maximally allowed rate constant (10^{15}–10^{16} s^{-1}), and f_e, f_s, and f_v are the electronic, spin, and nuclear retardation factors, respectively.

For the case of non-radiative transitions, it is important to note that they may only occur between states that are isoenergetic (so they are 'horizontal' transitions in that sense). Strictly speaking – of course, the solvent may act as a reservoir to take or supply energy. We can re-express the golden-rule expression, for clarity:

$$\langle \theta_f S_f | \mathbf{H}' | \theta_i S_i \rangle^2 \langle \varphi_f | \varphi_i \rangle^2 \tag{2.12}$$

Here symbols have the same meanings introduced previously. Note that in last term we should consider that there is a unique overlap integral for each vibrational mode, which we have not explicitly written for simplicity. The interaction Hamiltonian, $\mathbf{H}'$ is either $\mathbf{H_{ic}}$ or $\mathbf{H_{so}}$ for internal conversion or intersystem crossing, respectively. The latter involves a transition between states of different multiplicities. The implication of the golden-rule formulation of non-radiative rates is also illustrated in Figure 2.21.

We can see that distorted excited states may be expected to decay faster since at higher vibrational levels most of the wavefunction density is at the turning points. At the same time, nested surfaces would promote a longer excited state lifetime (not considering the radiative rate) – in that regard, the very small coupling term (which absorbs the Franck-Condon factors) at very high vibrational levels overwhelms the density of states. It is these types of considerations that have given rise to rules of thumb such as the 'energy gap law' i.e. a larger energy separation implies a slower non-radiative rate of decay. Or that emission should typically occur from the lowest vibrationally excited level of a given electronic state (Kasha's rule), since internal conversion from higher vibrational levels can be expected to be fairly fast due to the large density of states. These statements should, however, always be viewed as derivatives of the more general golden-rule treatment.

We end our admittedly simplified discussion of transitions with yet another handy tool: the Strickler-Berg equation, which may be used to estimate the radiative rate constant using experimental data. The equation may be derived by using a golden-rule style treatment to obtain the rate for stimulated absorption/emission, and then equating with rates obtained independently by

Einstein in terms of the coefficients A and B (for spontaneous and stimulated absorption/emission, respectively, $\boldsymbol{A} = \frac{8\pi h\nu^3 n^3}{c^3}\boldsymbol{B}$). This allows for recasting in terms of quantities that may be obtained in a facile way using experiment. Originally developed for organic chromophores, the expression can be expected to yield reasonable results (order of magnitude) for any spin-allowed transition.

$$k_r = {}^1/_{\tau_0} = 2.88 \times 10^{-9} n^2 \langle \tilde{\nu}_f^{-3} \rangle^{-1} \int \varepsilon(\tilde{\nu})/\tilde{\nu}\, d\tilde{\nu} \tag{2.13}$$

n is the refractive index of the solvent, $\tilde{\nu}_f$ is the emission frequency in cm^{-1}, and ε is the extinction coefficient (which is integrated over all frequencies in the last expression). The radiative rate constant, k_r, may therefore be evaluated.

2.3 Excited States: Energetics and Dynamics

Using the simple molecular orbital picture seen in Figure 1.21, we are able to see how the excited state (we label it *S) is both a better oxidant and reductant than the ground state (we label it S). If we know the potentials for oxidation and reduction of the ground state $E^o(S^+/S)$ or $E^o(S/S^-)$, together with the excited state energy, $E_{0\text{-}0}$ (i.e. the zero-point energy difference between the ground and excited state), we can estimate the excited state potentials as follows, using the Weller equation:

$$E^o(S^+/{}^*S) = E^o(S^+/S) - E_{0-0}({}^*S/S)$$
$$E^o({}^*S/S^-) = E^o(S/S^-) + E_{0-0}({}^*S/S) \tag{2.14}$$

As we saw in section 2.2, the excited state may decay radiatively or non-radiatively – the set of equations 2.14 suggest we may also utilize it for reactivity within its lifetime. Thus, the fate of this excited state may be summarized using the following kinetic equations, if no photochemistry goes on:

$$*S \xrightarrow{k_r} S + h\nu'$$
$$*S \xrightarrow{k_{nr}} S + \text{heat} \tag{2.15}$$

And the following equations may be added if reactivity is involved:

$$*S \xrightarrow{k_p} \text{products}$$
$$*S + Q \xrightarrow{k_q} S^+ + Q^- \text{ (alternatively, } S^- + Q^+)$$

(2.16)

Where we note that k_q is the *bimolecular* quenching rate constant, and therefore must be multiplied by the quencher concentration in order to convert it to a unimolecular rate constant. In principle, the excited state may be quenched by electron or energy transfer processes, but we only concern ourselves with the former in this thesis.

We can define a quantum yield for any of these processes:

$$\phi_i = \frac{k_i}{k_r + k_{nr} + k_p + k_q[Q]}$$

(2.17)

where the denominator may be re-expressed as: $k_{obs} = k_r + k_{nr} + k_p + k_q[Q] = {}^{1}/_{\tau_{obs}}$, in terms of the observed excited state lifetime. In this thesis, k_p is typically not a concern either, and the vast majority of the analysis concerns only the set of equations in 2.15. Electron transfer reactivity of the excited states is also tested using different quenchers, however, so k_q is sometimes relevant. Electron transfer quenching may proceed via dynamic or static mechanisms. The former involves diffusional encounter between an excited state and quencher molecule, resulting in the excited state's deactivation – the excited state lifetime should therefore be lowered. Static quenching involves, for instance, complexation in the ground state and therefore the lifetime of the uncomplexed population should not be affected. Accordingly, k_q (and the mechanism of quenching) is conveniently determined using the Stern-Volmer equation and conducting both steady-state and lifetime quenching experiments:

$$\frac{I_o}{I} = 1 + k_q\tau_o[Q] \text{ and } \frac{\tau_o}{\tau} = 1 + k_q\tau_o[Q]$$

(2.18)

Here, I_o is the emission intensity at a given wavelength (typically the maximum) in the absence of quencher, I is the emission intensity at the same wavelength in the presence of quencher concentration *[Q]*, k_q is the bimolecular quenching rate constant, and τ_o is the excited state lifetime in the absence of quencher. Therefore, a plot of $\frac{I_o}{I}$ (or $\frac{\tau_o}{\tau}$) with the quencher concentration *[Q]* can be expected to be linear with the slope equal to $k_q\tau_o$ or K_{sv}, the Stern-Volmer constant if a single quenching mechanism is operative. If the quenching process involves both static and dynamic mechanisms however, the Stern-Volmer plot for $\frac{I_o}{I}$ is parabolic instead. Then time-resolved measurements can help sift out the dynamic quenching rate constant, and the static quenching rate constant may be evaluated from the $\frac{I_o}{I}$ plot.

Since electron transfer has been mentioned, we ceremonially close this section by writing out the expression for electron transfer using Marcus theory[59]:

$$k_{el} = \frac{2\pi}{\hbar}|\mathbf{V}_{AB}|^2 \frac{1}{\sqrt{4\pi\lambda k_B T}} exp\left(-\frac{(\lambda + \Delta G^o)^2}{4\pi\lambda k_B T}\right) \tag{2.19}$$

k_{el} is the rate constant for electron transfer, $\mathbf{V}_{AB}$ is the electronic coupling between the initial and final states, λ is the reorganization energy, and ΔG^o is the total free energy change of the reaction, and the other symbols have their usual meanings. A key prediction of Marcus theory is that of the inverted region – when ΔG^o exceeds the reorganization energy, the rate of electron transfer *decreases*. The similarities with the golden-rule expressions considered above are evident: and indeed, non-radiative transitions may be treated within a Marcus-style framework, if desired[60].

2.4 Ligands

We saw in the introduction that coordination chemistry started off with the use of ligands such as Cl^-, NH_3, CN^- etc. These are the so-called classical ligands, which – again as we noted in chapter 1 – slowly gave way to modern chelating motifs, such as 2,2'-bipyridine. The variety of ligands available today is immense, ranging from cryptands to macrocycles. One popular motif is the scorpionate[61,62] and Smith has noted that the tris(pyrazolyl)borate anion is the common ancestor to all scorpionate ligands[63]. Scorpionates typically form homoleptic complexes with first-row metals, showcasing a close to octahedral geometry. Meanwhile, the past few decades have also seen utilization of *N*-heterocyclic carbenes (NHCs) as ligands[m], with their exceptional steric and electronic properties[64,65] resulting in breakthroughs in organometallic synthesis[66] and catalysis[67].

The best of both worlds is perhaps found in the relatively unique *scorpionate*-NHC[68–70], i.e. NHCs constrained to a tripodal framework. This motif was first reported by Fehlhammer in 1996[71], and a facile synthetic route was developed by Smith in 2005[70]. Later, a phenyl group was incorporated on the boron[72], resulting in [phenyl(tris(3-methylimidazol-1-ylidene))borate]$^-$ (L) – the ligand whose complexes are the subjects of the chapters that follow. By some

[m] a carbene has six valence electrons as opposed to the usual eight, and is therefore highly reactive, and must be stabilized by, for e.g. use of bulky substituents. The carbon is characterized by three sp^2 and an unhybridized p-orbital; two of the sp^2 orbitals are engaged in bonding with substituents, which leaves one sp^2 and one p-orbital available. In a singlet carbene, the former will house the lone-pair of electrons, making the carbene a strong sigma-donor; the empty p-orbital allows for π back-donation as well. NHCs, as the name implies, are carbenes which feature heterocycles containing nitrogens.

metrics[73], L is the strongest tripodal sigma-donor known. If we look at the MO diagrams in Figure 2.13, the ligand-σ orbitals can be expected to be lifted higher in energy than what is illustrated, and the e_g* set therefore substantially destabilized. This is an interesting situation to contrast with a typical polypyridyl that more prominently features π-interactions.

3. Methods

I need a weapon.

– John-117, *Halo 2*

In this section, we review the techniques employed in the following chapters for the study of electronically excited states. Since the theory behind these methods is very well documented, it is dealt with briefly, and the emphasis is instead placed on considerations that are specific to transition metal complexes when using these methods. Without due precaution, in certain cases, erroneous conclusions may be drawn: some relevant cases from current literature are surveyed to highlight the fact.

3.1 Steady-state Spectroscopy

Sample absorbance can be determined using the Bouguer-Lambert-Beer law:

$$A = \varepsilon c l = \log \frac{I_0}{I} \tag{3.1}$$

where A is the absorbance, ε is the molar decadic extinction coefficient (typically expressed in M^{-1} cm^{-1}, and a direct reflection of the transition moment), c is the concentration of the analyte (in M), and l is the absorption pathlength (in cm, for consistency of units such that the absorbance is unitless). I_0 and I are the incident and transmitted light intensity, respectively. Therefore, if ε for a given species is known, its concentration may be evaluated; conversely, a solution of known concentration may be used to determine the extinction coefficient of a given absorption band. This can already serve as a useful starting point for TMCs: as outlined in the theory section, absorptions having different electronic origins can be expected to have varying extinction coefficients, ranging from a few hundred $M^{-1}cm^{-1}$ for spin-allowed d-d bands to typically thousands for charge-transfer transitions. Figure 3.11 illustrates two typical examples. Spin-forbidden d-d bands on the other hand can sometimes have

extinction coefficient values <1 $M^{-1}cm^{-1}$ and be extremely broad and featureless, making them difficult to detect unless large concentrations or path lengths are employed. It is in any case advisable to check linearity of absorption bands with concentration – deviations can be diagnostic for chemical or physical interactions in the system, *e.g.* formation of aggregates. Finally, linear absorption is perhaps the simplest coherent spectroscopy, i.e. the field produced due to the molecular response, that determines the absorption line shape, has a fixed phase relationship with the incident light (a phase-shift of π for the signal field, in the semi-classical picture[n]).

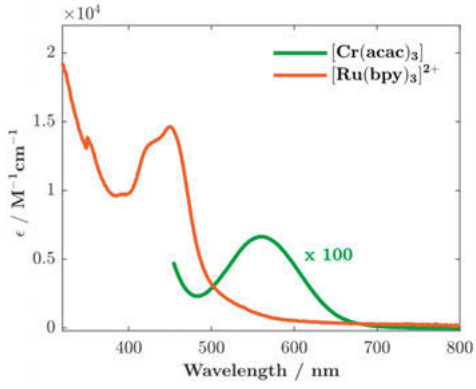

Figure 3.11. Absorption spectra of $[Ru(bpy)_3]^{2+}$ and $[Cr(acac)_3]$ (acac=acetylacetonate) recorded in acetonitrile seen in orange and green, respectively. The lowest energy bands centred at ca. 450 and 560 nm can be adjudged charge-transfer (MLCT) and metal-centred (MC, $^4A_2 \rightarrow {}^4T_2$) in character. Note the difference in extinction coefficients.

By contrast, spontaneous emission from a sample is incoherent, and unrelated to the phase of the incident light. The emission quantum yield is a useful parameter to determine:

$$\phi_x = \phi_s \times \frac{I_x}{I_s} \times \frac{A_s}{A_x} \times \frac{\eta_x}{\eta_s} \tag{3.2}$$

where ϕ_x is the quantum yield of the sample, ϕ_s is the known quantum yield of the standard, I_x and I_s are the integrated emission intensities of the sample and standard, respectively, and η_x and η_s are the respective refractive indices of the sample and standard solutions, often approximated as those of the solvents for dilution solutions. Finally, A_x and A_s are the absorbances of the sample and standard, typically kept as close as possible at the given excitation wavelength, and below 0.1 to avoid filter effects (i.e. due to absorption or trivial re-absorption of emitted light by the analyte). In some situations, high

[n] This statement must be qualified by the fact that the semi-classical view of destructive interference between the incident and signal electromagnetic field interpreted as absorption violates energy conservation in the first-order approximation; to account for the 'missing' photon, a fully quantum mechanical treatment or consideration of higher-order density matrices in the semi-classical treatment is necessary.

concentrations are unavoidable (see chapter 4), and front-face detection can be employed; use of very small path-lengths (<100 μm) is also a possibility.

Emission spectroscopy is typically a few orders of magnitude more sensitive than absorption, since it is not a difference measurement, and only limited by how low we can make the background. This makes it an excellent probe of molecular information and at the same time rather susceptible to impurities. One should be especially careful about the latter when, i) dealing with samples with low emission quantum yield[o], and ii) exciting in the blue, where several species tend to absorb, which may include photoproducts. To verify that the observed emission originates from the species of interest in the sample, it is routine practice to measure it as a function of several excitation wavelengths and confirm its invariance. Further, the excitation spectrum – i.e. scanning a range of excitation wavelengths, typically spanning the sample absorbance, while detecting at a fixed emission wavelength – should reproduce the ground state absorption line shape of the species in question (barring, e.g. Kasha-breaking behaviour, energy transfer etc.), and can usually be taken as good evidence for attributing the emission to a given band from the complex. Nevertheless, the information is not sufficient in isolation, especially for TMCs which display several transitions. For instance, a very rare case of dual (called "Janus"-type) emission from ligand-to-metal (LMCT) as well as metal-to-ligand (MLCT) has recently been reported from Fe(III)-cyclometalated complexes[74], the latter occurring from a band in the blue (<400 nm). Although the excitation spectrum matches the absorption band, it is notable that there is onset of ligand absorption in the region, and no control for the ligand emission is presented. Taken together with the low quantum yield (~10^{-4}, seeing as it is on the order of Raman bands) and nanosecond lifetime the results demand further scrutiny: indeed, a complete picture cannot be constructed without probing the excited state dynamics (*vide infra*).

3.2 Time-resolved Spectroscopy

Everything is a transient on some timescale. To truly appreciate the statement, we may consider the fact that the universe is some hundred million times older than the relatively longer-lived (ca. 100 years) specimens of the human species. As we saw in the introduction, the triplet MLCT state of $[Ru(bpy)_3]^{2+}$ has a lifetime that is around a million times greater than that of the ~100 fs of $[Fe(bpy)_3]^{2+}$, and the human lifespan is 10^{22} times longer than the latter. It is

[o] It is important to consider that (especially with increasing detector sensitivity) with large enough bandwidths and long enough integration times, nearly anything may be regarded as luminescent: a cut-off could be worthwhile.

evident that the notion of *relative* timescales is of critical importance: on the timescales of the universe we are transients, but on that of (even the longest-lived) electronically excited states, we are eternal. Philosophical exposition aside, light absorption takes place in ~1 fs – the dynamics of the excited states which result and we seek to observe are thus some of the fastest processes extant in nature. The need for such a time resolution necessitates the use of laser pulses, and ~100 fs, ~300 ps, as well as ~4 ns pulses have been used in this thesis.

Short pulse generation is achieved via mode-locking, i.e. the summing of a large number of frequencies (modes) in phase. In principle the pulse-width is only limited by the time-bandwidth product, and the broader the spectral width, the shorter the pulse: accordingly, fs pulses can be as broad as 100 nm in the visible, while ps pulses are nearly monochromatic with widths of a tenth of a nm. Longer pulses in the ns range are typically produced using Q-switching: a population inversion is allowed to build up in a non-resonant laser cavity, and a passive or active 'switch' (a Pockels cell which changes the polarization of light is an example of an active switch, while a saturable absorber is a passive one) makes the cavity resonant after an optimal build-up time (a few hundred microseconds, for most systems), allowing a single cavity mode to be amplified by the entire inverted population: the resulting ns pulse is therefore spectrally narrow.

The broadband nature of fs pulses has interesting implications: since all frequencies in the pulse envelope are in-phase, the excitation of several vibrational modes in a complex can result in the formation of a wavepacket, which can sample the potential energy surface; indeed, coherent oscillations may be analysed to identify, for example, specific decay pathways. In this thesis, however, such an analysis will not be made, and we shall restrict ourselves to monitoring population states, and not coherences. Spectrally broad pulses produce more trivial effects as well, such as group velocity dispersion, dubbed 'chirp' – a consequence of different frequencies having different propagation velocities through a medium – which must be corrected for. This is not a matter of concern for spectrally narrow excitation sources.

3.21 Transient Absorption Spectroscopy

Transient absorption (TA) or pump-probe in the UV-Visible range is perhaps one of the most used time-resolved spectroscopic techniques. The core principle across timescales is the same; a light pulse (designated pump) excites a sample and probe pulse measures absorption changes in time:

$$\Delta A = A_{pumped} - A_{unpumped} = \Delta \varepsilon c l \tag{3.3}$$

where $\Delta\varepsilon$ is the *differential* molar extinction coefficient. A few differences exist between typical fs and ns measurements: the latter can utilize a conventional white light probe source (e.g. a Xe lamp), and dynamics can be measured in real-time due to fast electronics (which can go down to a few picoseconds). To preserve the time-resolution in a fs measurement, however, fs pulses must be used to probe the sample as well – time is accounted for using an optical delay stage, which allows for the probe pulse to follow a longer path, and sub-micrometer movements can afford time-stamps down to a few fs: the total measurement is a collection of these snapshots. Given that TA probes absorption differences, it is a powerful tool to probe dark states – which as we have learned, those of many TMCs tend to be, particularly of the first-row. It is also relatively less sensitive to impurities.

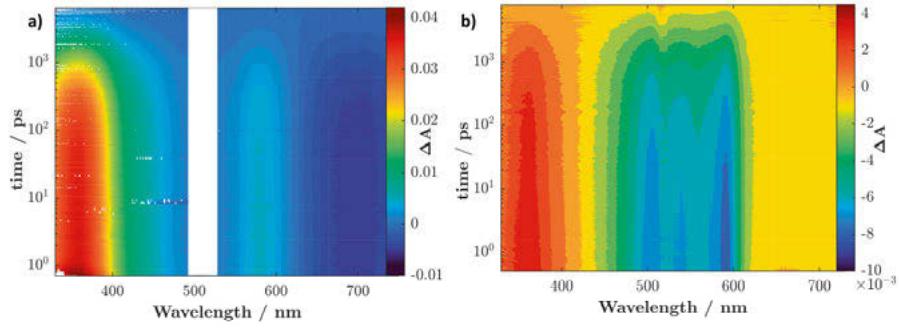

Figure 3.21. Transient absorption data for two different iron complexes, recorded in acetonitrile, after exciting into the lowest energy absorption band(s) at 500 and 520 nm. **a:** $[Fe^{III}L_2]^+$, where L=[phenyl(tris(3-methylimidazol-1-ylidene))borate]$^-$ which is the complex discussed in chapter 4 and illustrated in Figure 1.23. The white rectangle marks the region of pump scatter. **b:** $[Fe^{II}L'_2]^{2+}$ where L'=(2,6–diimine)pyridine. Please note color bar gradients are different in the two figure panels.

Three types of signal contributions can exist: excited state absorption (ESA), ground-state bleach (GSB), and stimulated emission (SE – note it is spontaneous emission for a ns measurement). Sample excitation leads to a depletion of the ground state population – more light therefore reaches the detector where the ground state absorbed, resulting in a negative GSB signal. Likewise, the formed excited state absorbs, and less light reaches the detector resulting in a positive ESA. Interaction with a probe photon can trigger emission from the excited state, and, since once again more light arrives at the detector, the resulting signal is stimulated emission. The net shape (and sign) of the ΔA signal at different wavelengths is a superposition of all contributions[p]: this is

[p]some extra details are provided in the appendix for the interested reader, which are necessary, for instance, to explain coherent artefacts

best understood by looking at some data, seen in Figure 3.21. Both surfaces feature a net positive signal in the blue region, due to ESA. The GSB from around 450 to 600 nm manifests as a net negative signal for the Fe-polypyridyl (Figure 3.21, right), while it leads to a reduction in the ESA for the Fe-carbene (Figure 3.21, left – for a clearer view of the band shape, the reader is directed to Figure 4.12). Finally, a negative ΔA which represents a SE signal is seen towards the red for the Fe-carbene, but this is not the case for the polypyridyl, which is not emissive.

Despite the general similarity in spectral features and lifetimes (~2 ns), their electronic origins are entirely different, being a charge-transfer state for the Fe-carbene, and a metal-centred state for the Fe-polypyridyl. In this particular case we have the benefit of having an emissive charge-transfer excited state to have greater certainty in our assignments (together with other measurements, see chapter 4) – but the fact remains that in many cases, transient data in the UV-Vis will be characterized by an ESA and bleach, making distinction between charge-transfer and ligand-field state manifolds a challenging task. Spectroelectrochemical data (see section 3.31) is useful to determine diagnostic spectral features for CT states, but it is by no means water-tight. A case in point is that of long-lived CT states in Fe^{II}-amido complexes reported by Herbert and co-workers[75]: the observed spectral features in the TA were in good agreement with the spectroelectrochemical data, leading to a CT assignment. Follow-up investigations by the same group – which now include time-resolved X-ray measurements – have revealed this to be the usual low-lying quintet metal-centred state ($^5T_2$) common in most Fe-complexes, however[76].

Nevertheless, TA remains an invaluable tool in conjunction with other methods. Returning to the case of Janus-emission discussed at the end of section 3.1, it is notable that the observed lifetime in TA and emission measurements does not agree (the TA signals disappear entirely in <500 ps, while emission lifetimes in the ns range are reported). An agreement between TA and emission lifetimes is a good indication of the emission originating from the same species. Furthermore, the observed extinction coefficient of the absorption band (ca. 6000 cm^{-1}) suggests a radiative rate constant on the order of magnitude of ~10^8 s^{-1} via the Strickler-Berg relation mentioned in the theory section (although strictly applicable to transitions where there is no change in multiplicity, the claimed ns lifetimes partly justify its application in this case). The observed emission lifetime (few ns) and quantum yield (around 0.01%) allow for an independent determination of the radiative rate ($\varphi_{em} = \frac{k_r}{k_r+k_{nr}}$) to about ~$10^4$ s^{-1}, leading to a discrepancy of up to 4 orders of magnitude. It is therefore wise to question the spectacular results.

We end this section by noting that additional complications arise in the analysis and interpretation of ultrafast TA data <500 fs[77], since many relevant photophysical processes in TMCs, from vibrational cooling to intersystem crossing may take place on these timescales, sometimes in parallel (this has not been discussed and truncated in Figure 3.21 for lucidity). Contributions from the IRF (instrument response function) – which is typically held as a fixed parameter in multiexponential fits, but may have a wavelength dependence – can influence the early time-constants at different wavelengths to an appreciable degree. Depending on resolution, ultrafast events may occur within the IRF, or at the least be heavily convolved with it. Coherent artefacts may be mistaken for signals[78,79]. A global analysis of the data and independent determination of the IRF using the solvent may to some degree help ameliorate such issues[80]; at the same time, single-wavelength analysis can provide insight in specific spectral regions which may be missed in a global fit of the data. The latter approach is adopted in this thesis, if conservative. There is always some trade-off, and at the end of the day, the importance of fit models and parameters being physically realistic cannot be stressed enough.

3.22 Time-resolved Emission Spectroscopy

Time-resolved photoluminescence (emission) (TRE) measurements track the decay of a luminescent excited state in time. Data collection and analysis is relatively straightforward (for single species) and serves to complement TA nicely – as mentioned in the previous section, agreement between the excited state lifetime determined from TA and TRE allows for attribution of the emission to the same species. It also provides a facile way of determining dynamic quenching rate constants; in conjunction with steady-state measurements, it can be used to differentiate between static and dynamic quenching mechanisms. TRE comes with the same caveats as steady-state emission measurements, however, in that it is sensitive, and one must remain mindful of impurities.

A frequently used method is ‘Time-correlated Single Photon Counting’ i.e. TCSPC, or SPC for short, which with very fast electronics and use of short pulses can measure excited states with lifetimes down to a few ps in the best case; even the most routine setup allows for ns time resolution. In principle, pulsed excitation creates an ensemble of excited states – in the ideal case scenario, we would be able to simultaneously measure the photons emitted by the entire population and obtain the mean decay time (and multi-channel SPC setups are indeed becoming more common). The core concept[81] of single-channel SPC is unique in that it reconstructs the ensemble decay by repeatedly measuring a single photon at a time; statistical conditions are met such that the ensemble is sampled in an unbiased fashion: this practically translates to

maintaining a low count-rate with respect to the excitation rate (otherwise, the measurement would be naturally skewed to the fastest decaying members of the ensemble by virtue of design). A representative example can be seen in Figure 3.22 (the instrument response function – IRF – is plotted in red, which depending on detector or light-source may be limited by either).

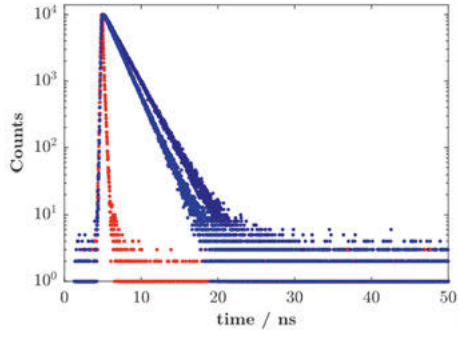

Figure 3.22. Typical data from an SPC measurement. Decays (blue) and the IRF (red).

3.3 Electrochemistry

A suite of electrochemical methods[82] involve the application of a potential and the measurement of the current response of the analyte; cyclic voltammetry (CV) enjoys particular popularity, as noted by Johnson[83] and sometimes the involved analysis for correctly interpreting the resulting curves may not be fully appreciated for coupled reaction schemes. Fortunately, for a large number of TMCs, determination of parameters of photophysical relevance (couple potentials, generally) is a simple task. The usual three-electrode setup may be utilized, consisting of a working, reference and counter electrode. The potential is scanned at a given (linear) sweep rate up to a vertex potential, typically determined by the solvent window, and then scanned back up to the starting point. The couple potential – which is the thermodynamic parameter of interest – may be determined by taking the average of the anodic and cathodic peak potentials. To ensure correct assignment of a given couple to a metal or ligand centred redox event, it is useful to measure the latter on its own as a reference – this is not always possible, however, e.g. for carbene ligands which are generated in-situ to bind with the metal and cannot persist in solution.

In addition to cyclic voltammetry, differential pulse voltammetry (DPV) has also been used in this thesis; the primary difference between the two techniques is that in the latter small amplitude potential pulses are applied on a linear ramp, and the difference between values on either side of the pulse is recorded. This allows for a substantial reduction in capacitive contributions to the current response, resulting in both greater sensitivity, and allowing for stretching the limit of the solvent window. Reversible couples appear as symmetric peaks in a DPV, with the peak potential equalling the aforementioned couple potential.

The determination of ground state potentials can be used to estimate the excited state potentials in a first approximation using the Weller formalism, as

shown in section 2.3. Unlike metal-centred states, whose energies can be tracked using Tanabe-Sugano diagrams, charge-transfer transition energies should rather depend on the reduction potentials of the metal and ligand. Indeed, the potential difference between a ligand oxidation/reduction and that of a metal couple should vary with the observed charge-transfer absorption band energy *if* the orbitals probed electrochemically are the same as those involved in the optical transitions. The approach is similar to that used for the determination of HOMO-LUMO gaps in organic chromophores. Finally, electrochemical potentials may also be used to make informed comparisons, regarding, for example, electron density on the metal in different complexes, but care must be taken to account for outer-sphere effects[84].

3.31 Spectro-electrochemistry

As alluded to in section 3.21, spectro-electrochemistry is by far one of the most robust and accessible methods to determine diagnostic features for charge-transfer states, which take centre-stage in this thesis. The potential may be held either anodic or cathodic of a given couple, and the absorption changes recorded with time, until conversion is complete. The final spectrum is thus representative of the oxidized/reduced ligand or metal, and an appropriate superposition can be used to approximately simulate the excited state spectrum. The general setup is the same as for a CV measurement, except the working electrode is typically switched from a standard 1 or 2 mm working electrode to a mesh electrode with large surface area, together with a smaller path-length optical cell, which allows for swift electrolysis (<10 min for sample volumes of around 0.3 ml) and concomitant monitoring of spectral changes. Clean conversion from one species to another can be confirmed from the presence of isosbestic points, and cycling a few times to check reversibility of the spectral changes is always good practice. A current-time curve may be measured in tandem with the bulk electrolysis – the area under the curve can furnish the total charge transferred, and be used to confirm the one-electron nature of the process.

4. A Fluorescent Fe-NHC Complex

The last decade has seen many ingenious attempts to make the charge-transfer excited states of Fe-complexes mimic those of Ru, so much so that it has led to paper titles such as, "Is Iron the New Ruthenium?"[47,48], where Wenger has elucidated the various strategies that may be employed. As the generic molecular orbital diagrams shown in Chapter 2 suggest, typical approaches may seek to stabilize t_{2g} orbitals or destabilize e_g* orbitals to effect larger field-splitting; accordingly, reports have used high-symmetry[85,86] (McCusker, Heinze), cyclometalation[87–92] (Dixon, Jakubikova, Bauer), nested potentials[93] (Vura-Weis), and strong sigma-donation[94–100] (Wärnmark, Gros), with the last one necessarily featuring different types of carbene ligands. On a different, perhaps more interesting track, the possibility of accessing strained high multiplicity CT states has also been suggested[101,102] (Damrauer). Cumulatively, the work has resulted in the enhancement of CT lifetimes from the sub-ps to tens of ps and even a few ns for iron-based complexes.

$[Fe^{III}L_2]^+$ is the subject of this chapter (Papers **I** and **II**), an exemplar of the strong sigma-donation strategy – and a successor of $[Fe(btz)_3]^{3+}$ (btz = 3,3'-dimethyl-1,1'-bis(p-tolyl)-4,4'-bis(1,2,3-triazol-5-ylidene), which possessed a weakly luminescent 100 ps ^{2}LMCT excited state[103]. At the time it was published in 2019, the fluorescent 2 ns ^{2}LMCT excited state of $[Fe^{III}L_2]^+$ became the longest and brightest known for iron-based CT states, capable of engaging in demanding bimolecular electron transfer reactivity. Let us revisit the complex, now with the benefit of nearly five years of hindsight in a rapidly evolving field, which has included several more publications on it[104–108].

4.1 Fundamental Photophysics and Excited State Dynamics

$[Fe^{III}L_2]^+$ is a low-spin ground state doublet, i.e. one unpaired electron in the metal-based orbitals (t_{2g}^5), which is in contrast to the more prevalent fully-filled t_{2g} set in Fe^{II}-polypyridyls. This is a direct consequence of the strong σ-donation of the ligand framework, which has a propensity to stabilize higher oxidation states. The absorption spectrum in acetonitrile is presented to the right of Figure 4.11 – the rose-red solution is characterized by a moderately

strong band in the visible, peaking at 502 nm (ε = 2950 $M^{-1}cm^{-1}$) with a very minor shoulder at 545 nm; the extinction coefficient together with the electrochemical potential difference between the ligand oxidation and the $Fe^{III/II}$ couple potential confirms an LMCT assignment, together with other measurements and analyses (see Paper **I** and its SI for details). Excitation into this lowest energy absorption band results in bright orange photoluminescence peaking at ca. 650 nm, with an emission quantum yield of 2%: the emission lifetime is 2 ns, and is in excellent agreement with the transient absorption data (Figure 4.12 and its caption), which confirms the ^{2}LMCT nature of the emissive excited state[q], which can therefore be adjudged as a fluorescence. Relevant photophysical and electrochemical properties of both $[Fe^{III}L_2]^+$ and $[Ru(bpy)_3]^{2+}$ are collated together in the Latimer diagram seen to the left of Figure 4.11. This is not just a nice cosmetic exercise, but allows us to see important similarities and differences between the two.

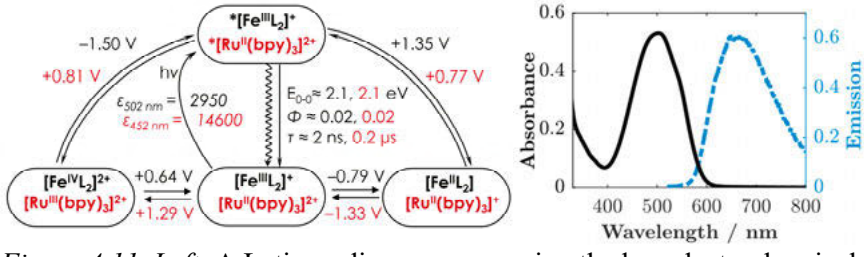

Figure 4.11. Left: A Latimer diagram comparing the key electrochemical and photophysical properties of $[Fe^{III}L_2]^+$ and $[Ru(bpy)_3]^{2+}$ in aerated acetonitrile; all potentials are referenced to SCE. *Right:* Normalized absorption and emission data for $[FeL_2]^+$.

Fe-carbene features excited state potentials ($*Fe^{III}/Fe^{II}$ = +1.35 and $Fe^{IV}/*Fe^{III}$ = −1.50 vs. SCE) that far exceed those of $*[Ru(bpy)_3]^{2+}$, thus priming it for photoinduced electron-transfer reactivity. Given the virtually identical $E_{0\text{-}0}$ value, the superior oxidizing and reducing power can be linked to the ground state potentials for oxidation and reduction of the metal centre. In fact, close scrutiny shows us that *both* the first reduction and oxidation events in $[Fe^{III}L_2]^+$ occur on the metal centre. This contrasts not only with $[Ru(bpy)_3]^{2+}$ where the first reduction occurs on a bpy ligand and oxidation on the metal centre[109], but with a large class of investigated polypyridyls for which it serves as prototype[110]. This has interesting implications for the reactivity of $*[Fe^{III}L_2]^+$, which we will return to shortly. For the moment, we end our comparative commentary by noting the order of magnitude smaller extinction coefficient of Fe-carbene, and its relatively short lifetime when compared to that of $*[Ru(bpy)_3]^{2+}$, whose transition back to the ground state is spin-forbidden.

[q] The LMCT nature of the transition means that in the ES the radical character moves from the metal to the ligand; since there is only one unpaired electron, however, a doublet multiplicity remains the only possibility, much as in the excited states of organic radical species

On the other hand, the photostability of Fe-carbene is far greater when irradiated under identical conditions in aerated acetonitrile for ca. 160 hours with no quenchers present (Figures S21 and S22 of Paper **I**). The doublet nature of its excited state also makes it immune to quenching by oxygen, unlike triplets.

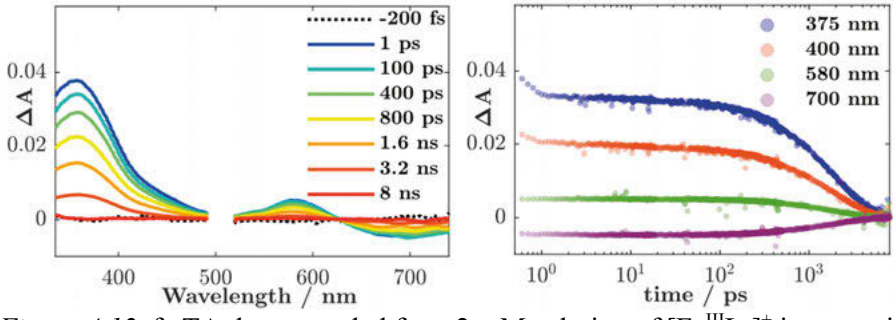

Figure 4.12. fs-TA data recorded for a 2 mM solution of $[Fe^{III}L_2]^+$ in acetonitrile. λ_{ex}=502 nm, power = 2 μJ/pulse. Spectra at selected time points as indicated in the legend (left) and kinetics at wavelengths as indicated in the legend (right). The excited state absorption in the blue agrees very well the spectroelectrochemical signature of $[Fe^{II}L_2]$ (see Figure 6.11), indicating the formation of the transiently reduced metal centre in the LMCT excited state; the ground state bleach centred at 502 nm appears as a trough in the ESA, with stimulated emission seen further towards the red beyond 600 nm, in agreement with the observed steady-state emission seen in Figure 4.11. The decays are monoexponential with a fit lifetime of ~2 ns.

4.2 Reactivity

Before embarking on a discussion of the reactivity results for $*[Fe^{III}L_2]^+$, it may be worthwhile to consider the physical implications of quenching an excited state with a lifetime of 2 ns – a situation which can be thought to be prevalent for a number of first-row metal-based CT excited states under investigation in the literature currently. *Assuming* a diffusion-controlled bimolecular quenching rate constant of $\sim 10^{10}$ $M^{-1}s^{-1}$, a quencher concentration of 0.05 M would be required to quench 50% of the excited state. Thus, to see appreciable quenching, concentrations of ca. 0.1 M may be nominal to test. The use of such concentrations on the practical level speaks to trivial limitations, such as limited solubility, and, depending on where the quencher absorbs, a difficulty in probing certain wavelengths using transient absorption spectroscopy. Fortunately, a large suite of reductive quenchers such as aromatic and aliphatic amines are either liquids or can be dissolved to appreciable extents in solvents such as acetonitrile (the one used here), and typically absorb only <350 nm. The oxidative side of matters is somewhat more challenging; MV^{2+} (methyl-viologen dication) and its derivatives may be used, but

other popular candidates such as 1,4-Benzoquinone are rendered unusable due to both solubility and absorbance constraints.

Then there are conceptual distinctions to make when employing such high quencher concentrations: at ~0.1 M, for typical quencher and chromophore radii, some 35% of quenchers can be expected to be in the sphere-of-action[r] (i.e. quencher present next to the chromophore at the moment of excitation, essentially translating to behaviour akin to static quenching), resulting in so-called "contact pairs". This suggests that the evaluation of rates under a diffusional assumption may not disentangle the behaviour of various reactant subpopulations. The situation of inhomogeneous reactant distributions in the solution phase and its consequences for charge separation has been dealt with in detail by a number of groups, notably that of Vauthey[111–116], and earlier by Mataga[117–119], and the interested reader is directed there. A key take-home is that since parameters such as electronic coupling and the reorganization energy are in fact sensitive functions of distance, one has to be careful when evaluating the intrinsic charge-separation rate constant, which should incorporate a reaction-diffusion model. In our case, we note the caveat, and with this backdrop, review the reactivity data presented in Paper **I**.

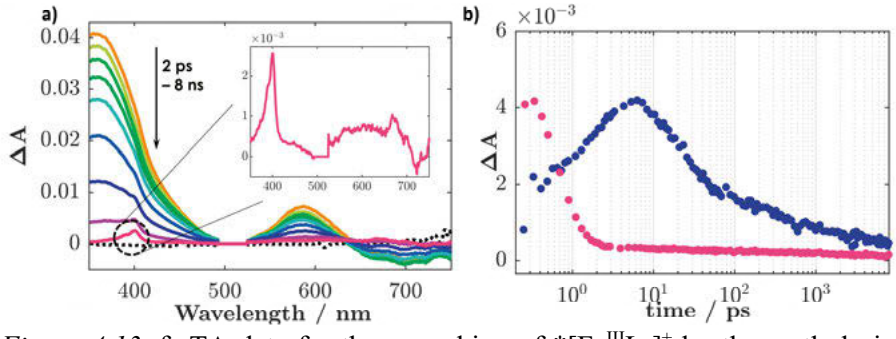

Figure 4.13. fs-TA data for the quenching of $*[Fe^{III}L_2]^+$ by the methyl-viologen dication (MV^{2+}) and diphenylamine (DPA), with oxidative electron transfer as the mechanism for the former and reductive electron transfer for the latter. **a:** Spectral data for quenching by MV^{2+} (conc. = 0.25 M, where the excited state is ca. 65% quenched), with an inset illustrating the cage escape products; earlier timescale spectral data can be found in Figure A2. **b:** Kinetics monitored at 625 nm, which is an isosbestic point in the excited state decay (see Figure 4.12), and allows for unambiguous monitoring of the product formation. MV^+, Fe^{IV} (oxidative quenching products and DPA^+ (reductive quenching product) absorb there. MV^{2+} is pink, DPA is blue. Data has been scaled for comparison.

[r] This is an idealized scenario assuming no interaction between chromophore and quencher

*$[Fe^{III}L_2]^+$ is quenched oxidatively and reductively by MV^{2+} and DPA, respectively, to yield electron transfer products with total yields of around 5% for the two cases. These translate to cage escape yields of ~6% and ~8% when accounting for the associated quenching efficiency at the concentrations tested. Since the relevant long timescale data is already presented in Figure 4 and supporting information of Paper **I**, we here take the opportunity to take a look at events occurring on shorter timescales, see Figure 4.13 a) and b). We focus on oxidative quenching by MV^{2+}, since reports on reductive quenching already exist[104,105]. Given the low yields, it is unsurprising to find recombination rates in excess of ~10^{11} s^{-1}, in good agreement with those reported for the reductive quenching cases. We can note that >90% of the signal amplitude has decayed <1 ps – with much of the formation and decay convolved with the IRF. This is in contrast with the somewhat slower product formation and decay dynamics for DPA: the latter was tested at 2.5 times lower concentration, however. Ultimately, the low yields for both cases can be traced to the spin-allowed nature of the recombination process, as illustrated in Figure 4.14.

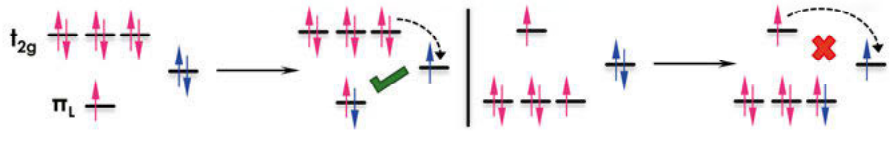

Figure 4.14. Simplified schematic showing how charge-recombination is spin-allowed in the case of a doublet excited state (left), and spin-forbidden for a triplet excited state (right).

Such a hypothesis has now been further corroborated by a report from Aydogan and co-workers[105], which reports high yields of cage escape (~60%) when using a halogenated solvent, dichloromethane; controls using other halogenated solvents could confirm the reasoning. This leads to the unusual result of improved cage escape yield for charge-transfer products in a solvent of relatively low polarity. Nevertheless, it would appear *$[Fe^{III}L_2]^+$ *is* a relatively poor electron-donor: yields of cage escape for all other (neutral) oxidative quenchers tested is ~0%, in contrast to a few percent for most reductive quenchers (see Appendix Figure A3). One possible rationale is that reductive quenching occurs on a ligand-based orbital, in contrast to oxidative quenching occurring on a metal-based orbital: the quencher could have greater electronic coupling with the former due greater accessibility i.e. proximity. Put differently, the ^{2}LMCT is already transiently an Fe^{II}, so reductive quenching can be thought to be favoured. It is actually fortuitous that yields are seen with MV^{2+} - likely due to the advantage of electrostatic repulsion in the charge separated products.

4.21 Symmetry-Breaking Charge Separation (SB-CS)

As promised in section 4.1, we now examine the consequences of a metal-centred oxidation preceding the ligand oxidation in Fe-carbene, the situation illustrated in Chart 1 c) of Paper **II**. It can be alternatively expressed in the form of the following two reaction equations, 4.21 and 4.22, with the help of the Latimer diagram in Figure 4.11. Here we use the oxidation state label to denote the complex for simplicity (i.e. $*Fe^{III} = *[Fe^{III}L_2]^{+}$, $Fe^{IV} = [Fe^{IV}L_2]^{2+}$ etc.):

$$*Fe^{III} + e^{-} \rightarrow Fe^{II} \qquad E^0 = +1.35\ V \qquad (4.21)$$

$$Fe^{IV} + e^{-} \rightarrow Fe^{III} \qquad E^0 = +0.64\ V \qquad (4.22)$$

Subtracting 4.22 from 4.21 and re-arranging yields: $*Fe^{III} + Fe^{III} \rightarrow Fe^{II} + Fe^{IV}$, with an $\Delta E^0 = 0.71$ eV. The excited state can therefore oxidize or reduce its own ground state, resulting in charge disproportionation reaction which proceeds with a *substantial* driving force – to understand why this is unusual, the reader is encouraged to execute the aforementioned exercise for *Drosophila* $[Ru(bpy)_3]^{2+}$ and confirm for themselves that lies are not being peddled. In fact, the two cases for TMCs in the literature where SB-CS has been implicated are a Ni-complex[120] and Ir-complex[121,122]. Based on the reported values of the couple potentials and the excited state energy, however, the SB-CS reaction can be expected to be around 0.22 and 0.38 eV uphill for the Ir and Ni complex, respectively – therefore, it is probable that the process is driven by other coupled reactions. In fact, for TMCs such as $[Ru(bpy)_3]^{2+}$, excited state energy is lost during intersystem crossing, and SB-CS can therefore typically be expected to be endergonic. Meanwhile, SB-CS is very common in organic chromophore assemblies[123,124]: this is because their optical transitions correspond to the HOMO-LUMO gap. The driving force for SB-CS is therefore usually close to zero[125–128], and the solvent work-term typically drives charge separation. Put in context, the paradigm for SB-CS in Fe-carbene – where it proceeds with a significant driving force – is unique to the point of being singular to this class of complexes.

Having said that, as mentioned previously, of course, bimolecular reactivity within the 2 ns lifetime is only possible at high concentrations: the experiments were therefore conducted on 70 mM solutions in 25 µm path-length cell in order to ensure optical transparency. Barring these considerations, the SB-CS process may be treated as any other photoinduced bimolecular ET within the ambit of the solvent-cage model, where the symbols have their usual meanings:

$$^2[*Fe^{III}] + {}^2Fe^{III} \xrightarrow{k_d} {}^{3,1}\{*Fe^{III\cdots}Fe^{III}\} \qquad (4.23)$$

$$^3\{*Fe^{III\cdots}Fe^{III}\} \xrightarrow{k_{et}} {}^3\{Fe^{II\cdots}Fe^{IV}\} \qquad (4.24)$$

$$^3\{Fe^{II\cdots}Fe^{IV}\} \xrightarrow{k_{bet}} {}^2Fe^{III} + {}^2Fe^{III} \quad (4.25)$$

$$^3\{Fe^{II\cdots}Fe^{IV}\} \xrightarrow{k_{sep}} {}^1Fe^{II} + {}^3Fe^{IV} \quad (4.26)$$

$$^1Fe^{II} + {}^3Fe^{IV} \xrightarrow{k_{rec}} {}^2Fe^{III} + {}^2Fe^{III} \quad (4.27)$$

Here, 4.23 would apply for the diffusional pairs, but not for the contact pairs. Given the reactants are both doublets, and the product is a triplet, spin conservation should statistically favour the formation of the triplet in the diffusional encounter complexes, and can proceed with a maximal rate constant of $¾k_d$.

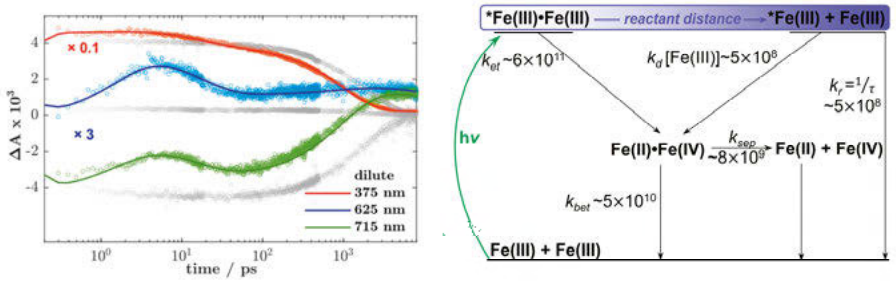

Figure 4.21. Left: fs-TA data for a ca. 70 mM solution of Fe(III) in acetonitrile. λ_{ex}=502 nm, power = 2 μJ/pulse. Kinetics measured at 375 nm (Fe^{II} maximum), 625 nm (isosbestic point in the unperturbed ES decay), and 715 nm (Fe^{IV} maximum). Product formation is clearly seen as a rise in the first few ps at the latter two wavelengths where absorption from Fe^{IV} attenuates the stimulated emission signal from the unquenched excited state. Data scaled as indicated for clarity. Data recorded at ca. 2 mM shown in grey for comparison. *Right:* Kinetic parameters of the SB-CS process obtained from global analysis of the data using a sum of exponentials fit model; all rate constants in s^{-1}. Figure adapted from Paper **II**.

In-line with expectations, SB-CS is clearly observed, and the critical results are summarized in Figure 4.21 and its caption. Interestingly, there is a correspondence between the early timescale kinetics observed at the isosbestic point of 625 nm for this case and reductive quenching by DPA, featuring near-identical sub-ps rate constants of charge separation. Note that a sum of exponentials global fit applied to a sequential model was used to determine the parameters, with contact and diffusional pairs considered separately; accordingly, the first two exponents modeled charge separation and geminate recombination in the contact pairs (k_{et} and k_{bet} in the scheme shown in Figure 4.21), while the third exponent gave the lifetime of the quenched excited state (k_r=1/τ, which could also be determined independently from SPC data). k_{et} ~6×10^{11} s^{-1} and k_{bet} ~5.2×10^{10} s^{-1} could be evaluated, the latter with k_{sep} calculated from the Debye-Smolchowski equation. The determined values are in good agreement with the follow-up study which could reproduce the results[108]. It can be noted that the slower k_{bet} could well be a consequence of

recombination occurring in the inverted region (driving force of 1.4 eV). Although yields remain modest due to the spin-considerations mentioned previously, this first case of SB-CS in a TMC is promising, since ligand design offers the opportunity to tune driving forces such that the recombination lies deeper in the inverted region.

4.3 Remarks

Having surveyed its properties, one would not be incorrect to state that several photophysical characteristics of the ^{2}LMCT excited state of $[Fe^{III}L_2]^+$ resemble those of organic radicals – though with some thermodynamic advantage when it comes to driving photoinduced electron transfer reactions, which tap into the redox activity of the metal centre. It is worthwhile to note that while the SB-CS process possible with the complex opens up a new avenue, it also suggests a more complicated picture for another: the conclusions of Paper **I** mention that the complex may be utilized in conjunction with semiconductor materials. However, any application – e.g. dye-sensitized solar cells – which involves high concentration of the complex (in a coating or otherwise) will necessarily feature SB-CS as a competing pathway to interfacial charge injection from the excited dye. Fe^{II} from the charge-separated products could be harvested, but geminate recombination would need to be outcompeted.

Returning to the fluorescent nature of the excited state, while it is true – also as Paper **I** mentions – that energy loss is minimized in the system since there is no intersystem crossing event, the spin-allowed nature of the transition will ultimately limit its lifetime. Such a statement is corroborated by the temperature dependence of the emission lifetime, which features only about a fourfold increase to 8.4 ns at 80 K. The key non-radiative decay pathways are therefore related to the intrinsic decay of the ^{2}LMCT to the ground state, most likely not via the metal-centred states which have already been substantially destabilized owing to the strong sigma-donation. Modifications of the ligand scaffold on the phenyl ring by introduction of electron-donating or withdrawing substituents has shown negligible impact on the photophysics[106] – this allows for imparting functionality on the one hand, but also indicates that the phenyl ring does not electronically communicate with the carbene framework to a substantial degree[s]. Further advances therefore demand more substantial alteration of the ligand-set.

[s] At the time of writing this thesis, a pyrene substituted version of the complex – both on the phenyl ring and the boron – was presented at the 25th International Symposium on the Photophysics and Photochemistry of Coordination Compounds. Expectedly, no change in the LMCT lifetime could be observed; this highlights the fact that typical strategies implemented for polypyridyls may not always translate for carbenes.

5. The Dark Knight: A Long-Lived Mn-NHC Excited State

We now take the proverbial step back – in time and in the 3rd row of the periodic table – to look at $[Mn^{IV}L_2]^{2+}$, the less famous but equally (if not more!) photophysically interesting cousin of $[Fe^{III}L_2]^{+}$. Both the first synthetic report by Smith[73], as well as the photophysical characterization in the solid state of Mn-carbene predate that of the iron counterpart[129]. Possessing a d^3 electron configuration, $[Mn^{IV}L_2]^{2+}$ is a ground state quartet – one can therefore suspect its photophysical properties to bear some resemblance to that of well-studied Cr^{III} and V^{II} systems[130–133]. Indeed, the solid state showed spin-flip luminescence from the ^2E state which is typical for the aforementioned complexes. Interestingly, however, a weak emission was also reported from a CT state, with a lifetime of 50 ns. In this chapter, we turn our attention to the latter in the solution phase – and find that, if $[Mn^{IV}L_2]^{2+}$ was dissolved in solution first, perhaps history may have been written a little differently.

5.1 Excited State Energetics and Dynamics

It is good to start our endeavour with some book-keeping: having three unpaired electrons in the ground state, $[Mn^{IV}L_2]^{2+}$ can give rise to excited states having different multiplicities, and some of the most relevant ones for our discussion are shown in panel a) of Figure 5.11. The absorption of $[Mn^{IV}L_2]^{2+}$ in acetonitrile features a prominent band in the visible, peaking at 504 nm (ε = 6200 M^{-1} cm^{-1}) with a shoulder at ca. 550 nm (please see Figure 6.11 in Chapter 6 for the absorption data in terms of ε). The extinction coefficient together with the difference in electrochemical potential between the $Mn^{IV/III}$ couple (Figure 5.11 panel c)) and the ligand oxidation (not shown, occurs at ca. +1.8 V) supports an LMCT assignment. Excitation into this lowest energy absorption band results in a broad (ca. 600 to 750 nm) and very weak emission ($\varphi_{em} < 10^{-4}$) in the solution phase at room temperature, at detector limits (Figure 5.11 panel b)). The collection of reliable excitation spectra is precluded in the solution phase due to the low signals. However, the spectra qualitatively agrees with the previously reported solid-state data; the emission at ca. 820 nm from the ^2E state can also be clearly seen in solvent glass at 77K. Further,

the measured excitation spectrum on the solid-state sample traces out the lowest energy absorption band.

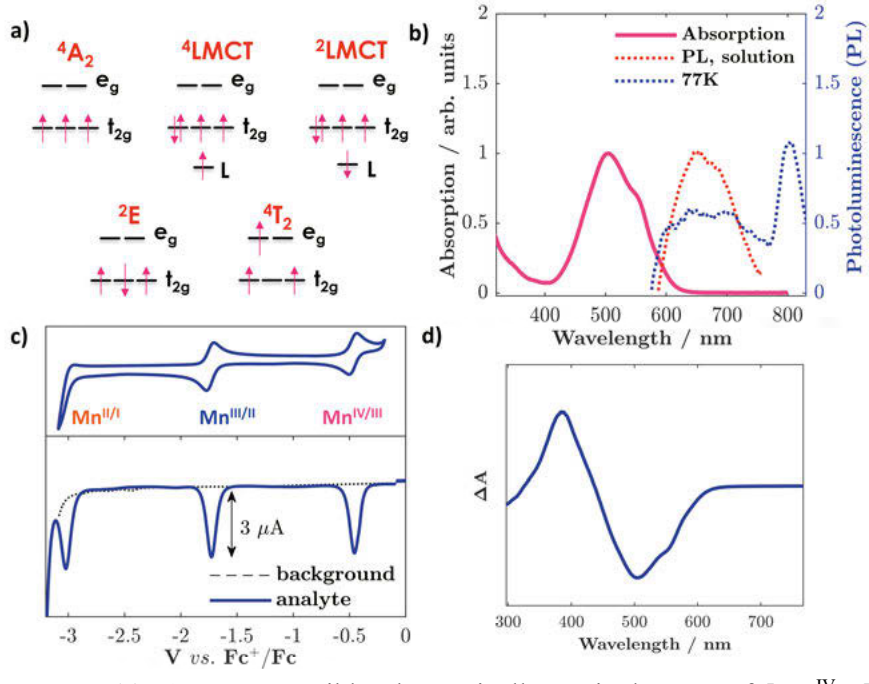

Figure 5.11. **a)** Some possible electronically excited states of $[Mn^{IV}L_2]^{2+}$, which is a ground state quartet (d^3). **b)** Normalized steady state absorption (solid pink) and corrected emission spectra of $[Mn^{IV}L_2]^{2+}$ in a ca. 80 μM solution in acetonitrile (dotted red), and at 77 K in butyronitrile glass (dotted blue). λ_{ex} = 500 nm, excitation and emission slit widths corresponding to a spectral resolution of 5 and 8 nm, respectively, with an integration time of 1 s. Note that the spectra have been corrected for solvent background, including Raman scatter, for clarity, due to the small emission signals. Uncorrected spectra are supplied in the extended data of Paper **III**. **c)** Cyclic voltammetry (100 mV/s) and differential pulse voltammetry data for ~1 mM $[Mn^{IV}L_2]^{2+}$ measured in acetonitrile with 0.1 M $TBAPF_6$ as supporting electrolyte, and, **d)** Expected spectral signature of the LMCT excited state as determined from spectro-electrochemistry. Note that contributions from the oxidized ligand are not included, since ligand oxidation occurs at the edge of the solvent window and spectral data cannot be reliably measured. See Figure 6.11 for spectra of the different oxidation states of the metal centre.

Thus, the emission – though homeopathic – can serve the useful purpose of evaluating $E_{0\text{-}0}$ from the intersection of the absorption and emission spectra, which comes to be ca. 2.1 eV. Taken together with the $Mn^{IV/III}$ couple potential of –0.47 V (vs. Fc^+/Fc), we get $^*Mn^{IV}/Mn^{III} \approx 1.63$ V (or nearly 2 V vs. SCE!). The impressive predicted oxidizing power of this excited state can be seen as

a direct consequence of the near 700 mV stabilization of the $Mn^{IV/III}$ couple compared to that of the iron analogue ($Fe^{IV/III}$ = 0.255 vs. Fc^{+}/Fc), which also has an $E_{0\text{-}0}$ of 2.1 eV. This observed lowering in couple potential is consistent with expected trends across a row; indeed, for other scorpionates such as tris(pyrazolyl)borates (Tp), a lowering of around 300 mV has been seen[134,135]. The more dramatic difference seen here could be a simple consequence of the strongly-donating nature of this ligand-set compared to Tp. Alternatively, it may be that this is partly due to better orbital overlap with Mn as compared to Fe (Mn>Fe): the twice as large extinction coefficient lends some credence to such a hypothesis.

Finally, spectro-electrochemistry allows for the determination of spectral markers of the LMCT excited state, and the expected difference spectrum is seen in panel d) of Figure 5.11, where the peak at ca. 380 nm is from Mn^{III}. Unfortunately, spectral signatures from the ligand cannot be reliably obtained since the ligand oxidation occurs at the edge of the solvent window. Nevertheless, measurements on the related iron complex suggest absorption from the oxidized ligand may be expected in the red (>600 nm), see SI of Paper **I**.

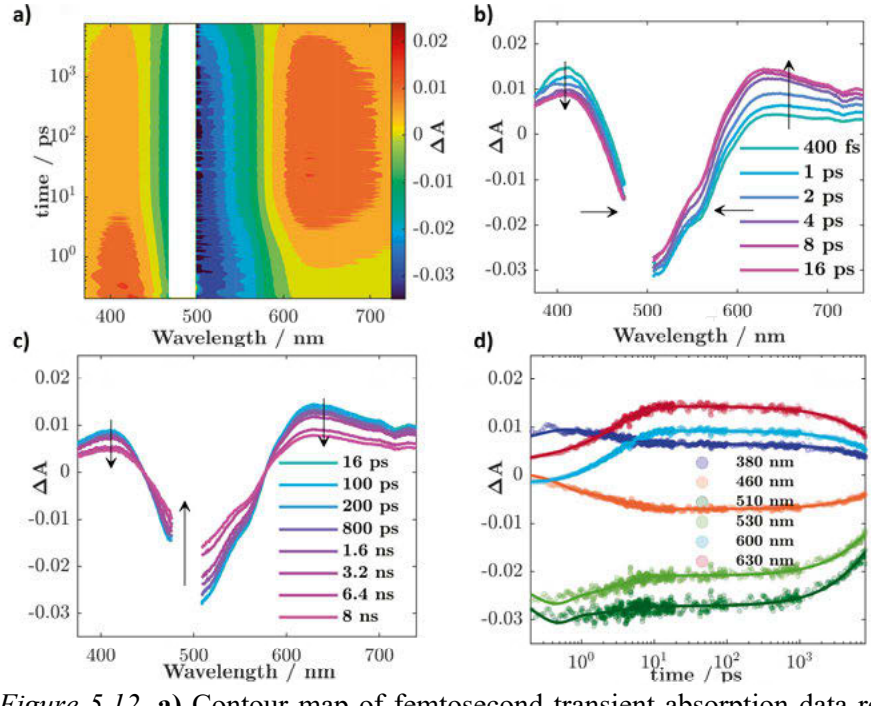

Figure 5.12. **a)** Contour map of femtosecond transient absorption data recorded for $[Mn^{IV}L_2]^{2+}$ (excitation wavelength = 480 nm, pulse energy = 0.7 µJ/pulse, absorption ≈ 0.35 at the excitation wavelength). **b)** and **c)** Spectral traces at selected time points (horizontal cuts from a)), with arrows to guide the spectral evolution. **d)** Vertical cuts from a) at selected wavelengths; a global analysis of the data yields fit components of 3 ps and 16 ns.

We are now ready to interpret the transient absorption data seen in Figure 5.12. The observed spectral shape at all timescales is suggestive of charge-transfer character, with an ESA in the blue characteristic of the transiently reduced Mn^{III} as expected from the spectro-electrochemical data, together with a GSB centred at ca. 500 nm, and contributions in the red from the oxidized ligand. The data is amenable to a biexponential fit and global analysis yields values of ~3 ps and ~16 ns (Figure 5.12 panel d)). The initial timescale spectral evolution is interesting, featuring a narrowing of the observed bleach and a simultaneous growth in the transient signal towards the red (Figure 5.12 panel b)): this is best interpreted as a loss of stimulated emission, given that emission from the LMCT can be expected in this region based on the steady-state data.

As we have learned in chapter 3, making definitive assignments to the identities of excited states based on UV-Vis transient data alone can be tricky. In this case, however, this may be possible to do. It is reasonable to assume that the initially formed Franck-Condon state is the ^{4}LMCT. Experience from related polypyridyl complexes[132,133] should suggest that the ^{4}LMCT already deactivates within the IRF (<100 fs) to yield the ^{2}E. Some things can be thought to speak against such a situation for the carbene, however: 1) there is clear loss of stimulated emission, suggesting that the initially formed ^{4}LMCT in fact disappears in around 3 ps, 2) the observed spectral signatures retain primarily charge-transfer contributions throughout, and 3) the observed reactivity is energetically incompatible with a ^{2}E state (*vide infra*). Given all these observations, we can make a tentative assignment of the observed time-constant to intersystem crossing from the initially formed ^{4}LMCT to the ^{2}LMCT. This would agree well with the comparatively subtle spectral changes observed. It could also help explain the nearly order of magnitude longer lifetime compared to the iron analogue, given the spin-forbidden nature of the transition back to the ground state.

Having made these arguments, it is important to mention that MCD data reported for $[Mn^{IV}L_2]^{2+}$ prior[129] exhibits sharp line shapes in the low-energy region of the observed absorption spectrum (i.e. at the shoulder). Analysis suggested that the observed structure was at least partly due to a vibrational progression, and comparison with recently reported low temperature data[108] for the iron analogue also suggests that this may well be the case (see Chapter 6 for details). At the same time, the presence of spin-forbidden transitions in the region could not be ruled out in MCD. Transient spectroscopy upon exciting into the lower energy shoulder yielded identical time constants, although some reduction in amplitude could be observed. Ultimately, based on the current dataset, a mixed metal-centre/charge-transfer character cannot be ruled out, but a predominantly charge-transfer assignment seems reasonable to make.

5.2 Reactivity

Some first reactivity data is shown in Paper **III**, with diphenylamine and DMF: the former has a potential of ca. +0.91 V vs. SCE, while the latter is around +1.5 V. We here take the opportunity to present some more data in order to test the limits of the approximated excited state potential of ca. 2 V vs. SCE. As we can see in Figure 5.21, the excited state is capable of oxidizing both 1,3–Dimethoxybenzene (+1.6 vs. SCE) and 4–Methylanisole (+1.8 vs. SCE). The total product yields remain low (~5%), virtually identical to the iron analogue, and the cause can once again be traced to the spin-allowed nature of the recombination. It is important here to note that relatively high quencher concentrations were employed in these cases, ca. 0.4 M. It could therefore be possible that the ^{4}LMCT is harvested due to quenchers in the sphere-of-action. However, this would suggest rather high yields of cage-escape if the signal is thought to be sourced entirely in the ^{4}LMCT. Furthermore, in the case of 4-Methylanisole, a shortening of the 16 ns lifetime is partly observed even on the ns-TA experiment. It would be interesting to conduct more experiments with a homologous series to delineate exactly how much energy is lost during the intersystem crossing process. In any case, the oxidizing power accessible is substantial.

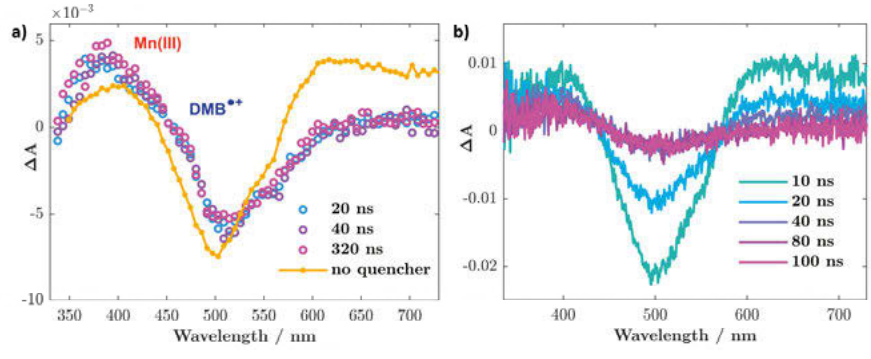

Figure 5.21. ns-TA spectral data for reductive electron transfer quenching of $*[Mn^{IV}L_2]^{2+}$ by **a:** 1,3–Dimethoxybenzene (+1.6 vs. SCE) and **b:** 4–Methylanisole (+1.8 vs. SCE), respectively. Excitation wavelength = 480 nm, pulse energy = 10 mJ/pulse, absorption ≈ 0.3 – 0.4 at the excitation wavelength, and integration time = 40 ns or 100 ns.

5.3 Remarks

With $[Mn^{IV}L_2]^{2+}$, we see the natural advantage of exploiting spin to achieve a long lifetime. And while Mn-carbene is able to show[t] that a paradigm similar to the heavy congeners may be realized with first-row metal-based charge-transfer states, there remain challenges. One in particular is the presence of low-lying spin-flip states (which, of course, have their own uses and applications) in this electronic configuration. Their energies can be expected to be independent of the ligand-field, and they may serve as efficient non-radiative decay pathways for the LMCT state. Variable-temperature measurements should help gain further insight into whether activated or non-activated pathways dominate the excited state decay.

[t] important here to note that d^3 V^{II}-complexes reported by Damrauer show similar behaviour for MLCT states, by virtue of which a ~1 ns lifetime is achieved with a conventional polypyridyl like bpy. The observed states there possess mixed MC/MLCT character, however.

6. First-Row Transition Metal Carbene Scorpionates: A Brief Survey

In 2003, McCusker published an incisive account on the fs-TA spectroscopy of transition-metal complexes with a focus on metal-polypyridyls[136]. In conclusion, it poetically read, '…virtually every ultrafast measurement carried out on an inorganic system represents new information, and inorganic chemistry provides an enormously rich variety of molecules to study.' As we have seen in the last two chapters, the carbene scorpionates present an interesting class of complexes to study. Accordingly, in this chapter, our first aim is documentation, with an eye toward trends. Since the field is still in its infancy, such a catalogue should prove useful to see what is known and what is not, in particular regarding timescales of excited state evolution and the identities of the states involved in the scorpionates. Although the current data-set is relatively minimal, our second aim is to see if any correlations may be found between the observed dynamics and the structure of these complexes. We also try to benchmark along the way, note possibilities, and make comparisons where appropriate.

6.1 Overview

Spectro-electrochemical data for the various $[M^xL_2]^{n+}$ complexes (where M=Mn, Fe, and Co) is presented in Figure 6.11. For convenience, a label of the metal together with its oxidation state is substituted to denote the complex (so $[Fe^{III}L_2]^+ = Fe^{III}$, $[Mn^{II}L_2] = Mn^{II}$ etc.). All metal couples are characterized by clean, reversible one-electron redox processes, and the associated spectral changes are reversible as well (under the usual oxygen and moisture-free electrochemical conditions). Of the several accessible oxidation states, Mn^{IV}, Fe^{III}, Fe^{IV} and Co^{III} (all low-spin) have been characterized by ultrafast optical spectroscopy, and can also be obtained as air and moisture insensitive crystals. Their key structural data is collected in Table 6.1. All complexes are characterized by a close to perfect octahedral environment (though formally D_{3d}[63,137]), featuring C-M-C bond angles $\geq 87^o$, making the bis(carbene)borate scorpionate motif competitive with some of the most symmetric polypyridyl ligands known, such as dqp (2,6-di(quinolin-8-yl)pyridine)[138] and dccp (2,6-bis(2-carboxypyridyl)pyridine)[85]. Bond lengths are 2.00 Å for Fe^{III} and Fe^{IV},

while Co^{III} features an average bond length of 1.94 Å which is 5% shorter than Mn^{IV}. The small variations in values across various metals and oxidation states can be taken to represent the rigidity of the ligand framework and the covalency of the M-carbene bond.

Table 6.1: Bond lengths (in Å) and angles (C···M···C) for various $[M^xL_2]^{n+}$ complexes. Extremes are mentioned with average values in brackets. Reference publications noted in text.

	Mn^{IV}	Fe^{III}	Fe^{IV}	Co^{III}
Bond length	2.03–2.05 (2.04)	1.98–2.01 (2.00)	1.99–2.01 (2.00)	1.93–1.95 (1.94)
C-M-C angle	86.83–86.95 (86.92)	86.42–87.12 (87.00)	87.26–87.72 (87.54)	88.36–92.38 (90.00)

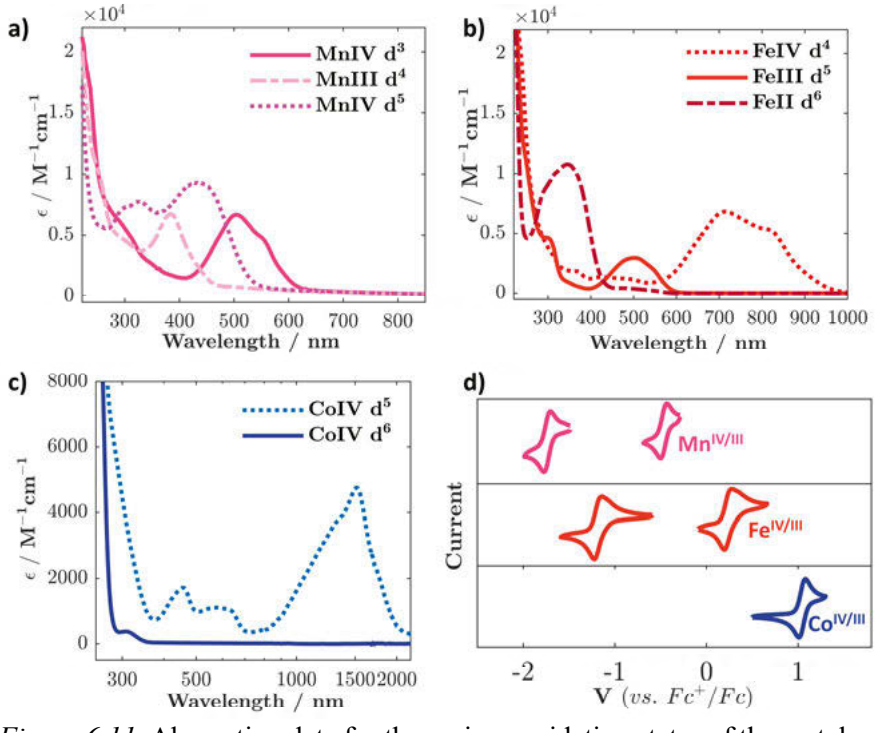

Figure 6.11. Absorption data for the various oxidation states of the metal centre as determined from UV-Vis-NIR spectro-electrochemistry for **a:** $[M^xL_2]^{n+}$, **b:** $[M^xL_2]^{n+}$, and **c:** $[M^xL_2]^{n+}$. **d:** Electrochemical data for $[M^xL_2]^{n+}$, where M=Mn, Fe, and Co. Note the log scale on the x-axis in panel c. Note that different line-styles are used in the different panels.

Fe^{II} and Mn^{III} are both oxygen sensitive, the former to the point that it is difficult to keep stable even in a glovebox over long periods. The latter too tends

to oxidize under air, albeit over several days, at least in powder form. A crystal structure has been obtained, and features bond lengths and angles virtually identical to the Mn^{IV} congener (2.02–2.04 Å, and 85.82–87.32°). As we shall see below, it has been possible to study the ultrafast photophysics of Fe^{II} by electrochemically reducing it and maintaining inert conditions and a constant potential bias throughout the experiment, to prevent contamination from the oxidation product. It should in principle be possible to study Mn^{III} by implementing the same methodology. Finally, apart from the absorption spectra shown in Figure 6.11, nothing is known about Mn^{II} and Co^{IV}.

We end this section by noting the nature of the charge-transfer bands seen, with the vast majority being LMCT transitions in-line with the strongly-donating nature of the ligand-set. The data is collected in Table 6.12. The assignment is in generally good agreement with the potential difference of the relevant metal couple (seen in Figure 6.11 d)) and ligand oxidation (which lies in between 1.6–1.8 V vs. Fc^{+}/Fc, see papers). Co^{III} is the only outlier, with no prominent charge-transfer absorption features in the vis-NIR; a more detailed analysis is presented in section 6.23.

Table 6.12: Charge-transfer transitions for various $[M^{x}L_2]^{n+}$ complexes. ε is in $M^{-1}cm^{-1}$ at the given absorption maximum in nm.

Ox. State/Metal	Mn	Fe	Co
II	MLCT $\varepsilon_{436}\approx 8870$	MLCT $\varepsilon_{348}\approx 10850$	–
III	LMCT $\varepsilon_{384}\approx 6200$	LMCT $\varepsilon_{502}\approx 2950$	?
IV	LMCT $\varepsilon_{504}\approx 6300$	LMCT $\varepsilon_{715}\approx 6850$	LMCT $\varepsilon_{1514}\approx 4754$

6.2 Comparative Cases

In order to systematize our study, we start simple by comparing Mn^{IV} and Fe^{III}, which happen to be the only two members (of this class of complexes investigated so far) which feature long-lived CT states in the nanosecond regime. Thereafter, we view pairs based on their shared electronic configurations d^4 and d^6, and see if commonalities can be found.

6.21 Mn^{IV} and Fe^{III} (d^3 and d^5)

Since we have already delineated the photophysics of the two subjects in question in chapters previous, we restrict ourselves to the most essential observations. Fe^{III} presents a limitation in its lifetime due to the spin-allowed nature of the ^{2}LMCT excited state's transition back to the ground state. Meanwhile, Mn^{IV} presents an improvement in lifetime, at least partly due to the spin-forbidden nature of the $^2\text{LMCT} \rightarrow {}^4A_2$ transition. At the same time, the presence of $^2E/^2T$ spin-flip states – whose energies are essentially independent of the ligand-field strength – may nevertheless present a leakage pathway for the CT state, limiting its lifetime.

Despite the difference in electronic configuration, both Mn^{IV} and Fe^{III} feature an interesting congruence in their absorption and emission spectra. In fact, a recent report[108] shows that the relatively unstructured absorption spectrum of Fe^{III} develops structure at low temperature – the shoulder at 545 nm becomes resolved, much like the room temperature spectrum of Mn^{IV}, which has a shoulder at 550 nm. Similarly, the emission also becomes structured, with three peaks showing energy separations of ca. 1100 cm^{-1}, which is very similar to those observed for the room temperature and 77K emissions for Mn^{IV}[129]. Taken together, the data strongly suggests a vibrational progression at least partly being responsible for the observed absorption and emission structure in the two complexes, with the B-C stretch mode occurring around the same frequency most likely implicated. At the same time, as pointed out in Chapter 5, the sharp line shapes observed on the low energy side in the MCD data collected for Mn^{IV} may also suggest the involvement of spin-forbidden states. That the Fe^{III} absorption and emission becomes similar to that of Mn^{IV} on lowering the temperature further supports the idea advanced in Chapter 5 that the ligand framework is probably best suited to a given size of the metal centre. Mn > Fe, and on lowering the temperature, contraction probably enables a better orbital overlap in Fe^{III} that is already extant in Mn^{IV} at room temperature.

As a final remark, it can be noted that both Mn^{II} and Co^{IV} are isoelectronic with Fe^{III} – what their photophysics is like, however, remains to be seen.

6.22 Mn^{III} and Fe^{IV} (d^4)

Both Mn^{III} and Fe^{IV} show low-spin triplet LMCT transitions differing by ca. 2 eV as reflected in their electrochemical couple potentials. Ultrafast spectroscopy on Fe^{IV} has been reported[139], and shows a sub-ps (0.8 ps) lifetime of the LMCT excited state. This decay component accounts for nearly 90% of the ground state recovery. This is followed by a ~16 ps component which completes the ground state recovery, most likely mapping the decay of a metal-

centred state. Given the available structural parameters, there is no reason to assume the ligand-field in this case should have a very large attenuation, but it could still be a possibility. It is not immediately clear why the Fe^{IV} congener should possess such a short lifetime and the initial report furnishes no explanation. We may find a clue by considering its Mn^{III} counterpart. Although Mn^{III} has not been spectroscopically characterized experimentally – owing to its tendency to get oxidized – an extremely detailed ligand-field theory analysis has been carried out on the complex[63], followed by another report using ab-initio methods to calculate its electronic structure[137]. The results have been benchmarked using other scorpionates ((tris-pyrazolyl)borates) which could be characterized fully using variable-temperature MCD. There, the ^5E pair of states has been found to lie at a low energies of ca. 14–15000 cm^{-1}.

A similar situation may prevail in the Fe^{IV}, and the ^5E states would then be isoenergetic with the broad LMCT absorption band. Since it is less evident how state-mixing or crossing should occur between the ^{3}LMCT and ^5E, given the multiplicity change of two, it is probable that the initially formed FC ^{3}LMCT undergoes rapid intersystem crossing to yield the ^{5}LMCT[u]. This ^{5}LMCT could be strongly coupled to the ^5E, and the short lifetime could then be explained by the presence of the low-lying ^5E states. On the other hand, a scenario where most of the initially formed LMCT directly decays back to the ground state cannot be excluded – though, once again, it is not immediately obvious *why* this would be the case for this complex in particular.

We end this section by asking ourselves where such an analysis leaves the Mn^{III}, and if it might be worthwhile to characterize photophysically? Given that the Mn^{III} LMCT lies at substantially higher energy (~26000 cm^{-1}), and all other metal-centred apart from the ^5E states have been computed to lie above 30,000 cm^{-1}, one could consider such an investigation a worthwhile endeavour. The relatively energetically isolated Mn^{III} LMCT state could potentially have a long lifetime. Additionally, the Mn^{III} LMCT excited state, much like that of the Fe^{III}, presents the possibility of SB-CS, i.e. undergoing photoinduced charge-disproportionation to yield Mn^{II} and Mn^{IV}.

6.23 Fe^{II} and Co^{III} (d^6)

The final pair we consider are isoelectronic Fe^{II} and Co^{III}, both of which have a t_{2g}^6 configuration in the ground state. Starting with the former, it is worth noting that the Fe-NHC complex, where the NHC is btz (=3,3'-dimethyl-1,1'-bis(p-tolyl)-4,4'-bis(1,2,3-triazol-5-ylidene)), possesses a 100 ps ^{2}LMCT excited state for $[Fe^{III}(btz)_3]^{3+}$ and a 500 ps ^{3}MLCT for $[Fe^{II}(btz)_3]^{2+}$ - i.e. long-

[u] Of course, rapid intersystem crossing from ^{3}MLCT to $^5T_2$ is something we already saw in Chapter 1 with $[Fe(bpy)_3]^{2+}$ - so a direct deactivation may not be immediately ruled out.

lived excited states for two different oxidation states of the same complex, which is very interesting. The photofunctionality of the two was also recently demonstrated[140]. We learn that a naïve expectation by analogy should prove to be false for the scorpionate-NHC under study herein, not just for the Fe^{IV}, but also for the Fe^{II} – albeit for entirely different reasons. Data obtained for Fe^{II} is shown in Figure 6.23, which shows a ^{3}MLCT lifetime of ca. 7 ps.

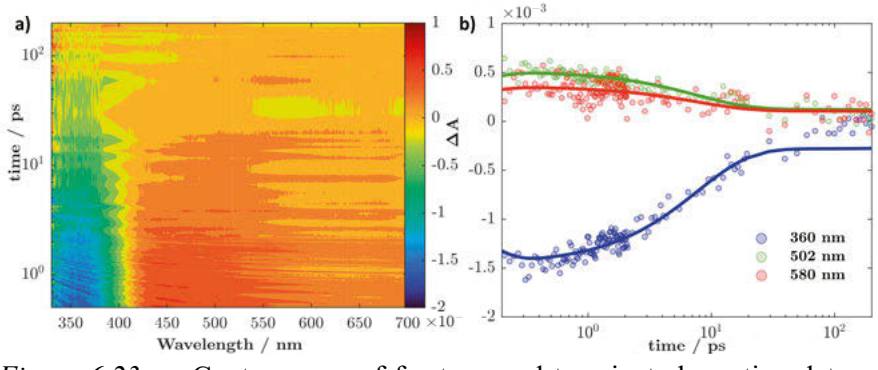

Figure 6.23. **a:** Contour map of femtosecond transient absorption data recorded for $[Fe^{II}L_2]$ (excitation wavelength = 400 nm, pulse energy = 0.56 µJ/pulse, absorption ≈ 0.3 at the excitation wavelength). **b:** Vertical cuts from a), showing the kinetics at selected wavelengths.

Depending on the benchmark, this may still be considered "long", but if the comparison is with the Fe^{III} ^{2}LMCT lifetime, this is three orders of magnitude shorter, quite unlike the Fe-btz. Part of the results may be explained by a lowered barrier for crossing to the ^{3}MC state (Paper X, not included in the thesis for brevity). However, it is notable that despite the use of inert conditions and a constant bias potential to avoid oxidation, the Fe^{II} gradually photodegraded under laser irradiation at 400 nm, making it difficult to obtain high quality data.

By contrast, if we look at Co^{III} – whose photophysics was reported in the literature[141] – it has been claimed that emission (λ_{max} = 690 nm, lifetime 0.8 µs in acetonitrile) can be observed from a ^{3}MC state, whose relaxed geometry is computed at an average Co-C bond elongation of nearly 20% – the latter can already be regarded as unusual given the observations made above, particularly regarding the relative rigidity of the ligand framework. Some remeasurements were made in the present thesis work to check the results, especially considering that both the TA and emission data in the original publication has only been reported at selected wavelengths. When using a CCD camera to measure the full spectral range, a large negative amplitude signal appears in the accessible 350–400 nm region during initial timescales from the first shot, which can be seen in Figure 6.24. As can be seen in panel c of Figure 6.11, Co^{III} only begins to absorb below 325 nm (that too with an extinction

coefficient of only ca. 400 $M^{-1}cm^{-1}$ at 307 nm, with substantial absorption only setting in below 300 nm). This is therefore not a ground-state bleach. Steady-state measurements show an emission in the region: the data is not shown, because it is unclear if this emission originates from the complex – even as the absorption does not change, excitation spectra which monitor this blue emission change upon irradiation, indicating that a potential photoproduct formed in the blue compensates for any lost absorption from the complex. The excitation spectra are included in the appendix.

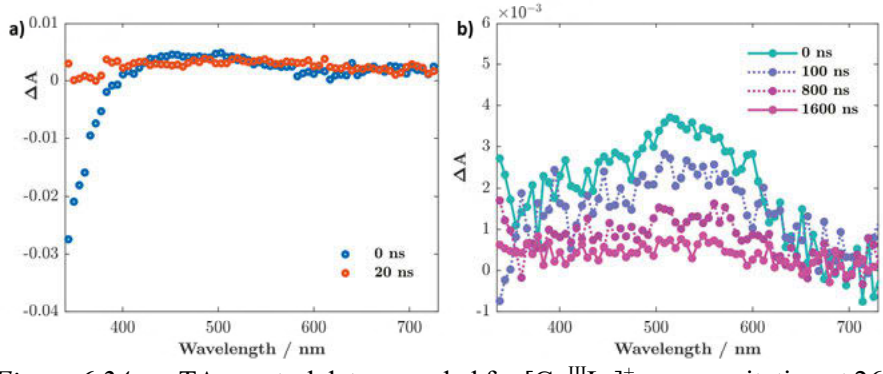

Figure 6.24. ns-TA spectral data recorded for $[Co^{III}L_2]^+$ upon excitation at 266 nm (pulse energy = 1 mJ/pulse). **a:** Single shot spectral traces collected at 0 and 20 ns without prior irradiation. Note that $[Co^{III}L_2]^+$ absorbs only below 300 nm, so this is not a ground state bleach. **b:** Long timescale transients in agreement with the published data measured using dielectric filters which measured kinetics in the range of 650 – 700 nm.

It is also worth pointing out that even in the original work, lifetime changes as large as 50% have been reported for different solvents (0.8 µs in acetonitrile, 1.6 µs in ethanol) – it is difficult to reconcile this solvent effect for a metal-centred state. On the other hand, the results would be perfectly compatible with photosubstitution chemistry that has been commonly observed in both $[Cr(CN)_6]^{3-}$ and $[Co(CN)_6]^{3-}$ in the past[142], among others[143–145]. A full explanation of the incompatible observations and the involved photochemistry will require a careful study, but that is not necessary to make the essential point that the Co^{III} complex is not as photostable as originally envisioned, and in that is quite unlike Fe^{III} and Mn^{IV}. This would make it rather similar in behaviour to isoelectronic Fe^{II} instead.

Ultimately, the relatively poor performance of the bis(carbene)borate framework with the d^6 configuration is perhaps rather simply understood when considering the simplified MO diagram shown in Figure 6.25. With a fully-filled t_{2g}, a high energy LMCT transition would necessarily populate metal orbitals with antibonding character. On the other hand, an MLCT transition would require that ligand-based π orbitals are populated. Unlike btz – which is

known to be both a strong sigma-donor and good π-acceptor – the bis(carbene)borate has poor π-accepting abilities, making it ill-suited to host MLCT transitions. We thus learn an important – if obvious – lesson that the paradigm routinely accessed in metal-polypyridyl which involves a fully-filled t_{2g} is incompatible with this ligand-set. But of course, this does not preclude the possibility of using other btz-like NHCs in a scorpionate framework to achieve a different outcome.

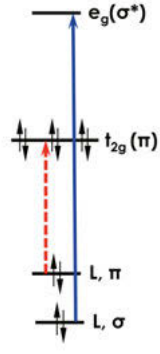

Figure 6.25. A simplified and truncated molecular orbital picture illustrating possible LMCT transitions when the t_{2g} orbitals are partially filled (dashed red) and when they are fully filled (solid blue).

7. Spectator NHCs in Brightly Shining organo-Au(I) Complexes

In the final part of our sojourn, we take a detour away from the scorpionate motif to take a look at a class of chromophores which hearken back – at least to some degree, if only by vague analogy – to the lakes mentioned in the introduction of this thesis. In modern times, Alizarin mostly enjoys photophysical attention as a model compound to study excited-state intramolecular proton transfer (ESIPT)[146,147]. As one would expect, the absorption (and emission) spectrum is fairly sensitive to pH, i.e. the protonation state of the dye. Substituents at the 1-position (capable of hydrogen bonding with the carbonyl) serve to bathochromically shift Alizarin's absorption (centred at ca. 430 nm); which is the same effect observed upon chelation with a metal[148]. Indeed, sometimes, the introduction of a metal can help to suitably modify the photophysical properties of an organic chromophore. The novel organo-Au(I) complexes that form the subject of this chapter exemplify such a situation, although protonation effects are certainly not involved. The structural motif can be seen in Figure 7.1.

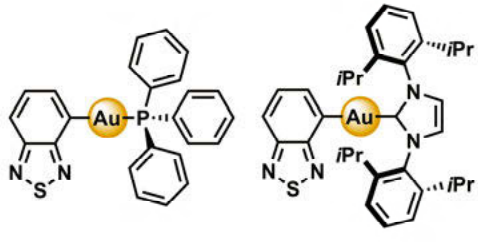

Figure 7.1. Representative structures of the linear organo-Au(I) complexes under investigation. The organic moiety is BTD (benzothiadiazole) while the auxiliary ligand is a phosphine (left) or N-heterocyclic carbene (right).

The photosensitivity of gold has been known from as far back as the early 1730s[149,150], where it was observed that 'invisible writing' on paper with a very dilute solution of gold in aqua regia took on a purple colour only upon light exposure. Surprisingly, the field of gold-based photophysics remained largely in hibernation until the pioneering work of Che and co-workers, who in 1989 first described the photoredox properties of a phosphorescent di-nuclear Au(I) complex[151]. Since then, a large body of work has focused on polynuclear Au(I) species[152–156], where the observed luminescence could often be

associated with the close Au—Au contacts (2.7–3.5 Å)[157] seen in crystal structures.[158] In the context of luminescent mononuclear gold complexes, however, perhaps the most well-known and investigated motif has been linear gold-alkynyls[159], which feature a bridging alkynyl unit between the gold atom and the organic chromophore. In 2017, Che et. al. reported a detailed characterization of several Au(I) (and Au(III)) complexes bearing this motif, with the former exclusively exhibiting fluorescence or delayed fluorescence phenomena at room temperature[160]. This study included alkynyl-bridged counterparts of the structures seen in Figure 7.1.

Meanwhile, the photophysics of complexes where an aryl moiety is directly bound to the gold – without an intervening alkynyl bridge, as those seen in Figure 7.1 – still remain relatively unexplored. A first report by Gray and coworkers emerged in 2007[161], where pyrenyl derivatives of Au(I) exhibited a pyrene-based ππ* phosphorescence at 77 K. More recently, Thompson et al. could observe both ILCT (inter-ligand charge transfer) and MLCT emissions in carbene-Au(I)-aryl complexes[162] at room temperature, and changing the electron donating strength of the aryl group allowed for tuning between the two emissive states. Thus, it can be interesting to investigate what happens if gold is directly bound to an electron-deficient unit such as BTD (benzothiadiazole) instead, *without* an intervening alkynyl bridge.

7.1 Excited State Energetics and Dynamics

The photophysical properties of the five complexes synthesized (two carbenes and three phosphines) were found to be largely similar (see Paper **IV** for details) – hence the title of the chapter.

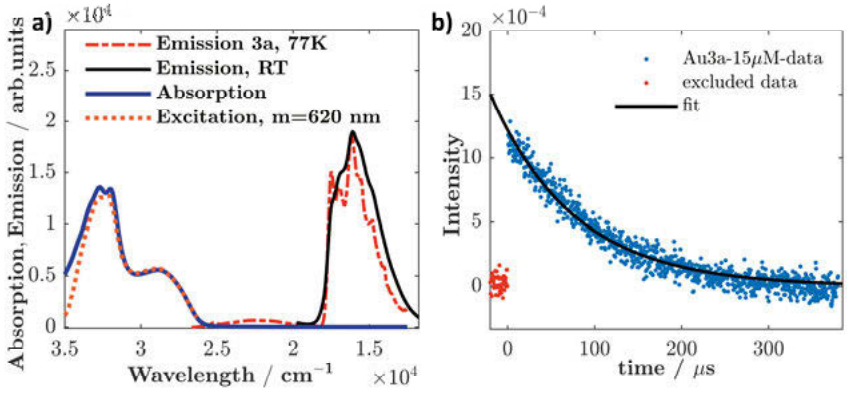

Figure 7.11. Representative photophysical data for complex **3a** recorded in 2Me-THF. **a:** Absorption, emission and excitation spectra as indicated in the legend. **b:** Time-resolved emission monitored at 620 nm (~16,000 cm^{-1}).

We will therefore limit ourselves to the discussion of the photophysical characteristics of one representative complex, **3a** (seen to the left of Figure 7.1 and photophysical data plotted in Figure 7.11; the corresponding carbene is shown in Paper **IV**). The absorption is characterized by two primary bands in the blue: a higher energy one centred at around 300 nm (33,000 cm^{-1}) and another one at ca. 350 nm (28,500 cm^{-1}). The former band is also present in unsubstituted BTD, while the latter is only present in the complex, i.e. it is a direct consequence of ligation with the gold. This observation somewhat contrasts with explanations invoked for the closest BTD-based alkynyl-bridged analogues reported by Che, mentioned previously[160]. In that case, the observed absorption was attributed to the dipole-allowed intraligand transitions of the arylacetylide ligands ($^1\pi\pi^*$(C≡CR)), with some charge-transfer character. Ligation with the gold was said to simply result in a bathochromic shift of the ^{1}IL band. However, given that the bridging alkynyl is entirely absent in this class of complexes, its involvement can be ruled out.

The origins of this lowest energy band are better understood when considering unsubstituted BTD's own transitions. Detailed spectroscopic analyses reported by Hollas[163] and others[164,165] have shown that while the strong band at 300 nm (33,000 cm^{-1}) is characterized by a $^1A_1 \leftarrow {}^1A_1$ transition, it tails off into a weaker band at ca. 328 nm which is formally $^1B_2 \leftarrow {}^1A_1$ (this is hardly visible in unsubstituted BTD's absorption spectrum, see Paper **IV**). About a fifth of this weak band's intensity was said to derive from the fully-symmetric ring contraction of the BTD, with b_2 vibrations also contributing and indulging in intensity stealing. It therefore stands to reason that introduction of gold at the para-position – or in Che's case, an alkynyl – should serve to perturb this transition: indeed, the spectral signatures observed for Che's ligand (without gold; i.e. BTD-alkynyl) are very similar to the ones observed for the complex here. Further support for such an analysis is found in a recent report which shows very weak phosphorescence in the solid state upon bromination of the BTD at the para positions[166].

Returning to the complexes under study here, excitation into this lowest energy band leads to bright orange luminescence in deaerated solutions; time-resolved emission measurements show lifetimes in the range of ~100 µs. The observed Stokes shift of ca. 12000 cm^{-1} further supports a triplet assignment. Quantum yields of phosphorescence lie between 3 to 6%. The observed vibrational progression bears resemblance to that reported for BTD's own extremely weak phosphorescence (only observed when deuterated or in halogenated solvents at 77K), suggesting that gold's large SOC promotes efficient population of BTD's triplet manifold. It may be worthwhile to contrast this observation of phosphorescence with the predominantly fluorescence and delayed fluorescence behaviour seen in the alkynyl-bridged counterparts reported by Che. Delayed fluorescence suggests formation of a triplet even in

the alkynyl-complexes. One possible reason that phosphorescence is observed here is that, in conjunction with a larger S-T gap (see computations in Paper **IV**), direct ligation of the gold to BTD results in a higher radiative rate constant.

7.2 Remarks

The introduction of a heavy metal atom has transformed a weak fluorophore into a room temperature phosphor, adding to the library of luminescent mononuclear Au(I) complexes. More formally, the observations made herein suggest that direct auration (at the appropriate position) in weak luminophores may allow for the construction of efficient phosphors with compact, robust structural motifs, which can find application where such properties are required (*e.g.* bio-imaging). Further, while in this study the role of the auxiliary ligand was minimal, it would be interesting to see what alternatives may be used to manifest greater electronic participation – and what new photophysical properties may emerge.

8. Epilogue

I've discovered the remains of Sinderion, an alchemist from Skingrad in Cyrodiil. He was exploring Blackreach in search of the Crimson Nirnroot, and appeared to be on the brink of an amazing discovery.

– "A Return To Your Roots", *The Elder Scrolls V: Skyrim, Dungeon Quest*

We have arrived at the end of our journey, dear reader, and if you are still here, then you are either supervisor, opponent or committee member – if *not*, however, something of worth may have been accomplished, after all. To recapitulate, we have acquainted ourselves with several bis(carbene)borate complexes. We first looked at a brightly fluorescent Fe(III)-carbene complex with a 2 ns ^{2}LMCT excited state. Owing to its unique electronic structure, this complex was also able to undergo optically triggered charge disproportionation with a significant driving force – and presents the first direct evidence for such a reaction in a TMC in the literature. We have also investigated the related Mn(IV)-complex, whose 16 ns long-lived ^{2}LMCT excited state happens to be dark, and also a potent photo-oxidant. Finally, having exhausted ourselves with a mess of metal-centred states, we have moved to the d^{10} configuration with benzothiadiazole-Au(I)-carbenes and phosphines, where ligation of the gold to the very weakly fluorescent heteroarene results in room temperature phosphorescence deriving from its triplet.

At the end of any journey, two key questions arise, "Have we reached our destination?" and, "Where to from here?". Both questions have contextual answers, best determined from the intended goal. Purely in terms of accessible photoinduced redox chemistry, the aims seem to have not only been met, but exceeded: for instance, the excited state potential of Mn(IV)-carbene (ca. 2 V vs. SCE) and also that of Fe(III)-carbene (1.35 V vs. SCE) already exceeds that of well-known photosensitizers such as $(Ir[dF(CF_3)ppy]_2(dtbpy))PF_6$ (+1.26 V vs. SCE)[167]. While this thesis has only demonstrated the first electron transfer reactivity step, it has been shown already for Fe(III)-carbene that it may be employed for useful photoredox transformations, that too with high yields. There are also other examples of first-row based excited states successfully accomplishing chemical transformations of utility[48]. The difficulty of mechanistic delineation, or the conditions (e.g. high quencher

concentrations) which the relatively short nanosecond lifetimes may impose, can be thought to not hinder the chemist engaged in more practical pursuits.

Of course, one may definitely seek to increase the lifetime to mimic excited states based on heavier metals in every aspect – for a number of reasons, not the least of which is doing so simply *because we can*. And so we have somewhere to go at the end of our journey: but how do we get there? The straightforward thing to think about is how we may modify the scorpionate motif we have used so far. In recent work carried out[168], coherences were thought to be diagnostic for what vibrations should be selectively targeted and hindered in the ligand framework in order to enhance the charge-transfer lifetime. It must be noted, however, that it is difficult to judge if the improved lifetime in the cage complex was a consequence of mode-specific effects as guided from coherence data vs. the general hindering effect of rigidity on vibrations. More importantly, for complexes such as the ones investigated here which already have lifetimes in the nanosecond regime, coherences may be too short-lived to prove useful diagnostics of vibronic deactivation pathways *or* the expected vibrational modes may lie in low-frequency regions where selective targeting may be difficult to do. And this is all under the assumption that the product state be unequivocally spectrally resolved from the reactant state to begin with, which may not be true for several transition-metal complexes.

Relying, therefore, for the moment on more traditional approaches, the collected data set at least putatively points to the fact that the rigidity of the scorpionate ligand predisposes it to favouring certain sizes – i.e. metals – for better orbital overlap. We have further seen that there may *still* be an advantage to be gained in making the ligand less flexible to further slow down non-radiative decay. Better π-accepting properties could also be desirable for the potential stabilization of MLCT excited states. Since substitutions on the boron or the phenyl have no bearing on the photophysics due to low electronic coupling[106], there must be an alteration within the carbene framework. A potential candidate which may fulfil all these criteria already exists: tris(benzimidazol-2-ylidene)borate[169]. Although it is a slightly weaker sigma-donor (yet only second to the ligand studied here), it may nevertheless stabilize metal-centred states sufficiently, while at the same time imparting the aforementioned advantages in-tandem. We could also be more radical, and advocate for the construction of a new scorpionate motif – one based on a CAAC (cyclic alkyl amino carbene) instead of an NHC[v], since the former are known to be both better sigma-donors as well as π-acceptors than the latter[170]. CAACs of course have been implemented to great success in realizing Cu-based ILCT emitters where non-radiative decay is shut-off entirely[171]. However, so far, mostly linear motifs exist for other metals, e.g. Fe(0)[172–174].

[v] some people consider the CAAC as an NHC variant inasmuch as it still contains a nitrogen

On the matter of metal-centred states, it is indeed the case that photochemical activity has been reported, even from low-lying, short-lived ones such as those of $[Fe(bpy)_3]^{2+}$[45]. Raised sufficiently in energy, they may become even more photochemically relevant – while the idea is an interesting one, it is important to acknowledge the possibility of ligand lability when some of these states get populated. Another remark can be made: while the octahedron is the favoured motif over a tetrahedron from a ligand-field perspective ($\Delta_t = 4/9\Delta_o$), for exploiting metal-centred states, a tetrahedral geometry could be worthwhile in terms of having greater intensity (d-d transitions are orders of magnitude more intense in tetrahedral complexes due to orbital mixing of metal p and d orbitals). In fact, from an intensity stealing perspective, non-octahedral geometries are more interesting – though other disadvantages are duly acknowledged.

In closing, whether the future is dark or bright remains to be seen – but with the spirit of curiosity of the spectroscopist and the creativity of the synthetic chemist, a never-ending adventure is guaranteed.

Popular Scientific Summary

The colours all around you are a consequence of light interacting with matter – the colours which are not absorbed or the ones which are emitted are the ones you see. This thesis, too, engenders a world of colour: it tries to understand what happens when visible light in particular is absorbed by a somewhat specific type of matter, called a transition-metal complex (TMC). TMCs usually consist of a metal centre which has formed bonds with other groups of molecules that are called "ligands" (from Latin, *ligare*, "to bind"). With different metals and ligands, the types of complexes accessible are practically infinite – it is all about creativity! We can make an attempt to classify and categorize complexes for ease of study, but in the end, each one of them is quite unique, and in that we may as well regard them as a beautiful people. Absorbing light makes complexes go to a higher energy level, something referred to as an 'excited state'. Indeed, depending on metal and ligand, a particular complex after absorbing light can do all sorts of things: it can emit light of a different colour, it can convert the light energy to separated charges like a little battery (only for some time, though!), it could even give away this charge to another molecule in the surrounding, or it can just dump the energy away as heat. For a long time, complexes based on earth-abundant metals – particularly those of iron – have only been capable of the last outcome: if at all they separate charges using light, this is done for a very *very* short time, and they most definitely do not glow.

The key finding of this thesis is that certain complexes of iron and manganese *can* achieve the above outcomes. This has been made possible by binding these metals to a special type of ligand. In fact, the ligand looks like a Scorpion, and that is what inspires the cover of this thesis. The two 'claws' and 'tail' attach themselves to the metal, and a metal can bind to two Scorpions, resulting in a cage-like structure, which is very stable. With the help of laser-based spectroscopic techniques an attempt has been made to understand what exactly happens in these complexes after they absorb light, and document their properties. The use of lasers is necessary because the events which follow light absorption are extremely fast – about a billion times faster than the blink of an eye! So very short laser pulses must be used to both excite and monitor the excited states of complexes: we cannot measure anything shorter than the least count of our ruler, after all. What are some interesting properties of these

complexes? Briefly, after absorbing light, the iron complex glows orange at room temperature, and it also separates charges long enough in order to be harvested. The manganese complex does not glow, but its capacity to give away charges to other molecules after absorbing is beyond that seen in most metal-based complexes. Some gold complexes have also been studied in this thesis, which also emit bright orange light at room temperature. They actually do so for a long time unlike the iron complex – they are phosphorescent, like glow sticks. This is made possible by attaching a gold metal atom to another molecule, and this time, it is the metal atom which gives rise to the shine! In the end though, in all cases, by assembling metals and other groups of atoms, i.e. “ligands” like little puzzle pieces, some fascinating results have been achieved.

Svensk Sammfattning

Färgerna runt omkring dig är en konsekvens av ljus som interagerar med materia – de färger som inte absorberas är de som du ser. Denna avhandling framkallar också en värld av färg: den försöker förstå vad som händer när synligt ljus absorberas av en specifik typ av materia, kallad ett övergångsmetallkomplex (*eng.* transition metal complex, TMC). TMC:er består vanligtvis av ett metallcentrum som har bildat bindningar med andra grupper av molekyler som kallas "ligander" (från latin, ligare, "att binda"). Med olika metaller och ligander är de tillgängliga typerna av komplex praktiskt taget oändliga - det handlar bara om kreativitet! Vi kan försöka klassificera och kategorisera komplex för att förenkla att studera dem, men i slutändan är var och en av dem ganska unik, och i det avseendet kan vi lika gärna betrakta dem som vackra individer. Att absorbera ljus får komplex att gå till en högre energinivå, något som kallas "exciterat tillstånd". Beroende på metall och ligand kan ett specifikt komplex, efter att ha absorberat ljus, göra alla möjliga saker. Det kan till exempel avge ljus av en annan färg, det kan omvandla ljusenergin till separerade laddningar som ett litet batteri (bara under en viss tid, dock!), det kan till och med överföra denna laddning till en annan molekyl i närheten, eller så kan det helt enkelt avge energin som värme. Under lång tid har komplex baserade på jordens vanligt förekommande metaller - särskilt järn - bara varit kapabla att nå det sista utfallet: om de överhuvudtaget separerar laddningar med hjälp av ljus, görs detta under en mycket kort tid, och de lyser definitivt inte.

Huvudresultatet av denna avhandling är att vissa komplex av järn och mangan kan uppnå flera av ovanstående utfall. Detta har gjorts möjligt genom att binda dessa metaller till en särskild typ av ligand. Faktum är att liganden ser ut som en skorpion, och det är det som inspirerar omslaget på denna avhandling. De två "klorna" och "svansen" fäster sig vid metallen, och en metall kan binda till två skorpioner, vilket resulterar i en burliknande struktur som är mycket stabil. Med hjälp av laserspektroskopiska tekniker har ett försök gjorts att förstå vad som exakt händer i dessa komplex efter att de absorberar ljus, och dokumentera vilka egenskaper de har. Användningen av laser är nödvändig eftersom händelserna som följer efter ljusabsorption är extremt snabba - ungefär en miljard gånger snabbare än ett öga kan blinka! Därför måste mycket korta laserpulser användas för att både excitera och studera de exciterade tillstånden hos komplexen, vi kan trots allt inte mäta något kortare än upplösningen på vår

linjal. Vad är då några intressanta egenskaper hos dessa komplex? Kort sagt, efter att ha absorberat ljus, lyser järnkomplexet orange vid rumstemperatur, och det separerar också laddningar tillräckligt länge för att kunna utnyttjas. Mangan-komplexet lyser inte, men dess förmåga att överföra laddningar till andra molekyler efter absorption överskrider det som ses i de flesta metallerbaserade komplex. I här avhandlingen har också vissa guldkomplex studerats vilka också sänder ut orange ljus vid rumstemperatur. Detta sker under lång tid, till skillnad från järnkomplexet, då guldkomplexen är fosforescerande, som lysstavar. Detta är möjligt genom att fästa en guldmetallatom till en annan molekyl, och den här gången är det metallatomen som ger upphov till ljuset! I slutändan har fascinerande resultat uppnåtts genom att sätta samman metaller och ligander, precis som små pusselbitar.

शोध-निबंध का सहज सारांश

आपके चारों ओर के रंग प्रकाश के पदार्थ के साथ अंतःक्रिया का परिणाम हैं - जो रंग अवशोषित नहीं होते हैं वे ही हैं जो आपको दिखाई देते हैं। यह शोध-निबंध भी इसी रंगो के संसार के बारे में है। इसके अंतर्गत यह समझने का प्रयास किया गया है की विशेष रूप से, दृश्यमान प्रकाश जब विशिष्ट प्रकार के पदार्थ द्वारा अवशोषित होता है, तब क्या होता है? यह विशेष पदार्थ हैं मध्य-धातु यौगिक, जिन्हें अगल भाषा में 'ट्रांजीशन मेटल काम्प्लेक्स', यानि टीएमसी कहा जाता ह। मध्य-धातु यौगिक में सामान्य रूप से एक धातु केंद्र होता है जो अणुओं के अन्य समूहों के साथ बंधन बनाता है जिन्हें "लिगैंड" कहा जाता है (यह शब्द लैटिन से लिया गया है, जिसका अर्थ होता है, "बंधन करना")। विभिन्न धातुओं और लिगेंड्स के साथ, सुलभ यौगिकों के प्रकार व्यावहारिक रूप से अनंत हैं - इनकी सीमा केवल हमारी रचनात्मकता पर निर्भर है! हम अध्ययन में आसानी के लिए इन परिसरों को वर्गीकृत करने का प्रयास कर सकते हैं, परन्तु अंत में, प्रत्येक अद्वितीय है, और इस दृष्टिकोण से यह यौगिक मूल्य-रूप से विभिन्न और सुन्दर मनुष्यों के सामान हैं! प्रकाश को अवशोषित करने से यौगिक उच्च ऊर्जा स्तर पर चले जाते हैं, जिसे 'ऊर्जा-पूर्ण अवस्था' कहा जाता है।

धातु और लिगैंड के आधार पर, प्रकाश को अवशोषित करने के बाद एक विशेष यौगिक अन्य प्रकार की प्रक्रियाओं का सृजन कर सकता है: यह एक अलग रंग की रोशनी उत्सर्जित कर सकता है, यह प्रकाश ऊर्जा को एक छोटी बैटरी की तरह अलग-अलग विद्युत्-आवेश में परिवर्तित कर सकता है (परन्तु कुछ समय के लिए ही!), यह उत्पन्न किये गए विद्युत्-आवेश को आसपास के किसी अन्य अणु को भी दे सकता है, या यह ऊर्जा को गर्मी के रूप में त्याग सकता है। लंबे समय से, पृथ्वी-प्रचुर धातुओं पर आधारित यौगिक - विशेष रूप से लोहे के - केवल अंतिम परिणाम में ही सक्षम रहे हैं: यदि वे प्रकाश का उपयोग करके विद्युत्-आवेश को विभक्त कर भी पाते हैं, तो यह बहुत ही अल्पायु के लिए किया जाता है, और वह ऊर्जा को पुनः प्रकाश के रूप में तो कदापि परिवर्तित नहीं कर पाते हैं।

इस अनुसन्धान का मुख्य निष्कर्ष यह है कि लोहे और मैंगनीज (एक सूरमे के प्रकार की धातु) के कुछ यौगिक उपरोक्त लिखे परिणामों को प्राप्त करने में सक्षम हैं। यह इन धातुओं को एक विशेष प्रकार के लिगैंड से बांधकर संभव बनाया गया है। वास्तव में, लिगेंड एक बिच्छू की तरह दिखता है, और इस किताब के आवरण पर प्रदर्शित चित्र उसी से प्रेरणा लेकर बनाया गया है। इस बिच्छू समान लिगैंड के दो 'पंजे' और 'पूंछ' धातु से बंधन बनाते हैं, और एक धातु के साथ दो बिच्छू बंधन करते है। इसके परिणामस्वरूप एक पिंजरे जैसी संरचना बनती है, जो अत्यधिक अचल होती है।

प्रकाश की स्पन्द किरणों (जिसको लेज़र कहा जाता है) के उपयोग द्वारा यह समझने का प्रयास किया गया है कि प्रकाश को अवशोषित करने के बाद इन यौगिकों में वास्तव में क्या होता है? उनमें क्या गुण हैं, इसकी व्याख्या भी की गई है। लेज़रों का उपयोग आवश्यक है क्योंकि प्रकाश अवशोषण के बाद होने वाली घटनाएँ अत्यधिक तीव्र होती हैं - पलक झपकने से लगभग एक अरब गुना गति! इसलिए अति न्यून प्रकाश स्पन्दों का उपयोग आवश्यक है, यौगिकों को ऊर्जा-पूर्ण स्थिति में ले जाने के लिए भी, और उस अवस्था की जांच करने के लिए भी। इस विचार को इस प्रकार समझा जा सकता है - हम किसी उपकरण की सबसे छोटी भुजा से भी छोटे आयाम को नहीं माप सकते। उसी प्रकार से हम तीव्र घटनाओं को मापने के लिए अति-तीव्र प्रकाश की किरणों का उपयोग करते हैं।

इन यौगिकों के कुछ विशेष गुण क्या हैं? संक्षिप्त में, प्रकाश को अवशोषित करने के बाद, लोहे का परिसर सामान्य तापमान पर नारंगी रंग के प्रकाश का उत्सर्जन करता है, और यह विद्युत्-आवेश को पर्याप्त समय के लिए विरक्त भी करता है, जिससे उसका उपयोग किया जा सके। मैंगनीज यौगिक प्रकाश उत्सर्जन में सक्षम नहीं हैं, परन्तु विद्युत्-आवेश विरक्त करने की इसकी क्षमता अधिकांश धातु-आधारित यौगिकों से सर्वोच्च है। इस शोध-निबंध में कुछ सोने के यौगिकों का भी अध्ययन किया गया है, जो सामान्य तापमान पर अति उज्जवल नारंगी रोशनी उत्सर्जित करते हैं। वे वास्तव में लौह यौगिक की तुलना में लंबे समय तक यह प्रकाश देते हैं - कुछ कुछ दिवाली की फुलझड़ी की तरह! यह एक सोने की धातु के परमाणु को दूसरे अणु से संग्रह द्वारा संभव हुआ हैं। अंततः हम यह कह सकते हैं की धातुओं और परमाणुओं के अन्य समूहों, यानी "लिगैंड्स", को छोटी पहेली के भागों की तरह एकत्रित करके, कुछ रोचक परिणाम प्राप्त किए गए हैं।

Acknowledgements

A thesis can only be written standing on the shoulders of giants. So, before anything, to all researchers from past to present, who have taught me, helped me, and inspired me – from near or far – I am in your debt. None mentioned, none forgotten as the Danish saying goes. Having said that…

Leif, for a performance *par excellence* in your role as supervisor: both plaudits and gratitude are due (*cf.* below).

Christer, for unswerving support all these years – without your encouragement, I would have never touched a laser.

Jeremy, your creation is the genesis of this thesis – thank you for trusting me with your complexes, an honour which I hope to continue to have for a long time to come.

Mauricio, thank you for loaning me your shiny gold creations to play with – and perhaps more importantly, thank you for everything else: from your invaluable friendship to the beautiful structures in this thesis, and your fantastic support throughout.

Om and **Kenneth**, thank you for entrusting me with your complexes, and the shared work on several publications.

Reiner, for introducing me to molecular photophysics and the shared work on several publications.

Thank you to all my co-authors, without whom the work was not possible. Thanks also to everyone in Hus 7 for maintaining a warm and collegial environment for doing research. **Sven**, in particular, the soul of Hus 7, as many would agree…

Vincent and **Luca**, for training me on the nanosecond system, and helpful advice always at the ready. Vincent especially, for grounding in me the importance of asking the right questions – and always staying in touch!

Julian and **Yocefu**, for training me on the femtosecond system, for very involved discussions about the intricacies of laser physics, data analysis, and much more… You two are still the ones I look up to as the gold standard for attention to detail and conceptual rigour. Your friendship is deeply valued.

Lei and **Robin**, for all our endless, incessant arguing which really trained my thinking – and for our friendship which always emerged victor.

Hans, for getting me deeply interested in molecular chemical physics. **Anders**, for taking the time to discuss physical inorganic chemistry with me: those were some of the best conversations I have had in my time here.

SoFiA team, for showing me the wonders and beauty of a truly multidisciplinary collaboration – much I have learned from all of you exploring the world of soap bubbles.

My students, for making me really think before I speak. **Ludmiła**, for being the perfect first student I had the joy to supervise.

Members of **WineClub**, present and past: those intense discussions have been the lifeblood of academic and personal growth. **Salauat**, for your care and understanding. **Martin**, my PhD-twin, for the many philosophical exchanges. **Belinda**, for the many laughs and engaging conversations. **Samir**, for being the most affable officemate. **Andrew**, for dealing with permanent desk annexation, and everything else. **Giorgio**, for the shared love of the history of science and the many fascinating discussions we have had. **Helena**, thank you for the translation notes of Werner's original paper. **Rima**, my diligent, cheerful nanosecond companion, I have had much fun opening up the laser with you. **Beri**, for all your help whenever needed, and our engaging discussions: academic or otherwise. **Andjela**, for being a care-bear, for all our times good and bad, but most especially for your genuineness and friendship.

Andrea, for being my ever-ready discussion companion for not just *everything* photophysics, but really everything. I am grateful for your penetrating insight into many matters, and your generosity. Thank you for great feedback and proofing my thesis at absurdly short notice.

My favorite seniors: **Starla**, without you, I would not have taken some very important decisions. Thank you for always standing beside me and providing sound advice. **Michał**, the only qualm I have is that we did not meet sooner. Thank you so much for patiently teaching me everything about 2D spectroscopy and taking the frazzled final year PhD student in stride – I look forward to a long future collaboration. **Jacinto**, for being incredibly supportive and understanding of my strong personality, for trusting me with some of your

projects and always offering a listening ear. I am very grateful. **Malin**, your creativity and dedication to science, always with a smile on your face, is an inspiration. Thank you for all the nice times together.

Lea, all these years later, and our connection has grown into something special. Thank you for your ever-ready understanding and advice. **Brigi**, practically my big sister: thank you for the amazing vegetarian food, the care, and patience you have had with me over the years, and everything we have shared.

Astrid, you are an amazing human being – I am so glad we met. Thank you for the wonderful friendship and connection, and of course for the scientific summary in Swedish.

Yocefu, **Aijie**, and **João** – thank you for being like family for two years, and your invaluable contribution to my personal and professional development. I will always cherish our time spent together and our friendship. Until we meet again.

Ben and **Hemlata**, my two most precious takeaways from Uppsala – thank you for effectively being a second set of parents to me. To many adventures to come!

Yocha, and everyone there – without the safe haven you offered me, I would not have been able to write this thesis. I will miss you all dearly, I wish we met sooner.

And once again, **Leif**… relegating you to the bottom half of this section is the highest form of gratitude I have to offer. Thank you for *everything*, especially for looking after me all these years during difficult times, academically and otherwise. This journey would be impossible to finish without your tireless support.

Mom and **Dad**, for loving me unconditionally – by far the hardest part of all this has been to be away from you, and I can only wonder if it has been worth it.

Bhaiya – chronological senior and astral twin – you are the source of the physical, emotional, and financial security that enables my creativity. Thank you for always being there, and reminding me of what is truly important in life.

सर्वो वै रुद्रतस्मै रुद्राय मम सर्वं समर्पयामि॥

References

1. Kauffman, G. B. The Discovery of Optically Active Coordination Compounds: A Milestone in Stereochemistry. *Isis* **66**, 38–62 (1975).
2. Kauffman, G. B. Coordination Chemistry: History. in *Encyclopedia of Inorganic and Bioinorganic Chemistry* (John Wiley & Sons, Ltd, 2011).
3. *Coordination Chemistry, A Century of Progress*. Edited by George B. Kauffman. ACS Symposium Series **565** (American Chemical Society, 1994). This text together with the references contained within is perhaps the most comprehensive documentation of the history of coordination chemistry (from 1800s to 1993) available in the literature.
4. Kragh, H. S. M. Jørgensen and His Controversy with A. Werner: A Reconsideration. *The British Journal for the History of Science* **30**, 203–219 (1997).
5. Kauffman opines that there is a high probability that animal matter (incl. bones and blood) and potash were heated together in antiquity to form ferricyanides – these were probably just not isolated.
6. Lippert, W. Gmelin's Handbook of Inorganic Chemistry. *J Chem Doc* **10**, 174–180 (1970).
7. Leopold Gmelin pioneered the concept of the objective chemical database, by publishing his 'Handbook of Chemistry' in 1817.
8. Gibbs, W. & Genth, F. A. Researches on the Ammonia-Cobalt Bases. *American Journal of Science and Arts* **24**, (1856).
9. Werner, A. Beitrag zur Konstitution anorganischer Verbindungen. *Zeitschrift für anorganische Chemie* **3**, 267–330 (1893).
10. Morgan, G. T. & Burstall, F. H. *Inorganic Chemistry: A Survey of Modern Developments*. (w. Heffer & sons Limited, 1936).
11. Blau, F. Die Destillation pyridinmonocarbonsaurer Salze. *Berichte der deutschen chemischen Gesellschaft* **21**, 1077–1078 (1888).
12. Constable, E. C. & Housecroft, C. E. The early years of 2,2'-bipyridine — A ligand in its own lifetime. *Molecules* **24**, 1–38 (2019).
13. Blau, F. Über die trockene Destillation von pyridincarbonsauren Salzen. *Monatshefte für Chemie und verwandte Teile anderer Wissenschaften* **10**, 375–388 (1889).
14. Blau, F. Über neue organische Metallverbindungen. *Monatshefte für Chemie und verwandte Teile anderer Wissenschaften* **19**, 647–689 (1898).
15. Werner, A. Über Spiegelbild-Isomerie bei Eisenverbindungen. *Berichte der deutschen chemischen Gesellschaft* **45**, 433–436 (1912).

16. Wyckoff, R. W. G. & Posnjak, E. The Crystal Structure of Ammonium Chloroplatinate. *J Am Chem Soc* **43**, 2292–2309 (1921).
17. Dickinson, R. G. The Crystal Structures of Potassium Chloroplatinite and of Potassium and Ammonium Chloropalladites. *J Am Chem Soc* **44**, 2404–2411 (1922).
18. Yamasaki, K. Absorptionsspektren von Metallkomplexsalzen des 2,2′-Dipyridyls. I. *Bull Chem Soc Jpn* **12**, 390–394 (1937).
19. Burstall, F. H. 34. Optical activity dependent on co-ordinated bivalent ruthenium. *Journal of the Chemical Society (Resumed)* 173–175 (1936).
20. Miller, R. R., Brandt, W. W., Puke, M. Sr. & Puke, O. S. F. Metal-Amine Coördination Compounds. V. The Ruthenium-2,2'-Bipyridine System1,2,3. *J Am Chem Soc* **77**, 3178–3180 (1955).
21. Arias-Rotondo, D. M. The fruit fly of photophysics. *Nat Chem* **14**, 716 (2022).
22. Ballhausen, C. J. & Gray, H. B. The Electronic Structure of the Vanadyl Ion. *Inorg Chem* **1**, 111–122 (1962).
23. Gray, H. B. & Beach, N. A. The Electronic Structures of Octahedral Metal Complexes. I. Metal Hexacarbonyls and Hexacyanides. *J Am Chem Soc* **85**, 2922–2927 (1963).
24. Tanabe, Y. & Sugano, S. On the Absorption Spectra of Complex Ions. I. *J Physical Soc Japan* **9**, 753–766 (1954).
25. Tanabe, Y. & Sugano, S. On the Absorption Spectra of Complex Ions II. *J Physical Soc Japan* **9**, 766–779 (1954).
26. Paris, J. P. & Brandt, W. W. Charge Transfer Luminescence of a Ru(II) Chelate. *J Am Chem Soc* **81**, 5001–5002 (1959).
27. Bolletta, F., Maestri, M., Moggi, L. & Balzani, V. Dynamic and static quenching of the tris(2,2'-dipyridyl)ruthenium(II) phosphorescence by anionic coordination compounds in various solvents. *J Phys Chem* **78**, 1374–1377 (1974).
28. Bock, C. R., Meyer, T. J. & Whitten, D. G. Electron transfer quenching of the luminescent excited state of tris(2,2'-bipyridine)ruthenium(II). Flash photolysis relaxation technique for measuring the rates of very rapid electron transfer reactions. *J Am Chem Soc* **96**, 4710–4712 (1974).
29. Low, K. S., Cole, J. M., Zhou, X. & Yufa, N. Rationalizing the molecular origins of Ru-and Fe-based dyes for dye-sensitized solar cells. *Acta Crystallogr B* **68**, 137–149 (2012).
30. Damrauer, N. H. *et al.* Femtosecond Dynamics of Excited-State Evolution in $[Ru(bpy)_3]^{2+}$. *Science* **275**, 54–57 (1997).
31. Decurtins, S., Felix, F., Ferguson, J., Gudel, H. U. & Ludi, A. The Electronic Spectrum of $Fe(bpy)_3^{2+}$ and $Os(bpy)_3^{2+}$. *J Am Chem Soc* **102**, 4102–4106 (1980).
32. Ferguson, J. & Herren, F. The Electronic Structure of the Metal-to-Ligand Charge-Transfer States of $M(bpy)^{2+}$ (M = Fe, Ru, Os). *Chemical Physics Letters* **89**, 371–375 (1982).

33. Yersin, H. et. al. Low-lying Electronic States of $[Rh(bpy)_3]^{3+}$, $[Pt(bpy)_2]^{2+}$ and $[Ru(bpy)_3]^{2+}$. A comparative study based on highly-resolved and time-resolved spectra. *Coord Chem Rev* **159**, 325–358 (1997).
34. Gawelda, W. *et al.* Ultrafast nonadiabatic dynamics of $[Fe^{II}(bpy)_3]^{2+}$ in solution. *J Am Chem Soc* **129**, 8199–8206 (2007).
35. Monat, J. E. & McCusker, J. K. Femtosecond Excited-State Dynamics of an Iron(II) Polypyridyl Solar Cell Sensitizer Model. *J Am Chem Soc* **122**, 4092–4097 (2000).
36. Wolf, M. M. N. *et al.* Sub-picosecond time resolved infrared spectroscopy of high-spin state formation in Fe(ii) spin crossover complexes. *Physical Chemistry Chemical Physics* **10**, 4264–4273 (2008).
37. Consani, C. *et al.* Vibrational Coherences and Relaxation in the High-Spin State of Aqueous $[Fe^{II}(bpy)_3]^{2+}$. *Angewandte Chemie International Edition* **48**, 7184–7187 (2009).
38. Cammarata, M. *et al.* Sequential Activation of Molecular Breathing and Bending during Spin-Crossover Photoswitching Revealed by Femtosecond Optical and X-Ray Absorption Spectroscopy. *Phys Rev Lett* **113**, 227402 (2014).
39. Bressler, Ch. *et al.* Femtosecond XANES Study of the Light-Induced Spin Crossover Dynamics in an Iron(II) Complex. *Science* **323**, 489–492 (2009).
40. Zhang, W. *et al.* Tracking excited-state charge and spin dynamics in iron coordination complexes. *Nature* **509**, 345–348 (2014).
41. Auböck, G. & Chergui, M. Sub-50-fs photoinduced spin crossover in $[Fe(bpy)_3]^{2+}$. *Nat Chem* **7**, 629–633 (2015).
42. Oppermann, M., Zinna, F., Lacour, J. & Chergui, M. Chiral control of spin-crossover dynamics in Fe(II) complexes. *Nat Chem* **14**, 739–745 (2022).
43. Jiang, Y. *et al.* Direct observation of nuclear reorganization driven by ultrafast spin transitions. *Nat Commun* **11**, 1530 (2020).
44. Dongare, P., Myron, B. D. B., Wang, L., Thompson, D. W. & Meyer, T. J. *$[Ru(bpy)_3]^{2+}$ revisited. Is it localized or delocalized? How does it decay? *Coordination Chemistry Reviews* **345**, 86–107 (2017).
45. Gualandi, A. *et al.* Organocatalytic Enantioselective Alkylation of Aldehydes with $[Fe(bpy)_3]Br_2$ Catalyst and Visible Light. *ACS Catal* **5**, 5927–5931 (2015).
46. Parisien-Collette, S., Hernandez-Perez, A. C. & Collins, S. K. Photochemical Synthesis of Carbazoles Using an $[Fe(phen)_3](NTf_2)_2/O_2$ Catalyst System: Catalysis toward Sustainability. *Org Lett* **18**, 4994–4997 (2016).
47. Wenger, O. S. Is Iron the New Ruthenium? *Chemistry - A European Journal* **25**, 6043–6052 (2019).
48. Wenger, O. S. Photoactive Complexes with Earth-Abundant Metals. *J Am Chem Soc* **140**, 13522–13533 (2018).
49. Wegeberg, C. & Wenger, O. S. Luminescent First-Row Transition Metal Complexes. *JACS Au* **1**, 1860–1876 (2021).

50. Larsen, C. B. & Wenger, O. S. Photoredox Catalysis with Metal Complexes Made from Earth-Abundant Elements. *Chemistry - A European Journal* **24**, 2039–2058 (2018).
51. McCusker, J. K. Electronic structure in the transition metal block and its implications for light harvesting. *Science* **363**, 484–488 (2019).
52. Zederkof, D. B. *et al.* Resolving Femtosecond Solvent Reorganization Dynamics in an Iron Complex by Nonadiabatic Dynamics Simulations. *J Am Chem Soc* **144**, 12861–12873 (2022).
53. Griffiths, D. J. & Schroeter, D. F. *Introduction to Quantum Mechanics*. (Cambridge University Press, 2018).
54. Dirac, P. A. M. *The Principles of Quantum Mechanics*. (Oxford University Press, 1930).
55. Inorganic Photochemistry Symposium Conference Proceedings, held at the ACS meeting, Seattle, 1983. *J Chem Educ* **60**, 783–913 (1983).
56. Kettle, S. F. A. *Physical Inorganic Chemistry: A Coordination Chemistry Approach*. (Springer Berlin Heidelberg, 2013).
57. Balzani, V., Juris, A. & Ceroni, P. *Photochemistry and Photophysics: Concepts, Research, Applications*. (WILEY-VCH, 2014).
58. Kitzmann, W. R., Moll, J. & Heinze, K. Spin-flip luminescence. *Photochemical and Photobiological Sciences* **21**, 1309–1331 (2022).
59. Marcus, R. A. On the Theory of Oxidation-Reduction Reactions Involving Electron Transfer. I. *J Chem Phys* **24**, 966–978 (1956).
60. Carey, M. C., Adelman, S. L. & McCusker, J. K. Insights into the excited state dynamics of Fe(ii) polypyridyl complexes from variable-temperature ultrafast spectroscopy. *Chem Sci* **10**, 134–144 (2019).
61. Trofimenko, S. *Scorpionates: The Coordination Chemistry Of Polypyrazolylborate Ligands*. (World Scientific Publishing Company, 1999).
62. Trofimenko, S. Polypyrazolylborates: Scorpionates. *J Chem Educ* **82**, 1715 (2005).
63. Forshaw, A. P. *et al.* Low-Spin Hexacoordinate Mn(III): Synthesis and Spectroscopic Investigation of Homoleptic Tris(pyrazolyl)borate and Tris(carbene)borate Complexes. *Inorg Chem* **52**, 144–159 (2013).
64. Nelson, D. J. & Nolan, S. P. Quantifying and understanding the electronic properties of N-heterocyclic carbenes. *Chem Soc Rev* **42**, 6723–6753 (2013).
65. Huynh, H. V. Electronic Properties of N-Heterocyclic Carbenes and Their Experimental Determination. *Chem Rev* **118**, 9457–9492 (2018).
66. Nolan, S. P. *N-Heterocyclic Carbenes: Effective Tools for Organometallic Synthesis*. (John Wiley & Sons, Incorporated, 2014). ISBN: 978-3-527-33490-2.
67. Herrmann, W. A. N-Heterocyclic Carbenes: A New Concept in Organometallic Catalysis. *Angewandte Chemie International Edition* **41**, 1290–1309 (2002).

68. Hu, X., Castro-Rodriguez, I. & Meyer, K. Copper Complexes of Nitrogen-Anchored Tripodal N-Heterocyclic Carbene Ligands. *J Am Chem Soc* **125**, 12237–12245 (2003).
69. Hu, X. & Meyer, K. New tripodal N-heterocyclic carbene chelators for small molecule activation. *J Organomet Chem* **690**, 5474–5484 (2005).
70. Nieto, I., Cervantes-Lee, F. & Smith, J. M. A new synthetic route to bulky 'second generation' tris(imidazol-2-ylidene)borate ligands: Synthesis of a four coordinate iron(II) complex. *Chemical Communications* 3811–3813 (2005).
71. Kernbach, U., Ramm, M., Luger, P. & Fehlhammer, W. P. A Chelating Tris-carbene Ligand and Its Hexacarbene Iron Complex. *Angewandte Chemie International Edition in English* **35**, 310–312 (1996).
72. Cowley, R. E., Bontchev, R. P., Duesler, E. N. & Smith, J. M. Removing the sting from the tail: Reversible protonation of scorpionate ligands in cobalt(II) tris(carbene)borate complexes. *Inorg Chem* **45**, 9771–9779 (2006).
73. Forshaw, A. P., Bontchev, R. P. & Smith, J. M. Oxidation of the Tris(carbene)borate Complex $PhB(MeIm)_3Mn^{I}(CO)_3$ to $Mn^{IV}[PhB(MeIm)_3]_2(OTf)_2$ *Inorg Chem* **46**, 3792–3794 (2007).
74. Steube, J. *et al.* Janus-type emission from a cyclometalated iron(iii) complex. *Nat Chem* **15**, 468–474 (2023).
75. Braun, J. D. *et al.* Iron(ii) coordination complexes with panchromatic absorption and nanosecond charge-transfer excited state lifetimes. *Nat Chem* **11**, 1144–1150 (2019).
76. Baldeep K. Sidhu *et al.* (Re)Assigning the Long-Lived Photo-Excited State in Fe-N(amido) Coordination Complexes. in *25th International Symposium on the Photophysics and Photochemistry of Coordination Compounds* (2023).
77. Beckwith, J. S., Rumble, C. A. & Vauthey, E. Data analysis in transient electronic spectroscopy–an experimentalist's view. *International Reviews in Physical Chemistry* **39**, 135–216 (2020).
78. Lorenc, M. *et al.* Artifacts in femtosecond transient absorption spectroscopy. *Appl Phys B* **74**, 19–27 (2002).
79. Dietzek, B., Pascher, T., Sundström, V. & Yartsev, A. Appearance of coherent artifact signals in femtosecond transient absorption spectroscopy in dependence on detector design. *Laser Phys Lett* **4**, 38–43 (2007).
80. Van Stokkum, I. H. M., Larsen, D. S. & Van Grondelle, R. Global and target analysis of time-resolved spectra. *Biochimica et Biophysica Acta - Bioenergetics* **1657**, 82–104 (2004).
81. O'Connor, D. V. & Phillips, D. Basic Principles of the Single Photon Counting Lifetime Measurement. in *Time-Correlated Single Photon Counting* 36–54 (Academic Press, 1984).
82. Bard, A. J. & Faulkner, L. R. *Electrochemical Methods: Fundamentals and Applications*. (Wiley, 2001).

83. Johnson, Ben. A. Interrogating Diffusional Mass and Charge Transport in Catalytic Metal-Organic Frameworks. Uppsala: *Acta Universitatis Upsaliensis,* p. 115 (2020).
84. Paulus, B. C., Nielsen, K. C., Tichnell, C. R., Carey, M. C. & McCusker, J. K. A Modular Approach to Light Capture and Synthetic Tuning of the Excited-State Properties of Fe(II)-Based Chromophores. *J Am Chem Soc* **143**, 8086–8098 (2021).
85. Jamula, L. L., Brown, A. M., Guo, D. & McCusker, J. K. Synthesis and characterization of a high-symmetry ferrous polypyridyl complex: Approaching the $^5T_2/^3T_1$ crossing point for FeII. *Inorg Chem* **53**, 15–17 (2014).
86. Mengel, A. K. C. *et al.* Boosting Vis/NIR Charge-Transfer Absorptions of Iron(II) Complexes by N-Alkylation and N-Deprotonation in the Ligand Backbone. *Chemistry - A European Journal* **23**, 7920–7931 (2017).
87. Dixon, I. M., Alary, F., Boggio-Pasqua, M. & Heully, J.-L. Reversing the relative ^{3}MLCT–^{3}MC order in Fe(ii) complexes using cyclometallating ligands: a computational study aiming at luminescent Fe(ii) complexes. *Dalton Transactions* **44**, 13498–13503 (2015).
88. Jakubikova, E. & Bowman, D. N. Fe(II)-polypyridines as chromophores in dye-sensitized solar cells: A computational perspective. *Acc Chem Res* **48**, 1441–1449 (2015).
89. Mukherjee, S., Bowman, D. N. & Jakubikova, E. Cyclometalated Fe(II) complexes as sensitizers in dye-sensitized solar cells. *Inorg Chem* **54**, 560–569 (2015).
90. Zimmer, P. *et al.* N-Heterocyclic Carbene Complexes of Iron as Photosensitizers for Light-Induced Water Reduction. *Eur J Inorg Chem* **2017**, 1504–1509 (2017).
91. Steube, J. *et al.* Excited-State Kinetics of an Air-Stable Cyclometalated Iron(II) Complex. *Chemistry – A European Journal* **25**, 11826–11830 (2019).
92. Leis, W., Argüello Cordero, M. A., Lochbrunner, S., Schubert, H. & Berkefeld, A. A Photoreactive Iron(II) Complex Luminophore. *J Am Chem Soc* **144**, 1169–1173 (2022).
93. Malme, J. T. *et al.* Nanosecond Metal-to-Ligand Charge-Transfer State in an Fe(II) Chromophore: Lifetime Enhancement via Nested Potentials. *J Am Chem Soc* **145**, 6029–6034 (2023).
94. Marri, A. R., Marekha, B., Penfold, T., Haacke, S. & Gros, P. C. Towards panchromatic Fe(ii) NHC sensitizers via HOMO inversion. *Inorg Chem Front* **10**, 118–126 (2022).
95. Liu, L. *et al.* A new record excited state ^{3}MLCT lifetime for metalorganic iron(II) complexes. *Physical Chemistry Chemical Physics* **18**, 12550–12556 (2016).
96. Duchanois, T. *et al.* An iron-based photosensitizer with extended excited-state lifetime: Photophysical and photovoltaic properties. *Eur J Inorg Chem* **2015**, 2469–2477 (2015).

97. Liu, Y., Persson, P., Sundström, V. & Wärnmark, K. Fe N-Heterocyclic Carbene Complexes as Promising Photosensitizers. *Acc Chem Res* **49**, 1477–1485 (2016).
98. Chábera, P. *et al.* FeIIHexa N-Heterocyclic Carbene Complex with a 528 ps Metal-To-Ligand Charge-Transfer Excited-State Lifetime. *Journal of Physical Chemistry Letters* **9**, 459–463 (2018).
99. Liu, Y. *et al.* A heteroleptic ferrous complex with mesoionic bis(1,2,3-triazol-5-ylidene) ligands: Taming the MLCT excited state of iron(II). *Chemistry - A European Journal* **21**, 3628–3639 (2015).
100. Harlang, T. C. B. *et al.* Iron sensitizer converts light to electrons with 92% yield. *Nat Chem* **7**, 883–889 (2015).
101. Shepard, S. G., Fatur, S. M., Rappé, A. K. & Damrauer, N. H. Highly Strained Iron(II) Polypyridines: Exploiting the Quintet Manifold to Extend the Lifetime of MLCT Excited States. *J Am Chem Soc* **138**, 2949–2952 (2016).
102. Fatur, S. M., Shepard, S. G., Higgins, R. F., Shores, M. P. & Damrauer, N. H. A Synthetically Tunable System to Control MLCT Excited-State Lifetimes and Spin States in Iron(II) Polypyridines. *J Am Chem Soc* **139**, 4493–4505 (2017).
103. Chábera, P. *et al.* A low-spin Fe(III) complex with 100-ps ligand-to-metal charge transfer photoluminescence. *Nature* **543**, 695–699 (2017).
104. Rosemann, N. W. *et al.* Tracing the Full Bimolecular Photocycle of Iron(III)–Carbene Light Harvesters in Electron-Donating Solvents. *J Am Chem Soc* **142**, 8565–8569 (2020).
105. Aydogan, A. *et al.* Accessing Photoredox Transformations with an Iron(III) Photosensitizer and Green Light. *J Am Chem Soc* **143**, 15661–15673 (2021).
106. Prakash, O. *et al.* Photophysical Integrity of the Iron(III) Scorpionate Framework in Iron(III)–NHC Complexes with Long-Lived 2LMCT Excited States. *Inorg Chem* **61**, 17515–17526 (2022).
107. Schwarz, J., Ilic, A., Johnson, C., Lomoth, R. & Wärnmark, K. High turnover photocatalytic hydrogen formation with an Fe(iii) N-heterocyclic carbene photosensitiser. *Chemical Communications* **58**, 5351–5354 (2022).
108. Rosemann, N. W. *et al.* Competing dynamics of intramolecular deactivation and bimolecular charge transfer processes in luminescent Fe(iii) N-heterocyclic carbene complexes. *Chem Sci* **14**, 3569–3579 (2023).
109. Campagna, S., Puntoriero, F., Nastasi, F., Bergamini, G. & Balzani, V. Photochemistry and Photophysics of Coordination Compounds: Ruthenium. *Top Curr Chem* **280**, 117–214 (2007).
110. Arias-Rotondo, D. M. & McCusker, J. K. The photophysics of photoredox catalysis: a roadmap for catalyst design. *Chem. Soc. Rev.* **45**, 5797–6080 (2016).
111. Vauthey, E. Direct Measurements of the Charge-Recombination Dynamics of Geminate Ion Pairs Formed upon Electron-Transfer Quenching at High Donor Concentration. *J Phys Chem A* **105**, 340–348 (2001).

112. Rosspeintner, A. & Vauthey, E. Bimolecular photoinduced electron transfer reactions in liquids under the gaze of ultrafast spectroscopy. *Physical Chemistry Chemical Physics* **16**, 25741–25754 (2014).
113. Vauthey, E., Högemann, C. & Allonas, X. Direct investigation of the dynamics of charge recombination following the fluorescence quenching of 9,10-dicyanoanthracene by various electron donors in acetonitrile. *Journal of Physical Chemistry A* **102**, 7362–7369 (1998).
114. Pagès, S., Lang, B. & Vauthey, E. Ultrafast Spectroscopic Investigation of the Charge Recombination Dynamics of Ion Pairs Formed upon Highly Exergonic Bimolecular Electron-Transfer Quenching: Looking for the Normal Region. *J Phys Chem A* **108**, 549–555 (2004).
115. Rosspeintner, A., Angulo, G. & Vauthey, E. Bimolecular Photoinduced Electron Transfer Beyond the Diffusion Limit: The Rehm–Weller Experiment Revisited with Femtosecond Time Resolution. *J Am Chem Soc* **136**, 2026–2032 (2014).
116. Morandeira, A., Engeli, L. & Vauthey, E. Ultrafast Charge Recombination of Photogenerated Ion Pairs to an Electronic Excited State. *J Phys Chem A* **106**, 4833–4837 (2002).
117. Ohno, T., Yoshimura, A. & Mataga, N. Bell-shaped energy-gap dependence of backward electron transfer occurring within geminate radical pairs produced by quenching of ruthenium(II) polypyridine complexes by aromatic amines. *Journal of Physical Chemistry* **94**, 4871–4876 (1990).
118. Kakitani, T., Yoshimori, A. & Mataga, N. Theoretical Analysis of Energy-Gap Laws of Electron-Transfer Reactions. in *Electron Transfer in Inorganic, Organic, and Biological Systems* **228** 4–45 (American Chemical Society, 1991).
119. Mataga, N. Photoinduced Charge Separation and Charge Recombination of Transient Ion-Pair States. in *Electron Transfer in Inorganic, Organic, and Biological Systems* **228** 91–115 (American Chemical Society, 1991).
120. Shields, B. J., Kudisch, B., Scholes, G. D. & Doyle, A. G. Long-Lived Charge-Transfer States of Nickel(II) Aryl Halide Complexes Facilitate Bimolecular Photoinduced Electron Transfer. *J Am Chem Soc* **140**, (2018).
121. Chambers, M. B., Kurtz, D. A., Pitman, C. L., Brennaman, M. K. & Miller, A. J. M. Efficient Photochemical Dihydrogen Generation Initiated by a Bimetallic Self-Quenching Mechanism. *J Am Chem Soc* **138**, 13509–13512 (2016).
122. Schreier, M. R., Pfund, B., Guo, X. & Wenger, O. S. Photo-triggered hydrogen atom transfer from an iridium hydride complex to unactivated olefins. *Chem Sci* **11**, 8582–8594 (2020).
123. Vauthey, E. Photoinduced symmetry-breaking charge separation. *ChemPhysChem* **13**, 2001–2011 (2012).
124. Ramirez, C. E. *et al.* Symmetry-Breaking Charge Separation in the Solid State: Tetra(phenoxy)perylenediimide Polycrystalline Films. *J Am Chem Soc* 1–14 (2020).

125. Kim, T., Kim, W., Mori, H., Osuka, A. & Kim, D. Solvent and Structural Fluctuations Induced Symmetry-Breaking Charge Transfer in a Porphyrin Triad. *The Journal of Physical Chemistry C* **122**, 19409–19415 (2018).
126. Ivanov, A. I., Dereka, B. & Vauthey, E. A simple model of solvent-induced symmetry-breaking charge transfer in excited quadrupolar molecules. *Journal of Chemical Physics* **146**, 164306 (2017).
127. Dereka, B. *et al.* Solvent tuning of photochemistry upon excited-state symmetry breaking. *Nat Commun* **11**, 1–11 (2020).
128. Kellogg, M. *et al.* Symmetry breaking charge transfer as a means to study electron transfer with no driving force. *Faraday Discuss* **216**, 379–394 (2019).
129. Harris, J. P. *et al.* Near-infrared $^{2}E_{g} \rightarrow {}^{4}A_{2g}$ and visible LMCT luminescence from a molecular bis- (tris(carbene)borate) manganese(IV) complex. *Can J Chem* 1–23 (2017).
130. Serpone, N. & Hoffman, M. Z. Chromium(lll)-Polypyridyls. *J Chem Educ* **60**, 853–860 (1983).
131. Sinha, N. *et al.* A Near-Infrared-II Emissive Chromium(III) Complex. *Angewandte Chemie - International Edition* **60**, 23722–23728 (2021).
132. Dill, R. D. *et al.* Long-Lived Mixed 2MLCT/MC States in Antiferromagnetically Coupled d^{3}Vanadium(II) Bipyridine and Phenanthroline Complexes. *Inorg Chem* **59**, 14706–14715 (2020).
133. Juban, E. A. & McCusker, J. K. Ultrafast dynamics of 2E state formation in Cr(acac)3. *J Am Chem Soc* **127**, 6857–6865 (2005).
134. Sharp, P. R. & Bard, A. J. Electrochemistry in Liquid Sulfur Dioxide. 4. Electrochemical Production of Highly Oxidized Forms of Ferrocene, Decamethylferrocene, and Iron Bis(tris(1-pyrazolyl)borate). *Inorg Chem* **22**, 2689–2693 (1983).
135. De Alwis, D. C. L. & Schultz, F. A. Metal-bis[poly(pyrazolyl)borate] complexes. Electrochemical, magnetic, and spectroscopic properties and coupled electron-transfer and spin-exchange reactions. *Inorg Chem* **42**, 3616–3622 (2003).
136. McCusker, J. K. Femtosecond Absorption Spectroscopy of Transition Metal Charge-Transfer Complexes. *Acc Chem Res* **36**, 876–887 (2003).
137. Colmer, H. E., Margarit, C. G., Smith, J. M., Jackson, T. A. & Telser, J. Spectroscopic and Computational Investigation of Low-Spin MnIII Bis(scorpionate) Complexes. *Eur J Inorg Chem* **2016**, 2413–2423 (2016).
138. Hammarström, L. & Johansson, O. Expanded bite angles in tridentate ligands. Improving the photophysical properties in bistridentate RuII polypyridine complexes. *Coord Chem Rev* **254**, 2546–2559 (2010).
139. Prakash, O. *et al.* A Stable Homoleptic Organometallic Iron(IV) Complex. *Chemistry - A European Journal* **26**, 12728–12732 (2020).
140. Ilic, A. *et al.* Photoredox catalysis via consecutive ^{2}LMCT- and ^{3}MLCT-excitation of an Fe(iii/ii)–N-heterocyclic carbene complex. *Chem Sci* **13**, 9165–9175 (2022).

141. Kaufhold, S. *et al.* Microsecond Photoluminescence and Photoreactivity of a Metal-Centered Excited State in a Hexacarbene–Co(III) Complex. *J Am Chem Soc* **143**, 1307–1312 (2021).
142. Conti, Claudio., Castelli, Francesco. & Forster, L. S. Photophysics of hexakis(cyano)chromate(3-) and hexakis(cyano)cobaltate(3-) in polyalcohol-water solutions at room temperature. *J Phys Chem* **83**, 2371–2376 (1979).
143. Endicott, J. F. Photochemical pathways. *J Chem Educ* **60**, 824 (1983).
144. Serpone, N. & Hoffman, M. Z. Chromium(III)-polypyridyls: A case study. *J Chem Educ* **60**, 853 (1983).
145. Kirk, A. D. & Wong, C. F. C. Photoaquation of trans-$[Cr(en)_2NCSF]^+$. *Inorg Chem* **18**, 593–597 (1979).
146. Lee, S., Lee, J. & Pang, Y. Excited state intramolecular proton transfer of 1, 2-dihydroxyanthraquinone by femtosecond transient absorption spectroscopy. *Current Applied Physics* **15**, 1492–1499 (2015).
147. Jen, M., Lee, S., Jeon, K., Hussain, S. & Pang, Y. Ultrafast Intramolecular Proton Transfer of Alizarin Investigated by Femtosecond Stimulated Raman Spectroscopy. *J Phys Chem B* **121**, 4129–4136 (2017).
148. Orna, M. V., Kozlowski, A. W., Baskinger, A. & Adams, T. Coordination Chemistry of Pigments and Dyes of Historical Interest. in *Coordination Chemistry: A Century of Progress* (ed. Kauffman, G. B.) **565** 165–176 (ACS Symposium Series, 1994).
149. Vogler, A. & Kunkely, H. Photoreactivity of gold complexes. *Coord Chem Rev* 489–507 (2001).
150. H. Hellot, 'Histoire de l' academie royale des sciences' 1737, p. 101.
151. Che, C.-M., Kwong, H.-L., Yam, V. W.-W. & Cho, K.-C. Spectroscopic properties and redox chemistry of the phosphorescent excited state of $[Au_2(dppm)_2]^{2+}$ [dppm = bis(diphenylphosphino)methane]. *J Chem Soc Chem Commun* 885–886 (1989).
152. Li, D. *et al.* Spectroscopic properties and crystal structures of luminescent linear tri- and tetra-nuclear gold(I) complexes with bis(diphenylphosphinomethyl)phenylphosphine ligand. *Journal of the Chemical Society, Dalton Transactions* 189–194 (1993).
153. Jia, G., Puddephatt, R. J., Scott, J. D. & Vittap, J. J. Organometallic Polymers with Gold(I) Centers Bridged by Diphosphines and Diacetylides. *Organometallics* **12**, 3565–3574 (1993).
154. Shieh, S. J., Hong, X., Peng, S. M. & Che, C. M. Synthesis and crystal structure of a luminescent one-dimensional phenylacetylide-gold(I) polymer with 2, 6-bis(diphenylphosphino)pyridine as ligand. *Journal of the Chemical Society, Dalton Transactions* 3067–3068 (1994).
155. Yam, V. W. W. & Choi, S. W. K. Synthesis, characterization and photophysics of luminescent organogold(I) phosphines. *Journal of the Chemical Society, Dalton Transactions* 2057–2059 (1994).
156. Hong, X., Cheung, K. K., Guo, C. X. & Che, C. M. Luminescent organometallic gold(I) complexes. Structure and photophysical properties of alkyl-,

aryl- and μ-ethynylene gold(I) complexes. *Journal of the Chemical Society, Dalton Transactions* 1867–1871 (1994).
157. Seifert, T. P., Naina, V. R., Feuerstein, T. J., Knöfel, N. D. & Roesky, P. W. Molecular gold strings: Aurophilicity, luminescence and structure-property correlations. *Nanoscale* **12**, 20065–20088 (2020).
158. Schmidbaur, H. The aurophilicity phenomenon: A decade of experimental findings, theoretical concepts and emerging applications. *Gold Bull* **33**, 3–10 (2000).
159. Pujadas, M. & Rodríguez, L. Luminescent phosphine gold(I) alkynyl complexes. Highlights from 2010 to 2018. *Coordination Chemistry Reviews* **408** 1–21 (2020).
160. Chan, K. T. *et al.* The interplay between fluorescence and phosphorescence with luminescent gold(i) and gold(iii) complexes bearing heterocyclic arylacetylide ligands. *Chem Sci* **8**, 2352–2364 (2017).
161. Partyka, D. v., Esswein, A. J., Zeller, M., Hunter, A. D. & Gray, T. G. Gold(I) pyrenyls: Excited-state consequences of carbon-gold bond formation. *Organometallics* **26**, 3279–3282 (2007).
162. Li, T. Y., Muthiah Ravinson, D. S., Haiges, R., Djurovich, P. I. & Thompson, M. E. Enhancement of the Luminescent Efficiency in Carbene-Au(I)-Aryl Complexes by the Restriction of Renner-Teller Distortion and Bond Rotation. *J Am Chem Soc* **142**, 6158–6172 (2020).
163. Hollas, J. M. & Wright, R. A. Vibrational analysis of the near ultraviolet spectrum of 2,1,3-benzothiadiazole and the analogous spectra of benzofurazan and 2,1,3-benzoselenadiazole. *Spectrochimica Acta* **25**, 1211–1226 (1969).
164. Henry, B. R. & Morrison, J. D. Studies of the electronic absorption and emission spectra of 2,1,3-benzothiadiazole. *J Mol Spectrosc* **55**, 311–318 (1975).
165. Gordon, R. D. & Yang, R. F. The Near Ultraviolet Spectra of 2,1,3-Benzothiadiazole and Its Deuterated and Substituted Derivatives'. *J Mol Spectrosc* **39**, 295–320 (1971).
166. Ishi-I, T., Kichise, R., Park, I. S., Yasuda, T. & Matsumoto, T. Room temperature phosphorescence in longer-wavelength red light region found in benzothiadiazole-based dyes. *J Mater Chem C Mater* **11**, 3003–3009 (2023).
167. Teegardin, K., Day, J. I., Chan, J. & Weaver, J. Advances in Photocatalysis: A Microreview of Visible Light Mediated Ruthenium and Iridium Catalyzed Organic Transformations. *Organic Process Research and Development* **20** 1156–1163 (2016).
168. Paulus, B. C., Adelman, S. L., Jamula, L. L. L. & McCusker, J. K. K. Leveraging excited-state coherence for synthetic control of ultrafast dynamics. *Nature* **582**, 214–218 (2020).
169. Muñoz, S. B. *et al.* Tris(carbene)borate Ligands Featuring Imidazole-2-ylidene, Benzimidazol-2-ylidene, and 1,3,4-Triazol-2-ylidene Donors. Evaluation of Donor Properties in Four-Coordinate {NiNO}10 Complexes. *Inorg Chem* **51**, 12660–12668 (2012).

170. Welz, E., Böhnke, J., Dewhurst, R. D., Braunschweig, H. & Engels, B. Unravelling the Dramatic Electrostructural Differences between N-Heterocyclic Carbene- and Cyclic (Alkyl)(amino)carbene-Stabilized Low-Valent Main Group Species. *J Am Chem Soc* **140**, 12580–12591 (2018).
171. Peltier, J. L. *et al.* Eliminating nonradiative decay in Cu(I) emitters: >99% quantum efficiency and microsecond lifetime. *Science* **363**, 601–606 (2019).
172. Ung, G., Rittle, J., Soleilhavoup, M., Bertrand, G. & Peters, J. C. Two-coordinate Fe0 and Co0 complexes supported by cyclic (alkyl)(amino)carbenes. *Angewandte Chemie - International Edition* **53**, 8427–8431 (2014).
173. Roy, S., Mondal, K. C. & Roesky, H. W. Cyclic Alkyl(amino) Carbene Stabilized Complexes with Low Coordinate Metals of Enduring Nature. *Accounts of Chemical Research* **49**, 357–369 (2016).
174. Soleilhavoup, M. & Bertrand, G. Cyclic (alkyl)(amino)carbenes (CAACs): Stable carbenes on the rise. *Acc Chem Res* **48**, 256–266 (2015).
175. Andrei Tokmakoff. Nonlinear and Two-Dimensional Spectroscopy Notes. Available at https://tdqms.uchicago.edu/2d-spectroscopy-notes/ (2011).

Appendix

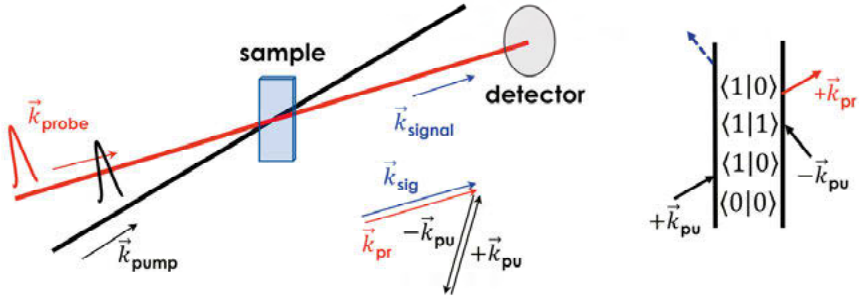

Figure A1. Consequences of detection geometry in pump-probe spectroscopy. Since the pump and probe are collinear, and the detection geometry is such that we detect signal *in the direction of the probe* – we force by considerations of vector addition that the pump must interact with the sample twice. Pump-probe is a third-order non-linear spectroscopy. The concept is also illustrated in the Feynman diagram (for stimulated emission) seen to the right; it is not possible to determine the time-ordering of the two interactions of the pump, since they come from the same field. Here we have assumed that the probe always follows the pump in terms of time ordering: when they overlap in time, however, a *coherent artefact* is generated. Figure concept from ref[175].

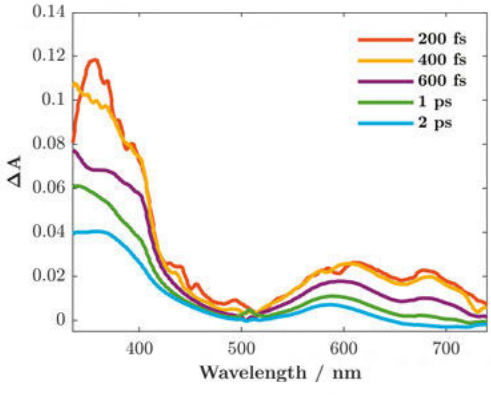

Figure A2. Earlier timescale spectral data for the oxidative quenching of $[Fe^{III}L_2]^+$ by MV^{2+} (in addition to that provided in Figure 4.13 panel a)). The early timescales <500 fs are convolved with the IRF; same measurement conditions.

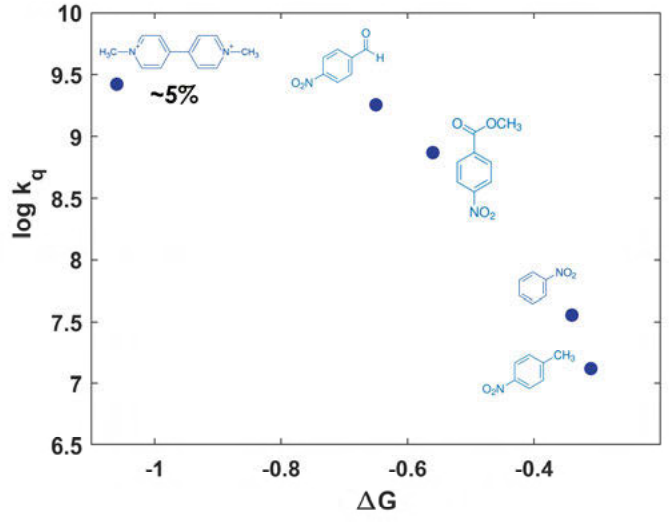

Figure A3. Compiled data for the oxidative quenching of $[Fe^{III}L_2]^+$ by various quenchers in acetonitrile. Dynamic quenching rate constants (k_q) determined from TCSPC. Cage-escape yields as determined from ns-TA are noted beside the quencher structure. No yields could be detected for any candidate tested except methyl-viologen.

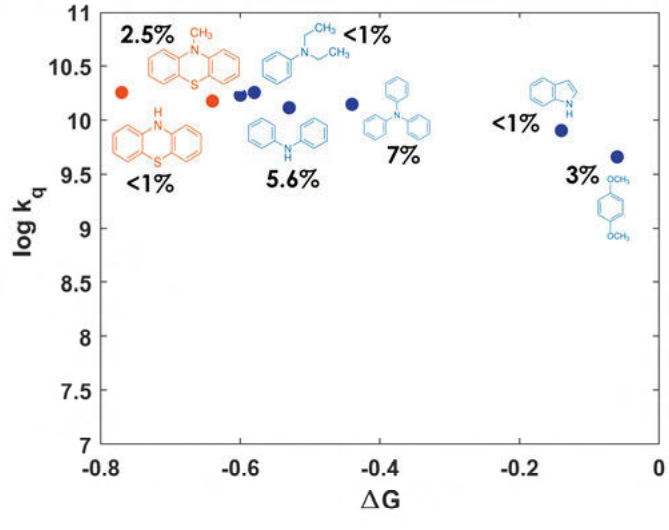

Figure A4. Compiled data for the reductive quenching of $[Fe^{III}L_2]^+$ by various quenchers in acetonitrile. Dynamic quenching rate constants (k_q) determined from TCSPC. Cage-escape yields as determined from ns-TA are noted beside the quencher structure.

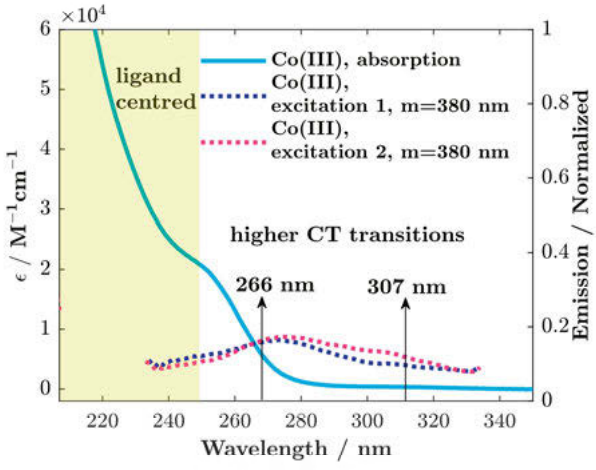

Figure A5. Absorption and excitation data for $[Co^{III}L_2]^+$. Excitation spectrum 2 was measured after irradiation.

Acta Universitatis Upsaliensis

Digital Comprehensive Summaries of Uppsala Dissertations from the Faculty of Science and Technology 2290

Editor: The Dean of the Faculty of Science and Technology

A doctoral dissertation from the Faculty of Science and Technology, Uppsala University, is usually a summary of a number of papers. A few copies of the complete dissertation are kept at major Swedish research libraries, while the summary alone is distributed internationally through the series Digital Comprehensive Summaries of Uppsala Dissertations from the Faculty of Science and Technology. (Prior to January, 2005, the series was published under the title "Comprehensive Summaries of Uppsala Dissertations from the Faculty of Science and Technology".)

Distribution: publications.uu.se
urn:nbn:se:uu:diva-508707

ACTA UNIVERSITATIS
UPSALIENSIS
2023